

Free Volume and Storage Stability of One-component Epoxy Nanocomposites

Dissertation

zur Erlangung des akademischen Grades
Doktor der Ingenieurwissenschaften
(Dr.-Ing.)

der Technischen Fakultät
der Christian-Albrechts-Universität zu Kiel

Muhammad Qasim Shaikh

Kiel

2010

1. Gutachter: Prof. Dr. Klaus Rätzke
 2. Gutachter: Prof. Dr. Wolfgang Jäger
- Datum der mündlichen Prüfung: 11.11.2010

Dedicated to my parents and my wife

Table of Contents

1. Introduction	1
2. Positrons and Positronium Annihilation	5
2.1 Introduction	5
2.2 Positrons and Positronium.....	5
2.2.1 Self Annihilation of Positrons and Positronium.....	6
2.2.2 Pick-off Annihilation of ortho-Positronium.....	6
2.2.3 Theoretical models for Positronium formation	7
2.3 Positrons sources for PALS.....	8
2.4 Positrons Annihilation Techniques (PATs).....	9
2.4.1 Positron Annihilation Lifetime Spectroscopy (PALS).....	10
2.4.1.1 Scintillator-Photomultiplier Detectors.....	11
2.4.1.2 Constant Fraction Diffraction Discriminators (CFDD).....	12
2.4.1.3 Time to Amplitude Converter (TAC).....	13
2.4.1.4 Multi-Channel Analyzer (MCA).....	13
2.5 Data Analysis of PALS spectrum	14
2.5.1 Analysis with LifeTime routine LT 9.0.....	14
2.5.1.1 Finite lifetime analysis	15
2.5.1.2 Continuous term analysis (with distribution).....	16
2.6 Tao-Eldrup Model for calculating the free volume in polymers	18
2.7 PALS studies on epoxy precursors	20
2.8 PALS studies on cured epoxy composites	21
2.9 PALS related to this thesis	21
3. Free Volume in Polymers	23
3.1 Introduction	23
3.2 Basic concept of the free volume.....	23
3.3 Definitions of the free volume.....	24
3.3.1 Empty volume	25
3.3.2 Excess free volume.....	25
3.3.3 Accessible free volume	26
3.4 Fractional free volume and related theories	27
3.5 Experimental techniques to determine free volume.....	28
3.6 Polymer properties characterized by the free volume.....	29
3.6.1 Glass-Transition temperature.....	30
3.6.2 Physical Ageing	31
3.7 Summary of this chapter	31

4. Johnson-Mehl-Avrami-Kohlmogorov Theory	33
4.1 Introduction	33
4.2 Basics of phase transformations	33
4.2.1 Nucleation and growth	33
4.3 Phase transformation Kinetics	36
4.4 Transformation mechanisms	37
4.5 Johnson-Mehl-Avrami-Kohlmogorov (JMAK) theory	38
4.5.1 Important assumptions	39
4.5.2 Derivation of Avrami equation	39
4.5.3 Avrami exponent ' n '	43
4.6 Time-Temperature Superposition	45
4.7 Summary of this chapter	46
5. One-component Epoxy Resin formulations	47
5.1 Epoxy Resins: An Introduction	47
5.1.1 Industrial applications of epoxy resin formulations	47
5.2 Current state of art and aim of this project	48
5.3 Basic principles of formulation	49
5.3.1 Epoxy resins	50
5.3.1.1 Diglycidyl ether of bisphenol A (DGEBA)	51
5.3.1.2 Bisphenol F Epoxy resin	52
5.3.2 Hardeners (Curing agents)	53
5.3.2.1 Amine curing	54
5.3.2.1.1 Dicyandiamide (DICY)	55
5.3.2.2 Anhydride curing	56
5.3.2.2.1 Methyl hexahydrophthalic anhydride (MHHPA)	58
5.3.3 Accelerators	58
5.3.4 Fillers	59
5.3.5 Micro and Nano/Encapsulation of Accelerators	59
5.4 Epoxy curing process and TTT diagram	60
5.5 Characterization of epoxy curing and cured epoxy networks	61
5.5.1 Traditional off-line methods	62
5.5.2 Modern in-situ methods	62
5.6 Summary of this chapter	63
6. Shelf life of one-component epoxy-resin formulation	65
6.1 Introduction	65
6.1.1 One-component formulation	65
6.1.2 Shelf-life and the curing mechanism	66
6.1.3 Transformed fraction and the JMAK theory	66
6.1.4 Free volume and PALS	67
6.2 Experimental	68

6.3	Results and Discussions	69
6.3.1	Analysis of Lifetime Spectra.....	69
6.3.2	Curing Kinetics and Avrami equation	71
6.4	Conclusion.....	75
7	Free and encapsulated accelerator formulations	77
7.1	Introduction	77
7.2	Experimental	79
7.2.1	Preparation of the epoxies.....	79
7.2.2	Modulated DSC	80
7.2.3	IR Spectroscopy	80
7.2.4	PALS	80
7.3	Results and Discussions	81
7.3.1	Part I: Precursor series (IR, PALS and JMAK).....	81
	7.3.1.1 Shelf calculated by IR Spectroscopy and PALS data at 60 °C	81
	7.3.1.2 JMAK fits to PALS data.....	82
7.3.2	Part II: Cured series (PALS and DSC).....	85
	7.3.2.1 Analysis of Positron Lifetime Spectra.....	85
	7.3.2.2 Micro-volumetric T_g and the co-efficient of thermal expansion	88
	7.3.2.3 Fractional hole free volume f_g (at T_g)	89
	7.3.2.4 Effect of cross-linking on T_g	89
	7.3.2.5 No effect of Positron irradiation	90
	7.3.2.6 The <i>ortho</i> -Positronium Inhibition	91
7.4	Conclusions	91
8	The effect of encapsulation on activation energy	93
8.1	Introduction	93
8.2	Experimental	94
8.2.1	Material.....	94
8.2.2	Analysis and Measurement	94
8.3	Results and Discussions	95
8.3.1	The <i>o</i> -Ps lifetime and the storage time	95
8.3.2	Transformed fraction and the JMAK fits	97
8.3.3	Avrami exponent and the Activation energies	99
8.4	Summary & Conclusions	102
9	Zeolite and Pyrogenic Silica filled Nanocomposites	105
9.1	Introduction	105
9.2	Experimental	107
9.2.1	Synthesis of Micro and Nano-sized encapsulations	107
9.3	Accelerator encapsulation in Zeolite carriers	107
9.3.1	Effects of varying accelerator concentration in μ -Zeolite carriers	107

9.3.2	Single-step micro and nano-sized encapsulations	111
9.3.3	Multi-stage micro and nano-Zeolite encapsulations	113
9.4	Accelerator encapsulation on Pyrogenic Silica carriers	116
9.4.1	Effects of varying accelerator concentration in 1K-formulations	117
9.5	Summary & Conclusions	121
10.	Summary & Outlook	123
11.	Bibliography.....	127
Appendices		
	<i>Appendix A</i>	135
	<i>Appendix B</i>	137
	<i>Appendix C</i>	139

Acknowledgments

List of Publications

1. Introduction

Epoxy resins are firmly established in a number of important applications, such as adhesives, protective coatings, laminates, and a variety of uses in building and construction.¹ The chemistry of epoxies and the range of modifications that are commercially available, allow cured polymers to be produced with a very broad range of properties. Successful performance of epoxy-based systems depends on proper selection and formulation of components. The components that have the most significant influence on the curing behavior and the network structure are the epoxy resin and the curing agents. As epoxy resins are converted into solid, infusible, and insoluble three-dimensional thermosetting networks for their applications, by curing with cross-linkers. Optimum performance properties are obtained by cross-linking the right epoxy resins with the proper cross-linkers, often called hardeners or curing agents. Selection of curing agent depends on various considerations, such as cost, ease of handling, pot life, cure rates, and the mechanical, electrical, or thermal properties required in the final resin. In order to lower the energy cost its important to achieve low temperature hardening and for this reason an accelerator must be added to speed up the reaction.

A single batch formulation is relevant for industrial applications, as for large scale applications, mixing the components directly before usage is not practical in industrial surrounding. As compared to a two-component epoxy-resin system, there is a limitation of shelf life when it comes to one-component systems, since the resin, hardener, accelerator, fillers and additives are all mixed together in one package. Therefore, a considerable shelf life of such ready to use one-component formulations is required. The epoxy curing process is an important factor affecting the performance of cured epoxies. To obtain desirable network structure and performance, it is imperative to understand the curing process and its kinetics to design the proper cure schedule. Epoxy curing process can be monitored by a number of experimental techniques and indirect estimation of cure conversion as a function of time is done with a combination of several experimental techniques and the available theoretical models. However, considering the product development in view it is still of utmost relevance, to establish reliable means of experimentally predicting the shelf life of new formulations of one-component epoxies, which is usually guessed from accelerated tests at elevated temperatures relying on selected reference measurements. In order to achieve predictability it is important to understand the complete curing mechanism of epoxies, so that the reaction

kinetics can be further elaborated in light of available standard models and further extrapolated to shelf life at storage temperatures.

Positron Annihilation Lifetime Spectroscopy (PALS), is presented here as a useful technique to study the curing kinetics of one-component epoxy resin formulations. Chapter 2 of this thesis discusses in detail the basics of positrons and positronium (Ps) formation in amorphous polymers. A brief overview of several positron annihilation techniques (PATs), is followed by an in-depth study of PALS technique, which is eventually the main focus of this PhD thesis. It is shown how a general setup of fast-fast coincidence functions and what information is experimentally obtained. Furthermore, data analysis of PALS by LifeTime routine 9.0 (LT9.0)² in its different modes is presented for the calculation of *ortho*-Positronium (*o*-Ps) lifetime $\tau_3 = \tau_{o\text{-Ps}}$. It is also shown that how this information can be correlated to the free volume in amorphous polymers, using a semi-empirical Tao-Eldrup model.³⁻⁴

Chapter 3 of this thesis stresses the importance of free volume and the characteristic properties of polymers directly affected by the free volume. It starts with the basic definition of the free volume and is followed by different ways of calculating the occupied volume. On one hand the change in free volume of the epoxy resin formulations, during the isothermal runs at elevated temperatures, is used to calculate the extent of curing i.e. the transformed fraction X . On the other hand, for a series of cured epoxy composites the temperature dependence of the free volume is used to calculate the glass-transition temperature (T_g) and the co-efficient of thermal expansion in the glassy and the rubbery phase.

The most significant achievement of this work is to study the curing kinetics of one-component epoxy resin formulations, using PALS data i.e. the change in free volume, in combination with Johnson-Mehl-Avrami-Kolmogorov (JMAK) equation,⁵⁻⁷ as discussed in Chapter 4. Isothermal and non-isothermal curing behaviors of epoxy resins has already been studied in the light of the Avrami equation in past, but only for high curing temperatures and neither growth exponent nor reaction constant have been interpreted or extrapolated to room temperature. This is of great importance for predicting storage stability of industrial one component formulations at room temperature. The origin of Avrami equation from metal physics, studied in the light of nucleation and growth theory for a liquid to solid phase transformation is also discussed in this chapter. This is followed by the derivation of Avrami

equation for a case of site-saturated homogenous nucleation. Furthermore, the Avrami exponent ' n ' and the reaction constant ' k ' are also discussed.

The composition of one-component epoxy resin formulations used in this work is discussed in Chapter 5 of this thesis. The basic rules of formulations, importance of maintaining the stoichiometric ratio of resin and hardener, the choice of accelerators and fillers are listed here. Please note that respecting the non-disclosure agreements concerning this work, the names of accelerators and the micro and nano-carriers used for encapsulation, will be treated as classified information.

The first results on the state of art one-component epoxy resin formulations, used as the benchmark system are mentioned in Chapter 6. It is shown that, how with increasing temperatures the reaction constant ' k ' varies and at the same time the Avrami exponent ' n ' remains constant. The boundary conditions for the fulfillment of JMAK equation are discussed and with the help of Arrhenius equation the shelf-life of epoxy resin formulation is extrapolated to storage temperatures.

Chapter 7 shows the results of PALS and IR-spectroscopy techniques, used for a series of one-component epoxy resin formulations in their precursor state. The affect of adding free and micro or nano-encapsulated accelerator on the shelf life is reported. The curing kinetics of one-component epoxy-resin systems is also discussed in the light of Avrami parameters and concluded with the possible reasons for the observed differences. Furthermore, the temperature dependence of the free volume for their cured composites is also studied in combination with PALS and DSC techniques.

The effect of accelerator encapsulation on curing kinetics and the activation energy is discussed in Chapter 8. Finally, a selected series of 1K-formulation containing Zeolite and nanosilica encapsulated accelerator are discussed in Chapter 9. Please note that the complete list of one-component epoxy resin formulations investigated during the course of this PhD thesis consists of 80 different formulations, with approximately 100 spectrums measured per sample on average, which is approximately 3 years of just the measuring time alone. Off course, this was possible due to the availability of three PALS machines at the Institute for Material Science, Multi-component Materials, University of Kiel. The data analysis includes the JMAK fits to the PALS data and t_{storage} from PALS in comparison to IR spectroscopy for

selected samples. Furthermore, the release behavior of accelerators is discussed in the light of Avrami parameters and compared with the hardening temperatures measured with DSC technique for selected samples.

The main aim of this PhD thesis on one hand, is to present the Positron Annihilation Lifetime Spectroscopy (PALS) as one of the state of art technique to characterize the in-situ curing kinetics of one-component epoxy resin formulations, by using the change in free volume as the measure of extent of curing in combination with the JMAK equation. On the other hand it is shown that PALS is also very useful when it comes to the characterization of the cured epoxy composites. This can give information about the interesting properties of cured composites, such as the temperature dependence of the free volume(V_f), the fractional free volume (FFV), glass-transition temperature(T_g), the thermal expansion co-efficient in the glassy and the rubbery phase.

2. Positrons and Positronium Annihilation

2.1 Introduction

Positrons are excellent probe particles to characterize defects of condensed matter. Upon annihilation with its anti-particle, the electron, they provide an indirect image of the structure, such as the concentration of vacancies and defect concentration in metals and semiconductors, sub-nanometre level free volume holes in polymers and they are even handy when it comes to characterization of larger pore diameters in highly porous materials. Positron annihilation has been, and continues to be, exploited in the study of structural changes associated with phase transitions, precipitation, deformation and physical ageing in various materials. The recent appearance of brilliant, reactor-based positron beams add a new dimension for the characterization and development of new thin-film probes, providing the research community with views on nature and possibilities in the development of advanced materials for future applications in everyday life.

The group of Prof. Dr. Franz Faupel at the Institute for Material Science – Multicomponent Materials, Engineering department of the Christian-Albrechts University of Kiel is involved in materials research with Positron Annihilation Lifetime Spectroscopy (PALS), since more than a decade. Some of the most noticeable works include free volume in bulk metallic glasses,⁸⁻¹⁰ amorphous alloys,¹¹ polyimides,¹² polymeric membranes with high permeability,¹²⁻¹³ Polymers of intrinsic micro-porosity,¹⁴ epoxy thin films¹⁵ and low molecular weight glass formers.¹⁶ In this chapter the basics of positrons and their detection as it relates to the sub-nanometre level free volume in bulk polymers are discussed, which is characterized in particular by the PALS.

2.2 Positrons and Positronium

In 1930 Paul AM Dirac¹⁷ postulated that a subatomic particle existed which was equivalent in mass to an electron but carried a positive charge. Carl Anderson observed these particles, which he named as the *positrons*, in cosmic ray research using cloud chambers in 1933.¹⁸ The positrons observed by Anderson were produced naturally in the upper atmosphere by the conversion of high-energy cosmic radiation into an electron–positron pair. Soon after this it

was shown that when positrons interact with matter they give rise to two photons which, are emitted simultaneously in almost opposed directions.

Positrons (e^+ or β^+) are the anti-particles of electrons (e^-), with a mass equal to that of electrons but having a positive charge. A positron in matter, can pick up an electron and this reaction of positron with an electron can lead to a meta-stable state called *Positronium*, abbreviated as (Ps).¹⁹ Positronium particles are similar to hydrogen atom in terms of size, but have a mass equivalent to two electrons.

2.2.1 Self Annihilation of Positrons and Positronium

The Ps annihilation events are governed by a selection rule resulting from charged parity (CP) invariance. The parity of the γ -photons is $(-1)^n$, and for ground-state Ps it is $(-1)^S$, where S is the total spin angular momentum of the Ps atom. If the positron and electron in the Ps have opposing spins (the singlet state, *para*-Ps or *p*-Ps) then the total $S = 0$ and consequently n has to be an even number, but if the positron and electron spins are parallel and $S = 1$ (the triplet state, *ortho*-Ps or *o*-Ps) then n has to be odd. The *p*-Ps principally decays into two 511 keV anti-parallel γ -rays, whereas *o*-Ps decays into three γ -rays whose total energy is $2mc^2$ or 1022 keV.²⁰

2.2.2 Pick-off annihilation of *ortho*-Positronium

The intrinsic lifetimes in vacuum for *p*-Ps and *o*-Ps are 0.125 ns and 142 ns, respectively (see Fig. 2.1). In ordinary molecular media, the electron density is low enough so that *o*-Ps can pick off electrons from the media that have anti-parallel spin to that of the positron, and undergo two-photon annihilation. The *pick-off annihilation* of *o*-Ps not only occurs in the form of two-photon annihilation, but it also shortens the *o*-Ps lifetime from 142 ns (self-annihilating *o*-Ps) to approximately ~ 1 to 10 ns in polymers.²¹

Experimental determination of *o*-Ps lifetime is one of the most useful methods for positron and positronium research. This is because *o*-Ps lifetime contains information about electron density, which governs the basic properties of chemical bonding in molecules and it is also controlled by the physical structure of molecules.

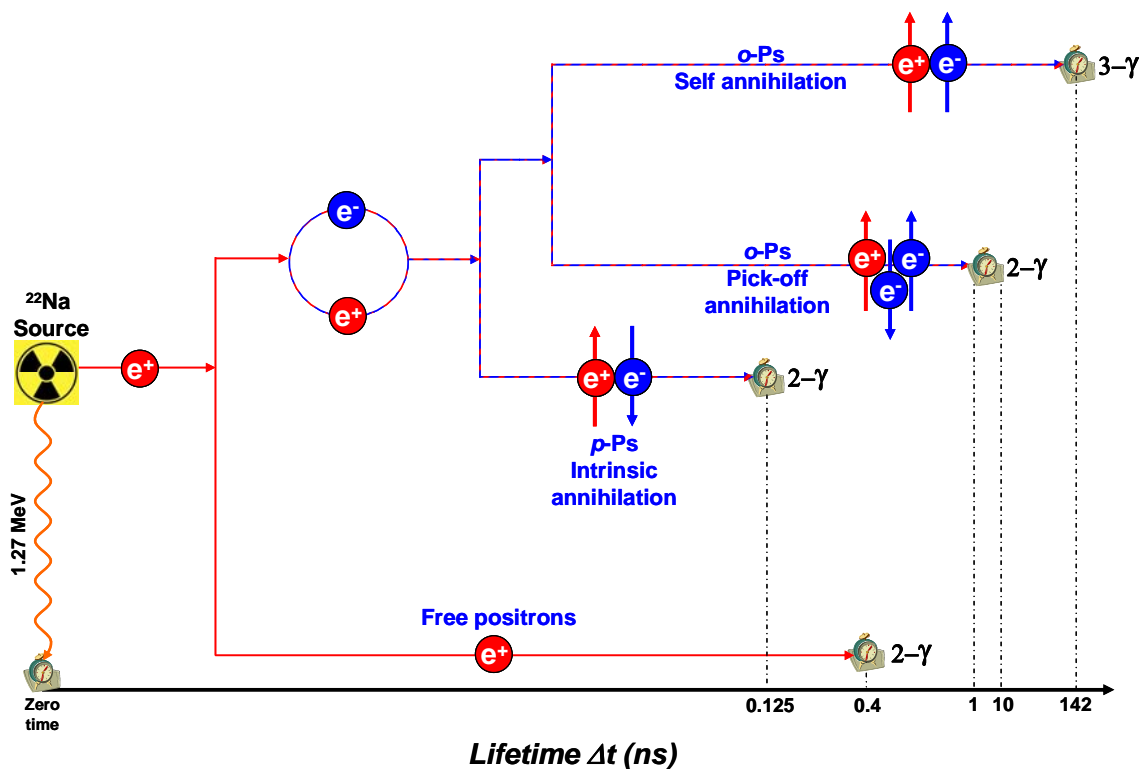


Fig. 2.1: Schematic of the most important positron and Ps formations and decay times in polymers.

The Ps formation probability $P^{\text{Ps}} = I_{p\text{-Ps}} + I_{o\text{-Ps}}$ and ($I_{o\text{-Ps}} = 3 P^{\text{Ps}}/4$, $I_{p\text{-Ps}} = P^{\text{Ps}}/4$), where $I_{p\text{-Ps}}$ and $I_{o\text{-Ps}}$ are the intensities of para and ortho positronium respectively and will be discussed in a later section in detail. The P^{Ps} is a very complex function and depends on different parameters such as the mobility of positrons and free electrons, the recombination of ionized molecules with free electrons, and the appearance of shallow or deep electron or positron traps. The two latter processes compete with combining of an electron and positron to form Ps.²²⁻²⁴

2.2.3 Theoretical Models for Positronium formation

The quasi-stable bound-state Ps cannot form in metals or semiconductors, as a result of electron screening (except above surface), but it can be formed in insulating solids and liquids. A small variety of models have been proposed to describe Ps formation in such solids and liquids, and their applicability depends to a large extent on the material under study.

The *Ore Model*,²⁵ considers Ps formation to occur principally in the range of energies from $(E_i - B)$ to E_{ex} , where E_{ex} and E_i are the threshold energies for atomic excitation and ionization, respectively, and $B = 6.8$ eV is the ground-state binding energy of Ps. Above E_{ex} other interactions are assumed to out compete Ps formation. A second prominent model is the *Spur*

Model, due to Mogensen²⁶, in which the positron binds to an electron released in a spur during the slowing-down process, under conditions of small relative momentum. An extension of this model is to consider the end of the positron track to be a *Blob*, rather than a spur²⁷. A third, particularly considered with respect to Ps in polymers, involves the formation of Ps in open volumes or holes, the electron being picked up from the surface,²⁸ if the positron is not completely thermalized, then the Ps atom may undergo thermalizing collisions with hole walls.

2.3 Positron sources for PALS

There are many radioactive isotopes which decay under β^+ emission of positrons, a process which is often used to produce positrons. In the laboratory environment the choice of radioactive sources for positron experiments has always been a compromise between application and cost. At the Isotope lab, Institute for Material Science, Engineering Department of Christian-Albrechts University of Kiel, ^{22}Na is used because of the benefits of long half life (2.6 years) coupled with the possibility of a simultaneous release of the start γ quanta along with a positron. The activity is bought in the form of a NaCl salt solution for in-house source preparation by evaporative deposition on a $7\mu\text{m}$ thick DuPont™ Kapton® polyimide film, which is glued by a second piece of $7\mu\text{m}$ thick foil with the help of a special adhesive called “PYRALIN™” (HD Microsystems).

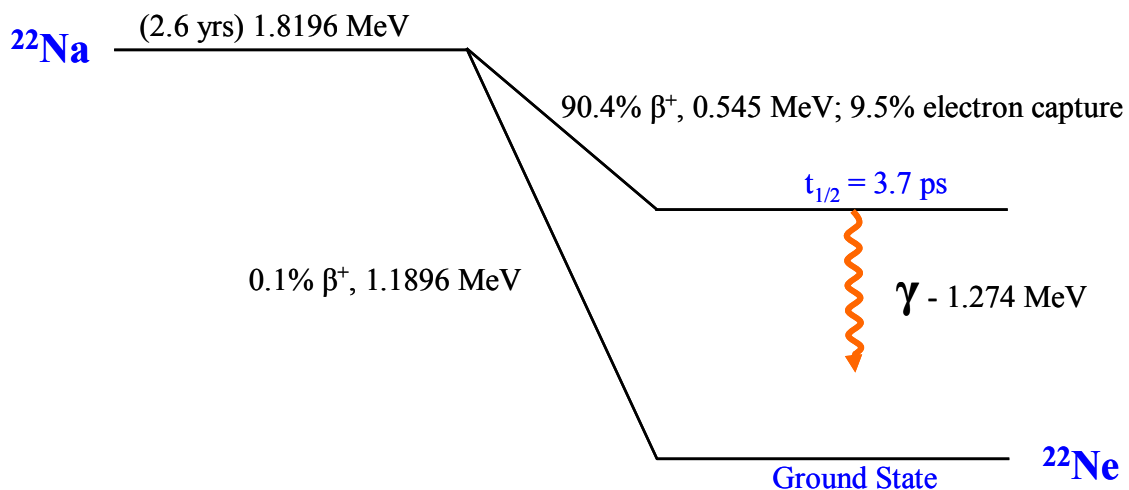


Fig. 2.2: Decay schematic of radioactive ^{22}Na isotope.

Positrons emitted by ^{22}Na sources have exhibit a broad energy distribution up to an energy of 540 keV and can penetrate deep into a sample.²⁹ The β^+ decay of ^{22}Na into ^{22}Ne ($^{22}\text{Na} \rightarrow ^{22}\text{Ne}$

$+ \nu + \gamma$), as shown in Fig. 2.2., is the most commonly used process for the emission of positrons, where ^{22}Na isotope gives a relatively high positron yield of 90.4%. It is observed that ^{22}Na decays by positron emission and electron capture, to the first excited state of neon nucleus (^{22}Ne) by the emission of an energetic positron and an electron neutrino. This excited state quickly de-excites to the ground state by the emission of a 1.274 MeV γ -ray with half-life $t_{1/2}$ of 3.7 ps. Approximately 9.5 % of the ^{22}Na will decay by electron capture, but it may also decay (0.1 %) directly to the ground state of Ne via the emission of a more energetic positron.

The decay of ^{22}Na results in the emission of the positrons (e^+) and a simultaneous release of a 1.27 MeV γ - quantum, which is often called the “birth” or “start” quantum of a positron. The lifetime of a positron is determined by the time between the birth quantum and its “annihilation” or the “stop” quanta. The half life of ^{22}Na is 2.6 years and the rate of its positron emission depends on the activity of the source. The higher the activity of a source, the shorter the time needed to complete the measurement of one spectrum. But too high activity can result in high background,³⁰ which can be problematic for analysis of long lifetimes, but are of no worry when analyzing polymers. The sources used throughout this thesis were approximately ~ 1 MBq, with a count rate of 400-500 counts per second. This means the time required to measure a spectrum of 5×10^6 annihilating events was in the range of 2-4 hours. This high number of total counts is important when analyzing the PALS spectrum with routine LT 9.0 software in its distribution mode and is discussed in detail in section 2.7.1.2.

2.4 Positron Annihilation Techniques (PATs)

There are several Positron Annihilation Techniques (PATs) available, which are successfully used with the annihilation radiation as shown in Fig. 2.3. The Positron Annihilation Lifetime Spectroscopy (PALS) is used to measure the lifetime Δt between the emission of the positron and the annihilation photons, whereas the Doppler broadening of Annihilation Line (DBAL) technique is based on measurement of the width of the annihilation gamma photon line, centred at 511 keV.

The Angular correlation of Annihilation Radiation (ACAR) technique is used for the measurement of angular distribution of the two annihilation photons ($180^\circ \pm \Delta\theta$), in the

direction transverse to the gamma emission, which directly yields information on the component of momentum of the annihilating pair. The Coincidence Doppler Broadening Spectroscopy (CDBS) can be used to investigate annihilations with core electrons to identify the chemical environment in which the positron decays.

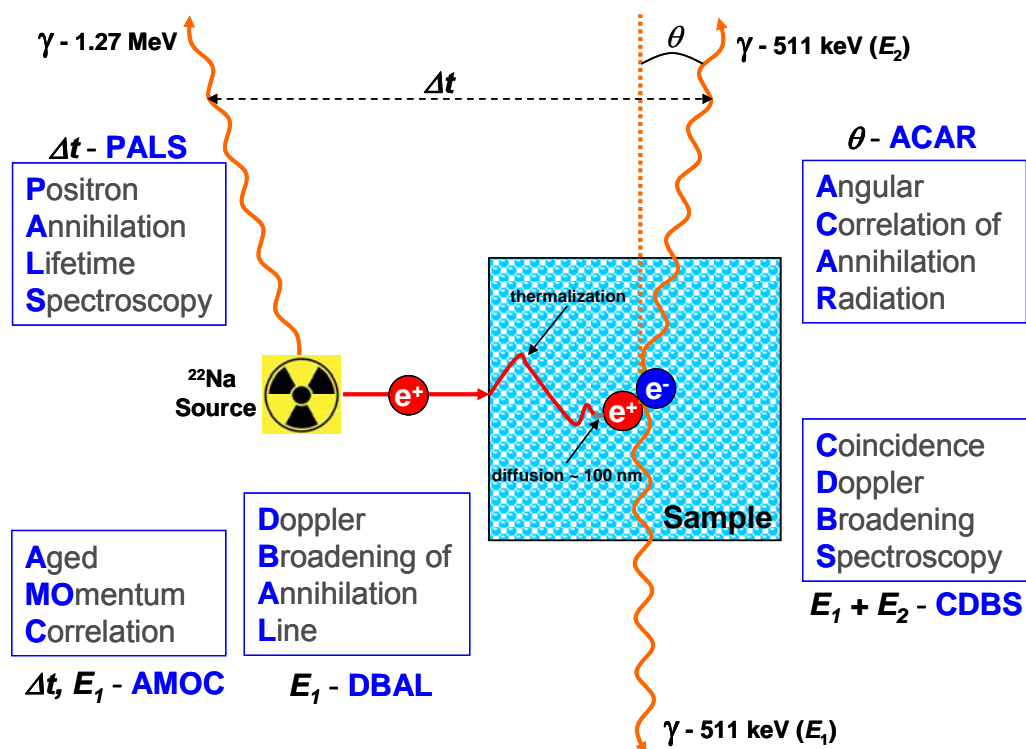


Fig. 2.3: Positron annihilation techniques.

The simultaneous measurement of positron lifetime and the momentum of the annihilating pair (i.e. PALS + DBAL) can give information on thermalization and transitions between positron states (and hence on chemical reactions of positrons or Ps, this technique is known as the Age-Momentum Correlation (AMOC). As mentioned earlier, the experimental technique used throughout this thesis was PALS, therefore in the following sections only the PALS technique is discussed in detail.

2.4.1 Positron Annihilation Lifetime Spectroscopy (PALS)

The positron lifetime of a single event can be measured by detecting the time difference between the birth γ -quantum of the β^+ -decay in the source and one of the annihilation γ -quanta with energy of 511 keV. The activity of the source must be sufficiently low in order to ensure that on average only one positron is in the sample. This avoids the intermixing of start and stop quanta originating from different annihilation events. A special “sandwich”

arrangement of ^{22}Na source, two identical samples, and detectors guarantees that all positrons emitted from the source are penetrating the sample material.

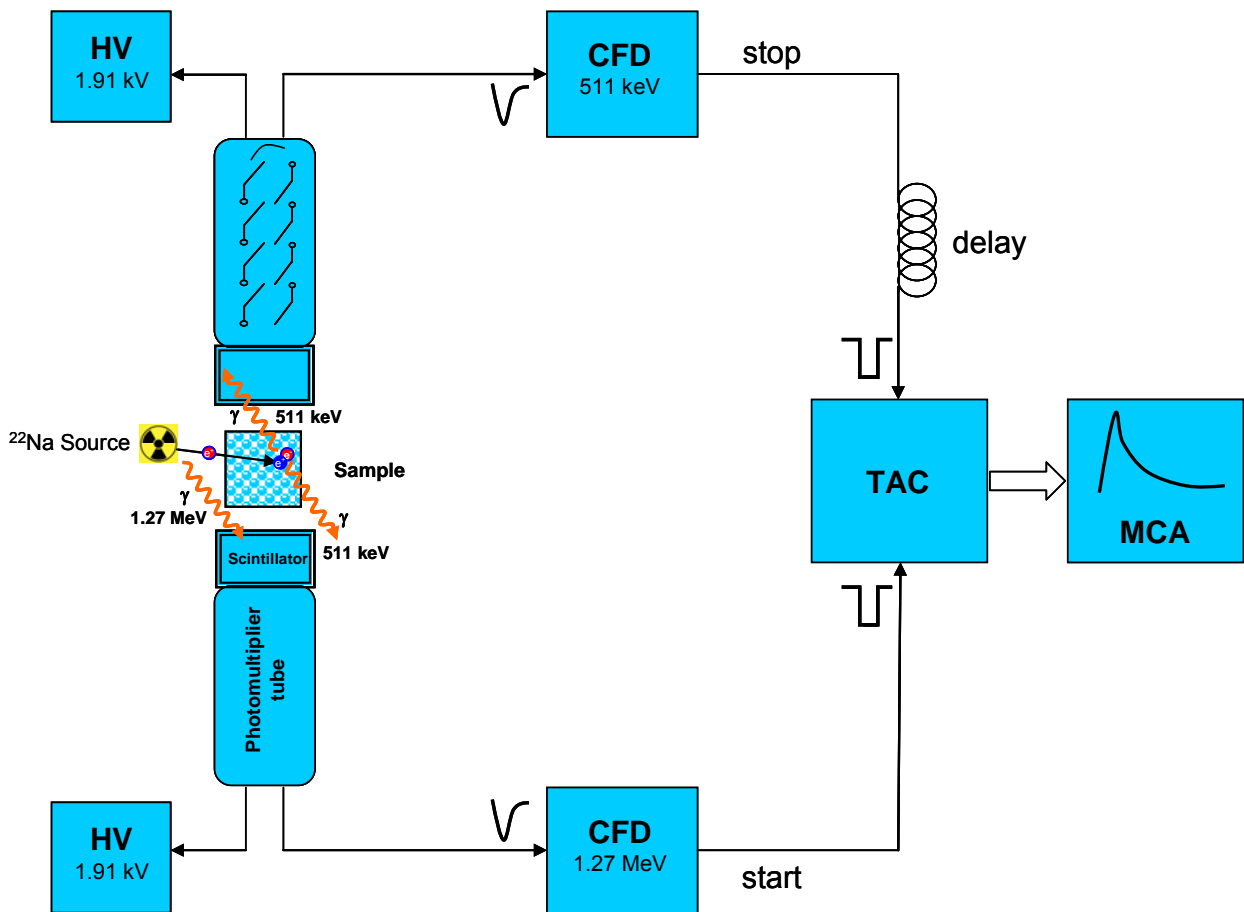


Fig. 2.4: Illustration of the experimental setup of positron annihilation lifetime spectroscopy (PALS), showing high voltage (HV) suppliers, photo-multiplier tubes (PMTs), constant fraction discriminators (CFDs), time to amplitude converter (TAC) and the multi-channel analyzer (MCA).

The experimental arrangement as shown in Fig. 2.4 is known as the “fast–fast coincidence” setup. The term is related to the fact that the time measurement as well as the energy selection is performed in a fast channel. A slow channel was used for energy selection when fast differential discriminators were not available at the beginning of positron lifetime experiments; this arrangement was called a fast–slow setup.²⁹

2.4.1.1 Scintillator-Photomultiplier Detectors

The scintillation-Photomultiplier tube detectors are the most common and successful mode for detection of 511 keV photons in PALS technique due to their good stopping efficiency. In the Isotope lab of Kiel University, these detectors consist of an appropriate choice of plastic

scintillator i.e. BC-420 ³¹ coupled to a (HAMAMATSU H1949-50) photomultiplier tube (PMT), with a short pulse rise-time are used to obtain a high time resolution for detection of the visible light.

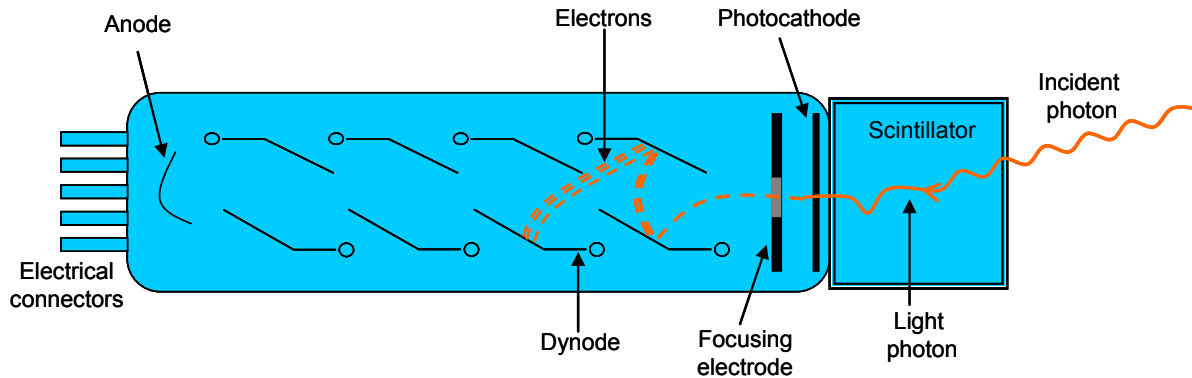


Fig. 2.5: Schematic diagram of a photomultiplier tube coupled with a plastic scintillator.

The γ -rays are converted by scintillator–photomultiplier detectors into analog electrical pulses. The PMTs consist of a vacuum enclosure with a thin photocathode layer at the entrance window. As shown in Fig. 2.5, an incoming scintillation photon deposits its energy at the photocathode and triggers the release of a photo-electron. Depending upon its energy, the photo-electron can escape the surface potential of the photo-cathode and in the presence of an applied electric field accelerate to a nearby dynode which is at a positive potential with respect to the photo-cathode. Upon impact with the dynode, the electron, with its increased energy, will result in the emission of multiple secondary electrons. The process of acceleration and emission is then repeated through several dynode structures lying at increasing potentials, leading to a gain of more than a million at the final dynode (anode). This high gain obtained from a photo-multiplier tube leads to a very good signal-to-noise ratio for low light levels and is the primary reason for the success and applicability of photomultiplier tubes for use in scintillation detectors.

2.4.1.2 Constant Fraction Discriminators (CFDs)

Discriminators with upper and lower levels, giving an output pulse only when the input pulse height lies between the two, are termed single channel analysers (SCA's). They are most often used to select pulses generated by gamma radiation within a certain energy range. A frequently used fast timing version of the SCA is the constant fraction discriminator (CFD) which combines fast low-jitter timing with pulse height selection. The discriminators suppress

noise and generate standard timing pulses by the constant-fraction discrimination principle. Another task is to guarantee that the 1.27-MeV and 511-keV quanta are accepted only in the appropriate channels. Their output pulses start and stop a time-to-amplitude converter as an “electronic stopwatch”. The stop pulse is coax-cable delayed in order to shift the time spectrum into a linear region of the TAC.

2.4.1.3 Time to Amplitude Converter (TAC)

The amplitude of the output pulse is proportional to the time difference between the birth and the annihilation γ -quanta and thus, represents a measure of the positron lifetime. The timing pulses are used to start and stop the charging of a capacitor in the time-to-amplitude converter (TAC). The time linearity is ensured there by constant-current charging that is stopped at the arrival of the stop pulse originating from the annihilation γ -quantum.

2.4.1.4 Multi-Channel Analyzer (MCA):

The final signal, whose amplitude is proportional to the lifetime of the positron is then fed into a multi-channel buffer (MCB) which records this in a histogram which, over time, describes the positron lifetime spectrum. An ORTEC® 919A multi-channel analyzer with about 16000 channels is used for storing the spectra. The multi-channel analyser (MCA), sorts pulses according to their height into several thousand channels or bins. MCAs can be multi-parameter, collecting for example spectra simultaneously in two dimensions and storing intensity contour plots.³² A single annihilation event is stored after analog–digital conversion in the memory of a multi-channel analyzer. Here the channel numbers represent the time scale, which can be easily converted by multiplying by the channel width. The three PALS instruments in the Isolab at the University of Kiel are configured to use 4096 channels each. The channel width used for the major part of this work was 25 ps, which is completely acceptable given that polymers have an *o*-Ps lifetime in the range of 1-10 ns. The time resolution of the spectrometer is determined mainly by the scintillator–multiplier part and is approximately 285 ps. The practical consequence of this relatively poor resolution is the limitation of the determination of positron lifetime components larger than about 50 ns. In order to obtain the lifetime spectrum with good statistics, more than 5×10^6 annihilation events were recorded.

2.5 Data analysis of PALS spectrum

The MCA builds a histogram over the probability $P(t)$, such that the annihilation of a single positron at a time t is registered. The spectrum S is a function of the total counts Index n , each of which represents a channel number in MCA, with the peak of spectrum coming from the maximum number of annihilation events. This gives the spectrum $S(n)$ with total number of coincidence counts N_0 , as follows:

$$S(n) = N_0 \int_{t_n}^{t_n + \Delta t} P(t) dt \quad (2.1)$$

where $t_{n+1} = t_n + \Delta t$, with Δt being the channel width of the spectrometer and t_n being the incident time of particular stop signal in addition to the channel width. The time dependent coincidence probability $P(t)$ can be summarize as;

$$P(t) = R(t) * [N(t) + B] \quad (2.2)$$

with $N(t)$ being the decay function, B is the signal background, and $R(t)$ is the resolution function of the instrument, generally determined by measuring a reference sample. For this purpose, Cu ($\tau_r = 122$ ps), Al ($\tau_r = 169$ ps), Si ($\tau_r = 219$ ps) or Kapton® ($\tau_{av} = 370$ ps)³³ can be used, where τ_r and τ_{av} are the reference and average lifetime values. The PALS spectrum for the reference must be obtained under the same experimental conditions and configurations as used in the samples in order to preserve the same instrument resolution.

2.5.1 Analysis with LifeTime routine LT 9.0

The positron lifetime spectrum must be analyzed by assuming a certain model spectrum, in order to obtain information about the properties of the inspected material. Positrons can annihilate in a crystal lattice in defect-free regions or after being trapped in the free volume holes of a polymer. Each of which gives a characteristic annihilation rate λ_i and characteristic lifetime $\tau_i = 1/\lambda_i$, respectively. In practice the lifetime distributions are usually obtained using a computer program such as the PATFIT,³⁴ CONTIN,³⁵ or MELT programs.³⁶ The reliability of these programs for measuring the *o*-Ps lifetime distribution in polymers was shown by Cao *et al.*³⁷ A detailed description of these methods of data analysis is already presented in literature.³² In PALS studies of polymers the decay function $N(t)$ of PALS spectrum can also

be analyzed by LifeTime routine LT 9.0.² The advantage of LT 9.0 over the other programs is that it can be easily used in a windows environment (except VISTA) and there is also a possibility of analyzing in two ways i.e. a finite lifetime analysis (discrete) or continuous lifetime analysis (with distribution).

2.5.1.1 Finite lifetime analysis

The life of a single positron has a well defined value between 0 and ∞ , if N number of positrons annihilate from a single state, they will have their lifetimes distributed according to Eq. (2.3)

$$N(t) = \frac{N}{\tau} \exp\left(-\frac{t}{\tau}\right) \quad (2.3)$$

but in reality positrons will usually annihilate from more than one state, each with its own individual lifetime. In the finite lifetime analysis the PALS spectrum are resolved into a finite number of negative exponentials decays. The experimental data $P(t)$ is expressed as a convoluted expression (by a symbol $*$) of the instrument resolution function $R(t)$ and a finite number of negative exponentials. So the decay function $N(t)$ is given as;

$$N(t) = \sum_{i=1}^{k+1} I_i \lambda_i \exp(-\lambda_i t) = \sum_{i=1}^{k+1} \frac{I_i}{\tau_i} \exp\left(-\frac{t}{\tau_i}\right) \quad (2.4)$$

Substituting this value in Eq. 2.2, one gets;

$$P(t) = R(t) * \left[\sum_{i=1}^{k+1} \frac{I_i}{\tau_i} \exp\left(-\frac{t}{\tau_i}\right) + B \right] \quad (2.5)$$

where, λ_i , is the inverse of the i -th lifetime component (τ_i) and I_i , is its intensity. The LT 9.0 is a routine that performs a weighted non-linear least square fit of Eq. 2.5 to the experimental spectrum. The user defines, the number of component i , to be fitted as well as initial guesses of the starting values. In polymers it is usually found that the spectra can be best resolved into three components. Where each lifetime corresponds to the average annihilation rate of a positron in different state. The shortest lifetime ($\tau_1 \sim 0.125\text{ns}$) is due to singlet para-positronium (p -Ps). The intermediate lifetime ($\tau_2 \sim 0.40\text{ ns}$) is due to positrons and positron-molecule species. The longest lifetime ($\tau_3 > 1\text{ ns}$) is due to the o -Ps localized in the free-volumes holes.

2.5.1.2 Continuous term analysis

The finite term analysis was basically developed for materials such as metals and semiconductors, which have often a single lifetime or a possibility of a number of discrete lifetimes due to atomic vacancies. Figure 2.6 shows as an example a schematic of free volume in polymers characterized by the *o*-Ps (shown as red circles).

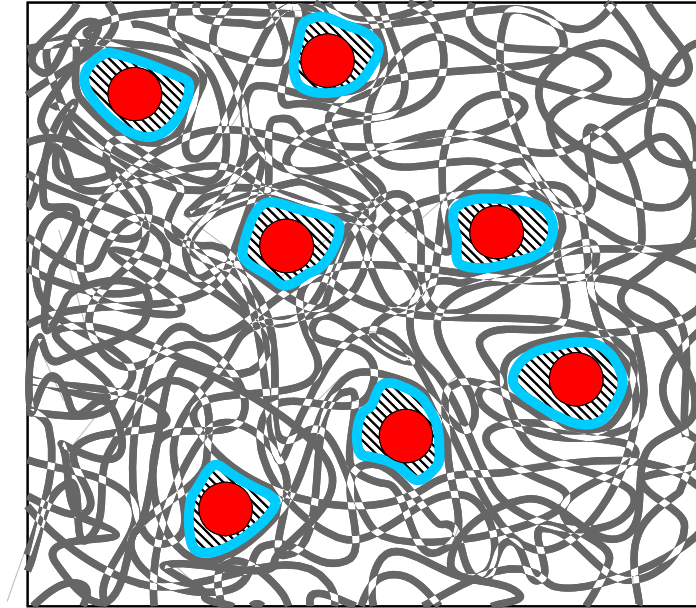


Fig. 2.6: Illustration of accessible free volume in polymers (area covered by blue boundaries), probed by *o*-Ps (red circles)

In polymers fitting to discrete lifetimes is not a good idea as there will always be a distribution of hole radii giving a distribution of lifetimes. This in particular is the advantage of the continuous lifetime analysis that one can obtain free volume hole size distributions, rather than the average values obtained in the finite analysis. In continuous lifetime analysis, a PALS spectrum is expressed in a continuous decay form, and is given by the Laplace transformation of the sum of the functions $\alpha_i(\lambda)\lambda$,

$$N(t) = \sum_{i=1}^{k+1} I_i \int_0^{\infty} \alpha_i(\lambda) \lambda \exp(-\lambda t) d\lambda \quad (2.6)$$

substituting Eq. 2.6 in Eq. 2.2, one gets;

$$P(t) = R(t) * \left[\sum_{i=1}^{k+1} I_i \int_0^{\infty} \alpha_i(\lambda) \lambda \exp(-\lambda t) d\lambda + B \right] \quad (2.7)$$

Here $\alpha_i(\lambda)$ is the distribution (probability density function, pdf) of the annihilation rate $\lambda = 1/\tau$ of the decay channel i , and LT 9.0 describes $\alpha_i(\lambda)$ by log normal functions;

$$\alpha_i(\lambda) = \frac{1}{\sigma_i \sqrt{2\pi}} \exp \left[-\frac{\ln(\lambda) - \ln\left(\frac{1}{\tau_0}\right)^2}{2\sigma_i^2} \right] \frac{1}{\lambda} \quad (2.8)$$

where τ_0 is the inverse of the mean log normal annihilation rate distribution and σ_i is the standard deviation related to the finite width of the distribution comes from the size (and shape) distribution of holes. So the continuous component depends on three model parameters i.e. the component intensity I , the mean-lifetime of each channel τ_i ,

$$\tau_i = \int_0^{\infty} \alpha_i(\lambda) d\lambda \lambda^{-1} = \tau_0 \exp\left(\frac{\sigma_0^2}{2}\right) \quad (2.9)$$

and the standard deviation from the mean-lifetime σ_i ;

$$\sigma_i^2 = \tau_0^2 \exp(\sigma_0^2) [\exp(\sigma_0^2) - 1] = \tau_i^2 [\exp(\sigma_0^2) - 1] \quad (2.10)$$

The time resolution is characterized by the full width at half maximum, FWHM, that is:

$$FWHM = 2\sigma\sqrt{\ln 2} \quad (2.11)$$

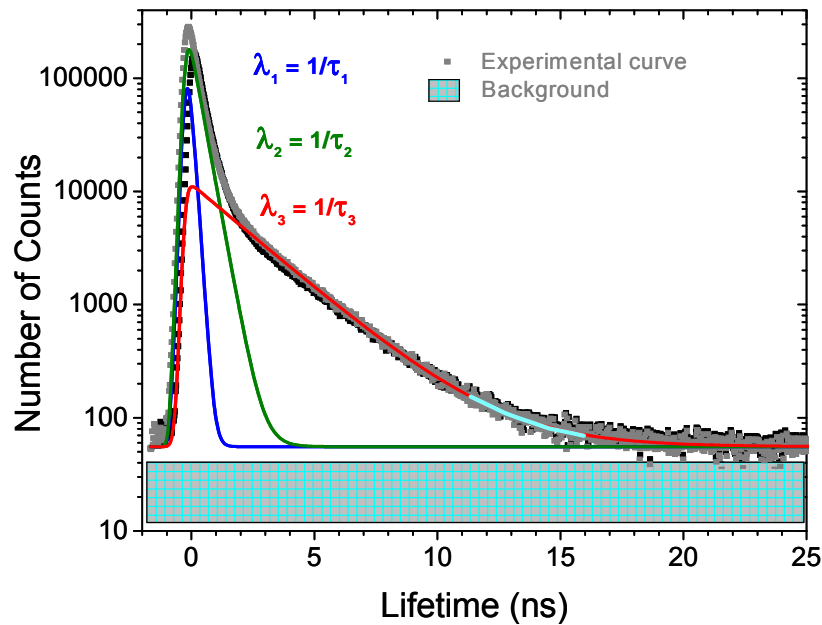


Figure 2.7: Spectrum of a cured DICY/Epoxy network analyzed by LT 9.0 in its distribution mode.

As an example, a typical positron lifetime spectra obtained from a cured DGEBA/Epoxy network is shown in Fig. (2.7). The experimentally obtained spectrum is analyzed with the help of LT 9.0 in its distribution mode. This continuous lifetime analysis approach was used throughout this thesis, which as explained above is of benefit to obtain free volume hole size distributions as compared to the discrete lifetime values obtained by the finite analysis.

It is generally observed that by increasing the number of parameters to be fitted one can reduce the χ^2 for a particular fit. To decompose a lifetime spectrum, the determination of the number of components in samples with unknown free volume distribution is started by a three-component fit of the spectrum. Additional components such as standard deviation σ_i ($i = 1,2,3$) and a second resolution function are added until the variance of the fit χ^2 is in the range of 1.0 to 1.15.

2.6 Tao-Eldrup model for calculating the free volume in polymers

In this simple semi-empirical model,³ it is assumed that *o*-Ps annihilates from an infinite square well potential. To model the overlap of the Ps wave-function with the surrounding molecules, the Ps wave-function is allowed to penetrate the potential well by a depth of δr as shown in Fig.2.8

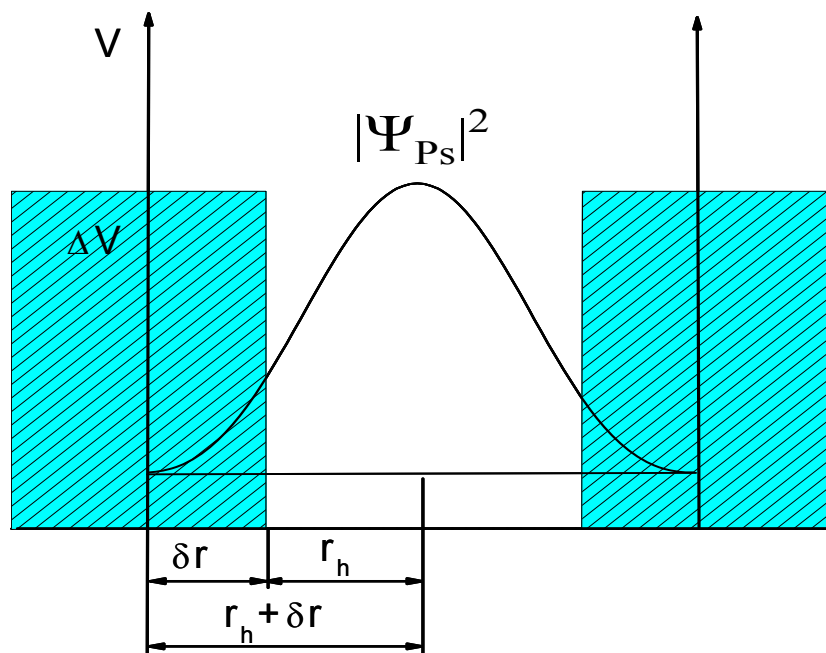


Figure 2.8: A schematic diagram of the positronium wave-function $|\psi|^2$, confined in a free volume hole of radius r_h . In the Tao and Eldrup model, this is approximated by an infinitely deep potential well of radius $r_h + \delta r$.

It follows from elementary quantum mechanics that the observed *o*-Ps pick off lifetime is related to the radius of the free volume hole (assumed to be spherical and the same size as the potential well) by the equation;

$$\tau_{o-Ps \text{ pickoff}} = \frac{0.5 \text{ ns}}{\left[1 - \frac{r_h}{r_h + \delta r} + \frac{1}{2\pi} \text{Sin}\left(\frac{2\pi r_h}{r_h + \delta r}\right) \right]} \quad (2.12)$$

where 0.5 ns is the spin averaged positronium annihilation lifetime and r_h is the hole radius. A value of $\delta r = 0.166$ nm is widely accepted and was determined empirically from fitting Eq. 2.12 to the *o*-Ps lifetime observed for free volumes holes of known size in various porous materials.^{4,38} Assuming the shape of holes as spherical, the hole volume v_h may then simply be calculated from

$$v_h = \frac{4}{3} \pi r_h^3 \quad (2.13)$$

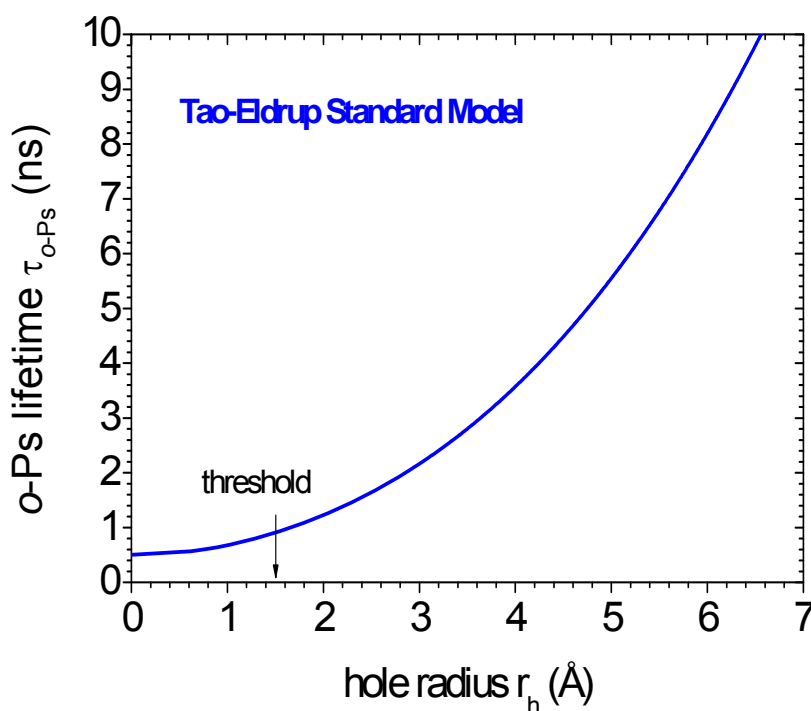


Figure 2.9: Correlation of *o*-Ps lifetime and the radius of free volume holes according to Eq. (2.12).

The *p*-Ps may also undergo pick-off annihilation, however the pick off annihilation rate (which can be assumed to be equal to $1/\tau_{o-Ps}$) is small as compared to the *p*-Ps self annihilation rate and so can be neglected. Unbound or ‘free’ positrons annihilate with a rate that reflects the electron density in the vicinity of the positron.³⁹ In polymers, this leads to an

average free positron lifetime of ~ 350 to 500 ps. It is conventionally assumed that the free positron lifetime is fixed for a given polymer. The free positrons may be trapped and annihilate in free volume holes and that the average free positron lifetime may also reflect the size of these holes.

To summarize, the average positron and positronium lifetimes in a polymer sample may be expressed as;

$$\tau_{p-Ps} = \frac{1}{(\eta\lambda_{p-Ps} + \lambda_{po})} \cong \frac{1}{(\eta\lambda_{p-Ps})} = 125 \text{ to } 200 \text{ ps} \quad (2.14)$$

$$\tau_{free} = \frac{1}{(\lambda_{free})} \cong 350 - 500 \text{ ps} \quad (2.15)$$

$$\tau_{o-Ps} = \frac{1}{(\eta\lambda_{o-Ps} + \lambda_{po})} \cong \frac{1}{(\eta\lambda_{po})} = 1 - 10 \text{ ns} \quad (2.16)$$

where λ_{p-Ps} and λ_{o-Ps} are the intrinsic annihilation rates of *p*-Ps and *o*-Ps respectively. λ_{po} is the pickoff rate and is assumed to be the same for both *p*-Ps and *o*-Ps. The value η is the relative contact density and reflects the change in the overlap of the electron-positron wave-functions compared to their state in vacuum.⁴⁰

2.7 PALS studies on epoxy precursors

Characterization of precursors or cured epoxy resin formulations by PALS, has been reported by various groups. For example, in-situ investigations on the cross-linking process of the epoxy resin system DGEBA and diethylenetriamine (DETA) in comparison with infrared (IR) spectroscopy was reported by J. Kanzow et al.⁴¹ The decrease in free volume of epoxy resin system is strongly connected with the cross-linking process of resin and hardener. It was observed that the free volume is dependent on the composition of the resin and the hardener. The isothermal curing of several epoxy-resin systems was studied by T. Suzuki et al.⁴²⁻⁴⁴ The decrease in *o*-Ps lifetime and simultaneous increase in its intensity were reported as the commencement of polymerization of the epoxy formulation, whereas the lower values of τ_3 were referred to as the termination of polymerization, these observations were supported by the higher values of I_3 with reached the saturation limits.

2.8 PALS studies on cured epoxy composites

Nanohole volume dependence on the cure schedule in epoxy thermosetting networks was reported by A. Somoza et al.⁴⁵ A strong dependence of the pre-cure temperature on the structure of amine cured epoxies was reported and it was suggested that the epoxy composites must be treated under similar conditions, specially when it comes to a comparison of PALS data with other techniques. Free volume changes with respect to the change in thermoplastic composition were reported by A.J. MacKinnon et al,⁴⁶ the change in the thermoset matrix material is termed as the major factor contributing to the phase structure of the cured composites, which eventually effects the mechanical properties. Pressure dependence of amine-cured epoxy polymers was studied above and below their glass-transition temperatures by Y.Y. Wang et al,⁴⁷ both *o*-Ps lifetime and its intensity decreases with increasing pressure. A second run with decreasing pressure was performed and the results were reproducible for the temperature above T_g , but this was not the case for the sample below T_g . This difference was attributed to the time scale for molecular relaxation below T_g , being lower than the experimental time scale of a few hours.

2.9 PALS related to this thesis

The work reported in this thesis is one step forward and the storage stability of one-component epoxy resin formulations is determined with the help of Johnson-Mehl-Avrami-Kolmogorov equation (JMAK) and Arrhenius law in combination with PALS data, the JMAK theory is discussed in Chapter 4 of this work. The effect of change in activation energies is also studied for free-accelerator and encapsulated accelerator formulations. Furthermore, the change in free volume, thermal expansion co-efficient and the glass-transition temperatures for several dicyandiamide (DICY) cured diglycidyl ether of bisphenol-A (DGEBA) formulations are studied, for an details of these formulations the reader is referred to the Chapter 5 of this thesis..

3. Free Volume in Polymers

3.1 Introduction

Free volume is an important characteristic property of polymeric materials which influences their numerous properties, such as viscoelasticity,⁴⁸⁻⁵⁰ diffusivity and permeability,⁵¹ penetration by solvents,⁵² impact properties⁵³ and the physical aging.⁵⁴ However, in contrast to other properties of polymers, free volume can be regarded as a complex physical object within polymers that can be characterized by the size and size distribution of micro-cavities or free volume element (FVE) that forms it. Initially, free volume was merely regarded as a theoretical concept that could explain many aspects of polymer behavior but could not be determined experimentally. Later, much attention was drawn to the problem of experimental evaluation of free volume in polymers and attempts to characterize the free volume resulted in development of various methods. In this chapter a quantitative discussion of various free volume definitions is done and compared with the hole free volume as characterized by positron annihilation lifetime spectroscopy (PALS).

3.2 Basic concept of the Free Volume

According to the free volume theory as first developed by Eyring⁵⁵ and others, molecular motion in the bulk state depends on the presence of holes, or places where there are vacancies or voids. When a molecule moves into a hole, obviously the hole also exchange places with the molecule, as illustrated by the motion indicated in Fig. 3.1.

Although Fig. 3.1 assumes small molecules, a similar model can be constructed for the motion of polymer chains, the main difference being that more than one “hole” may be required to be in the same locality, as cooperative motions are required. Thus, for a polymeric segment to move from its present position to an adjacent site, a critical void volume must first exist before the segment can jump.

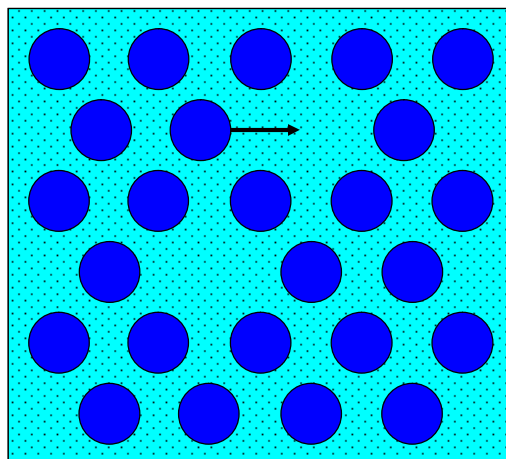


Fig. 3.1: A quasi-crystalline lattice exhibiting vacancies, or holes. Blue circles (●) represent molecules or the occupied volume, V_{occ} , and the remaining area (■) represent the specific free volume, V_f , whereas the arrow indicates the molecular motion.

It must be emphasized that beyond simple vibrational and rotational states, holes in materials are required for all types of molecular motion, so the important point is that molecular motion cannot take place without the presence of holes. These holes, collectively, are called the “**free volume**”.

3.3 Definitions of the free volume

The simplest assumption that can be made regarding free volume is based on its representation as the difference between the specific total and the occupied volume of the polymers. An expression of the free volume, $V_f(\text{cm}^3/\text{g})$, can be written as;

$$V_f = V_{tot} - V_{occ} \quad (3.1)$$

Where V_{tot} , is the specific total volume⁵⁶ and the occupied volume by the atoms is denoted as V_{occ} . The specific volume V_{tot} may be calculated from the inverse of the density $\rho(\text{g}/\text{cm}^3)$, However, V_{occ} has at least three different definitions and therefore refers to different definitions of free volume;

1. Calculated via the van der Waals excluded volume, or the *empty volume*.
2. The crystalline volume at 0 K, or the *excess free volume*.
3. *Accessible free volume*.

3.3.1 Empty volume

An approach to find the occupied volume of polymers was proposed by Bondi,⁵⁷ who suggested calculation of the van der Waals volume V_W , of repeat units of polymers by using the tabulated increments in V_W for smaller groups, which gives;

$$V_f = V_{tot} - V_W \quad (3.2)$$

In this model, the van der Waals volume is assumed to consist of a number of interpenetrating spheres. The radii of these spheres are equal to the van der Waals radii of the corresponding atoms and the separation of the centre of the spheres is equal to the bond lengths. Tabulated values of the van der Waals volumes of many of the most commonly occurring groups of atoms can be found in literature,⁵⁸ allowing the van der Waals volume of most polymers to be easily calculated. The free volume calculated as the difference between the total volume and the van der Waals volume represents the total free volume of the sample, which is often termed as the *empty volume*. It should be noted however, that not all of the total free volume defined in this way is available for the motion of the polymer chain segments.

3.3.2 Excess free volume

The concept of *excess free volume* is generally described as the free volume in the sample in excess of the volume occupied by the densest packing of molecules. According to this definition, the occupied volume consists of the van der Waals volume and the intrinsic interstitial free volume that occurs as a result of the equilibrium packing coefficient. Defining the free and occupied volume in this way acknowledges that the molecules can never fill the volume of the entire sample, so there must always be free volume analogous to the interstitial free volume in a crystal. Initially, in this model the crystal packing itself is used as the occupied volume and Bondi equated this occupied volume with the crystal polymer's volume at absolute zero, $V_c(0)$, and then postulated an empirical relation;

$$V_{occ} = V_c(0) \approx 1.3V_W \quad (3.3)$$

Connecting V_{occ} with the van der Waals volume.

$$V_f(T) = V_{tot}(T) - V_c(0) \quad (3.4)$$

$$V_f = V_{tot} - 1.3V_w \quad (3.5)$$

The tabulated values of V_c determined experimentally for a large number of common polymers can be found in literature.⁵⁸ The factor of 1.3 is due to the packing densities of polymeric crystals at absolute zero. This approach therefore describes the excess free volume as the volume that appears as a result of the irregular packing of the molecules. Clearly this approach represents a major simplification for defining the occupied volume as it assumes exactly the same packing efficiency for all polymers, and the assumption that the occupied volume doesn't change with temperature is not true. Furthermore, if V_c cannot be measured directly, an approximate value may be calculated using the van der Waals volume. As it is shown⁵⁸ for a large series of polymers, the crystalline volume at 298 K may be closely approximated by;

$$V_{occ} = V_c(298K) = 1.45 V_w \quad (3.6)$$

Another advantage of this excess free volume is that, it directly represents the volume available for motion of the polymer chain segments and is expected to be related to the physical and rheological properties of the polymer.

3.3.3 Accessible free volume

The *accessible volume* for a given penetrant molecule is the volume of the domain composed of points that can be occupied by the center of mass of the penetrant without any overlap between the van der Waals spheres of the polymer and that of the penetrant. For a spherical penetrant, accessible volume is most easily obtained by augmenting the radii of all polymer atoms and calculating the unoccupied volume. For a given matrix and a range of spherical probe molecules of progressively increasing radius, the accessible volume falls quasi-exponentially.⁵⁹⁻⁶⁰

Misra and Mattice⁶¹ utilized atomistic modeling via computer analysis, assuming hard spheres for the atoms. Central to the analysis was the use of mathematical probes, which analyzed the properties of the holes. Figure 3.3 shows that the maximum probe radius for polybutadiene at 300 K is around 1.5Å.

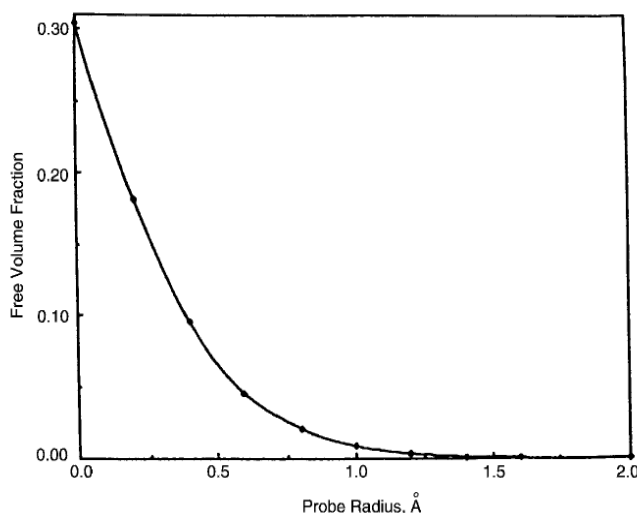


Fig 3.3: Theoretical free volume fraction as a function of the probe sized for polybutadiene.⁶¹

3.4 Fractional free volume and related theories

In most cases, a dimensionless, reduced value of the free volume, called the fractional free volume f , gives better correlations than V_f with transport properties within a family of polymers and is also a good measure of the openness of a polymer matrix. The fractional free volume is defined as the ratio of the specific free volume V_f , to the total volume V_{tot} ;

$$f = \frac{V_f}{V_{tot}} \quad (3.7)$$

Because of the different ways of defining the free volume, it is clear that the magnitude of the specific free volume and the free volume fraction will depend crucially on exactly how the occupied volume is defined. This difficulty is demonstrated by the wide range of values calculated by different free volume theories for the same polymer at the same temperature.

Table 3.1 - The free volume fraction f of PMMA at $T = T_g$ calculated from various free volume theories.⁶²

<i>Method</i>	<i>f(T_g)</i>
Simha-Somcynsky EOS theory	0.081
Simha-Boyer	0.137
Boyer-Spencer	0.235
Hirai-Eyring	0.056
Williams-Landel-Ferry (Doolittle)	0.013
Miller (Cohen – Turnbull)	0.032

An example is highlighted in table 3.1 which shows the fractional free volume of poly(methylmethacrylate) PMMA calculated at the glass transition temperature by various free volume theories. Since the above mentioned free volume theories are beyond the scope of this work, for this reason they are not discussed in detail.

3.5 Experimental Techniques to determine the free volume

Free volume distributions have been studied using kinetic theories(as briefly named in the previous section) and molecular dynamic simulations.⁶³ The attempts to characterize free volume resulted in development of various methods that are often united by the term “*probe methods*”. A common feature of these methods is that probes of different nature and size (atoms or molecules) are introduced into a polymer and observation of their behaviour, which is sensitive to free volume, makes it possible to deduce some information on nano-structure of free volume.

Just to name a few of these techniques, the experimental probes for free volume at molecular and atomic scales is possible using small-angle X-ray diffraction(SAXS),⁶⁴ inverse gas chromatography,⁶⁵ ¹²⁹Xe NMR spectroscopy,⁶⁶ spin-probe measurements,⁶⁷ wide-angle X-ray scattering(WAXS), photo-chromic and fluorescence techniques.⁶⁸

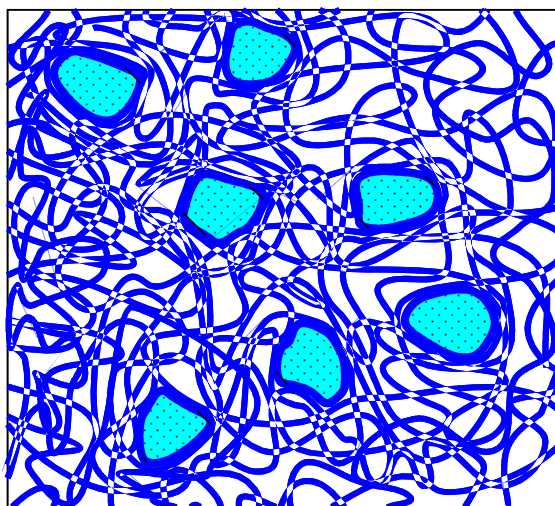


Fig. 3.2: Typical accessible free volume (■) sites in a polymeric structure due to the disordered packaging. The mean volume of these individual nanoscopic holes is determined by PALS and the total sum of all the free volumes can be obtained if number density N , of holes is known.

Positron annihilation lifetime spectroscopy has emerged as the unique method providing resolution of a few Angstroms in size and it has been shown that a good correlation exists

between the lifetime of *ortho*-Positronium (*o*-Ps) atoms and the free volume for not only polymers, but also applied to simple liquids as well.⁶⁹⁻⁷⁰ However, PALS calculate the hole free volume V_h , and the total free volume cannot be estimated directly with this method. In addition, it is important to realize that PALS is a dynamic method of measurement with a time scale of 10^{-9} s. The molecular vibrations with a frequency higher than 10^9 Hz will therefore contribute to the occupied volume.⁷¹ This thesis is based on experimental data obtained from the PALS technique only, which is already discussed quantitatively in Chapter 2.

Table 3.2 Methods used for probing free volumes in Polymers⁷²

<i>Method</i>	<i>Probe</i>	<i>Size</i>	<i>Information</i>
Positron Annihilation Lifetime Spectroscopy	<i>o</i> -Ps	1.06 Å	Size, size distribution, concentration of the FVE and dependence of the size of the FVE on temperature and pressure
Inverse gas chromatography	Organic Vapors	> 5 Å (>C ₃)	Temperature-averaged mean size of the FVE
¹²⁹ Xe NMR	¹²⁹ Xe	ca. 4 Å	Size of the FVE and its temperature dependence
Spin probe method	2,2,6,6-tetra-methylpyperidine-1-oxyl(TEMPO) and other stable nitroxyl radicals	> 100 Å ³	Information on the part of the size distribution of the free volume which corresponds to larger holes; temperature dependence of larger hole sizes
Photochromic probe method	Stilben and azobenzene derivatives	120-600 Å ³	
Electrochromic probe method	Azo-dyes	> 100 Å ³	

As indicated in table 3.2, a survey of some of the probe methods reveals that, the probes differ by their size and shape, whereas the methods are based on different principles of observation of behaviour of the probes in polymers. The smallest probe is used in the positron annihilation lifetime spectroscopy (PALS) and much larger probe molecules are used in the methods of spin-probe, electrochromic, photochromic and in inverse gas chromatography.

3.6 Polymer properties characterized by the free volume

Changes in free volume, V_f , can be monitored as a volumetric change in the polymer; by the absorption or release of heat associated with that change; the loss of stiffness; increased flow; or by a change in relaxation time.

3.6.1 Glass-Transition temperature

One of the most suitable approximations for analyzing the glass transition concerns the free volume.⁷³ As explained earlier, the free volume is the space in a solid or liquid not occupied by molecules; i.e., it is the empty space existing between molecules. In the liquid state the free volume is large, so molecular movements occur easily (the unoccupied volume facilitates the mobility of the molecules), and the molecules are therefore able to change their conformation freely. As shown in Fig. 3.4, the free volume, V_f , is represented by the shaded area, whereas α_r is the coefficient of thermal expansion for the "rubbery state" and α_g is the coefficient of thermal expansion for the "glassy state".

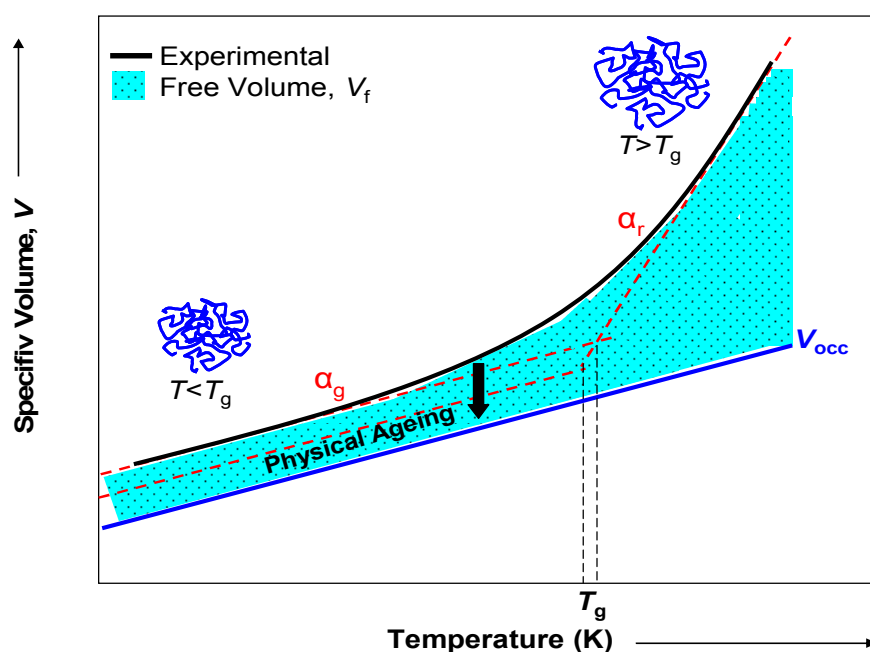


Fig. 3.4: A schematic diagram showing the determination of T_g from a plot of the specific occupied (V_{occ}) and the specific free volume (V_f) as a function of temperature for an amorphous polymer.

The free volume is sensitive to changes in temperature, thus the thermal expansion of the solid or molten polymer can be explained by a change in free volume. Below T_g only local conformational changes are permitted, and consequently the free volume shows a negligible temperature dependence, whereas above T_g there is a drastic change in the free volume, as indicated by the steeper slope in Fig. 3.4. Moving from very low temperatures, where the molecules are tightly compressed, it first passes through the solid state transitions. The material warms up and expands, the free volume increases which allows the localized bond movements i.e. bending and stretching. As the temperature and the free volume continue to

increase, the whole side chains and localized groups of four to eight backbone atoms begin to have enough space to move.

Furthermore, as the heating continues, the T_g or the glass transition temperature is reached, where the chains in the amorphous regions begin to coordinate long-range cooperative motions. One classical description of this region is that the amorphous regions have begun to melt, since the T_g only occurs in amorphous material, in a 100% crystalline material one does not see a T_g . Finally, the melt temperature T_m is reached, where large-scale chain slippage occurs and the material flows (not shown here). For a cured thermoset, nothing happens after the T_g until the sample begins to burn and degrade because the cross-links prevent the chains from slipping past each other.

3.6.2 Physical Ageing

While the molecular motion in the rubbery and liquid states involves 10 to 50 carbon atoms, molecular motion in the glassy state is restricted to vibrations, rotations, and motions by relatively short segments of the chains. As explained before, the extent of molecular motion depends on the free volume. In the glassy state, the free volume depends on the thermal history of the polymer. When a sample is cooled from the melt to some temperature below T_g and held at constant temperature, its volume will decrease (see Figure 3.4). Because of the lower free volume, the rate of stress relaxation, creep, and related properties will decrease.⁷⁴ This phenomenon is sometimes called physical aging, although the sample ages in the sense not of degradation or oxidation but rather of an approach to the equilibrium state in the glass.

3.7 Summary of this chapter

The glass-transition and physical ageing properties of some of the cured epoxy resin systems are studied with the help of the hole free volume obtained from PALS experiments and these results will be discussed in a later part (Chapter 7) of this thesis. But the major part of this work is focused on the investigation of the storage stability of single-component epoxy resin precursors as shown in Chapter 6, which are also studied with the help of Johnson-Mehl-Avrami-Kolmogorov (JMAK) equation and the transformed fraction calculated from the change in o -Ps lifetime, which in turn is the measure of hole free volume V_h . The JMAK

equation of phase transformations is discussed in the next chapter, whereas the PALS technique, as mentioned earlier is quantitatively discussed in Chapter 5.

4. Johnson-Mehl-Avrami-Kolmogorov Theory

4.1 Introduction

The main aim of this thesis is to provide industry with some more reliable and efficient means of determining the shelf-life of single-component epoxy-resin systems. In order to achieve this, it is necessary to understand the curing kinetics of these systems. This can be explained by the phase transformation from the precursor to the solid phase. In general, the theoretical basis for the overall transformation kinetics comes from the metal physics. The most important of them being the Avrami theory, also known as JMAK equation, named after Johnson and Mehl,⁷⁵ Avrami⁵⁻⁷ and Kolmogorov,⁷⁶ who significantly contributed to this equation. The Avrami theory is a widely accepted model to study the phase transformations, e.g. crystallization or austenite-to-martensite transformations.⁷⁷ In this chapter, the Avrami theory for the crystalline phase transformations is discussed. Here, this theory is applied for the first time to study the curing of epoxies, with the help of PALS data.

4.2 Basics of Phase Transformations

The emergence of a new phase within a parent phase, such as a solid within a liquid, involves the birth of a phase and its subsequent development. Normally with phase transformations, at least one new phase is formed that has different physical or chemical characteristics, with a possibility of a different crystallographic structure than the parent phase. Furthermore, most phase transformations do not occur instantaneously. In fact, they begin by the formation of numerous small particles of the new phase, which increase in size until the transformation has reached its completion. The progress of a phase transformation can be divided into two distinct stages: nucleation and growth.

4.2.1 Nucleation and Growth

Discussion of the theory of nucleation involves a thermodynamic parameter called free energy (or Gibbs free energy, G). A transformation will occur spontaneously only when ΔG has a negative value, where ΔG is the change in free energy. There are two types of nucleation i.e. homogeneous and heterogeneous. The distinction between them is made according to the site

at which nucleating events occur. For the homogeneous type, nuclei of the new phase form uniformly throughout the parent phase, whereas for the heterogeneous type, nuclei form preferentially at structural inhomogeneities, such as container surfaces, insoluble impurities, grain boundaries and dislocations. For the sake of clarity, only the homogeneous nucleation is discussed here, as these principles can be extended for a discussion of the heterogeneous type as well.

If the solidification of a pure material is considered, assuming that nuclei of the solid phase forms in the liquid phase. Figure 4.1, shows as an example the phase transformation from liquid to solid state. The growth of a nucleus, presumed to be of spherical shape with a radius r , volume $V = 4/3\pi r^3$ and an area of $A = 4\pi r^2$.

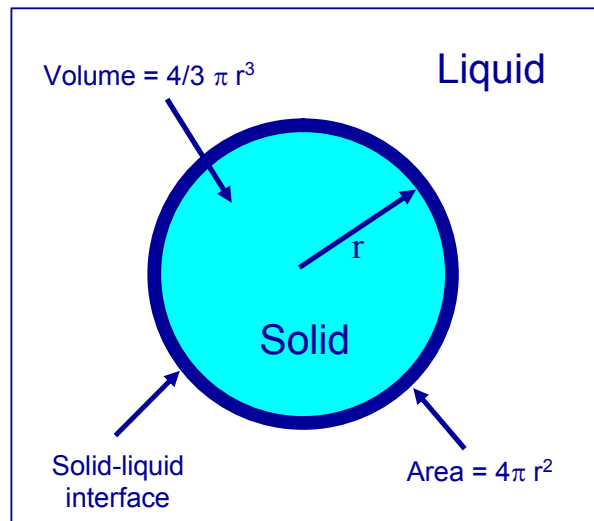


Fig 4.1: The figure showing nucleation of a spherical solid particle in a liquid.

There are two contributions to the total free energy change that accompany a solidification transformation. Firstly, change in the volume free energy of the phase after and the phase before transformation i.e. solid and liquid phases, $\Delta G_v = G_S - G_L$, and it will have a negative value if the temperature is below the equilibrium solidification temperature. The magnitude of its contribution is the product of ΔG_v and the volume of the spherical nucleus i.e. $V = 4/3 \pi r^3$. The second energy contribution results from the formation of the solid–liquid phase boundary during the solidification transformation. Associated with this boundary is a surface free energy, γ_{SL} , which is positive. Furthermore, the magnitude of this contribution is the product of γ_{SL} and the surface area of the nucleus i.e. $A = 4\pi r^2$. Finally, the total free energy change is equal to the sum of these two contributions i.e.,

$$\Delta G = G_{after} - G_{before} = V(G_S - G_L) + A \gamma_{SL} \quad (4.1)$$

$$\Delta G = -\frac{4}{3} \pi r^3 (G_L - G_S) + 4\pi r^2 \gamma_{SL} \quad (4.2)$$

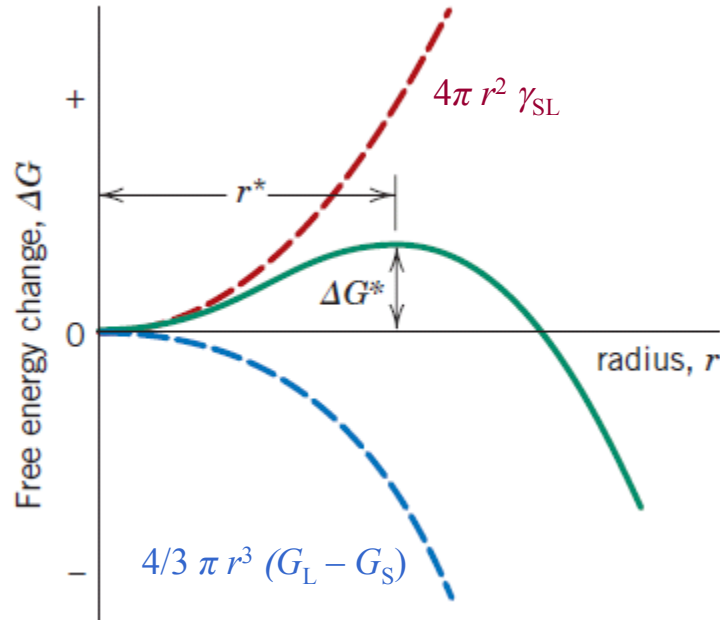


Fig 4.2: Schematic curves for volume free energy and surface free energy contributions to the total free energy versus embryo/nucleus radius. Also shown is the critical free energy change (ΔG^*) and the critical nucleus radius (r^*).⁷⁸

The volume, the surface, and the total free energy contributions are plotted schematically as a function of nucleus radius in Figure 4.2.⁷⁸ can be seen that for the curve corresponding to the first term on the right-hand side of Eq. 4.2, the free energy (which is negative) decreases with the third power of r . Furthermore, for the curve resulting from the second term in Eq. 4.2, energy values are positive and increase with the square of the radius. Consequently, the curve associated with the sum of both the terms, first increases, passes through a maximum, and finally decreases.

In a physical sense this means that when a solid particle begins to form, as atoms in the liquid cluster together, its free energy first increases. If this cluster reaches a size corresponding to the critical radius r^* , then growth will continue, accompanied by a decrease in free energy. On the other hand, a cluster of radius less than the critical will shrink and re-dissolve. This sub-critical particle is called an embryo, whereas the particle of radius greater than r^* is termed as a nucleus. A critical free energy ΔG^* , occurs at the critical radius and, consequently, at the maximum of the curve in Figure 4.2. This ΔG^* corresponds to an

activation free energy, which is the free energy required for the formation of a stable nucleus or it may be considered an energy barrier to the nucleation process.

Since r^* and ΔG^* appear at the maximum on the free energy-versus-radius curve of Figure 4.2, derivation of expressions for these two parameters is a simple matter. For r^* , the ΔG equation (Equation 4.2) is differentiated with respect to r , the resulting expression is set equal to zero, and then solved for ($r = r^*$). That is,

$$\frac{d(\Delta G)}{dr} = \frac{4}{3} \pi (G_L - G_S)(3r^2) + 4\pi \gamma_{SL}(2r) = 0 \quad (4.3)$$

this leads to the result,

$$r^* = \frac{2 \gamma_{SL}}{(G_S - G_L)} \quad (4.4)$$

Now, substituting this expression for r^* into Equation 4.2, yields the following expression for ΔG^* : (with $\Delta G = \Delta G^*$)

$$\Delta G^* = \frac{16\pi}{3} \frac{\gamma_{SL}^3}{(G_L - G_S)^2} \quad (4.5)$$

During the growth stage these nuclei increase in size, which results in the disappearance of some or all of the parent phase. The transformation reaches completion if the growth of these new phase particles is allowed to proceed until the equilibrium fraction is attained. Note that nucleation will continue to occur simultaneously with growth of the new phase particles. Off course, nucleation cannot occur in regions that have already transformed to the new phase. Furthermore, the growth process will cease in any region where particles of the new phase meet, as the transformation should have reached completion in these regions.⁷⁹

4.3 Phase Transformation Kinetics

The amount of material transformed can be calculated, subject to the restraints that are imposed on the kinetic process. The time dependence of rate, which is often termed as the kinetics of a transformation, is an important factor widely used in the study of numerous materials. The rate of transformation and the time required for the transformation to proceed to some degree of completion (e.g., time to 50% reaction completion, $t_{1/2}$) are inversely proportional to each other (Equation 4.6).⁷⁸

$$\text{rate} = \frac{1}{t_{1/2}} \quad (4.6)$$

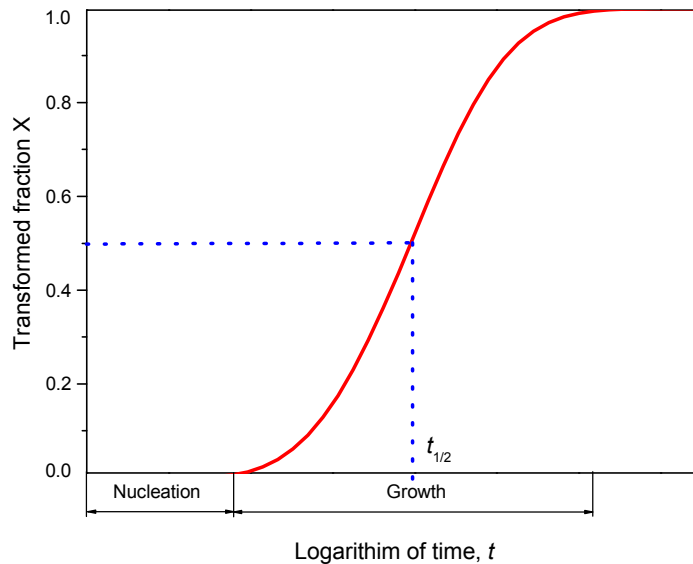


Fig 4.3: Plot of fraction reacted versus the logarithm of time, typical of many solid-state transformations in which temperature is held constant.

Thus, if this transformation is plotted against the logarithmic time (i.e., $\log t_{1/2}$), it generally results in an S-shaped curve i.e. slow at first, then accelerating and finally decelerating (as shown in Figure 4.3). It is often the case that the kinetics of phase transformations are represented using the Time-Temperature-Superposition and plotting the logarithmic time- (to some degree of transformation) versus-temperature plots.⁷⁷ (see e.g. section 4.6 and 5.4 of this thesis)

4.4 Transformation Mechanisms

There are several possibilities involving the nucleation and growth mechanisms, the two most important models for "grain size", which have been used for the results and discussion part of this thesis, are listed as under;⁸⁰

- (a) Continuous nucleation: nuclei added during transformation.
- (b) Site Saturated: all nuclei present at $t = 0$.

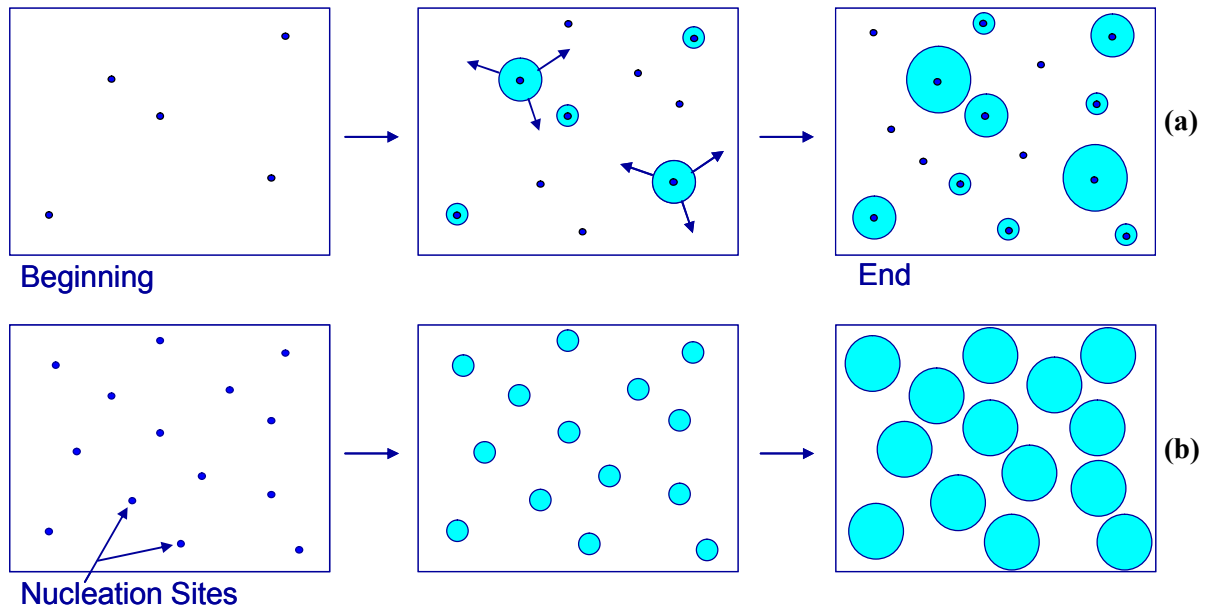


Fig 4.4: (a) Nucleation at constant rate during the whole transformation (b) Site-saturated: all nucleation occurs at the beginning of transformation.

A very simple nucleation mechanism, as shown in Fig. 4.4(a), is the one where the nucleation frequency is independent of the amount of material transformed, i.e. it is constant. This implies either steady-state homogenous nucleation or a specific type of heterogeneous nucleation where the number of nuclei activated is constant with time. Another possibility involving homogeneous nucleation as displayed in Fig. 4.4(b), is that all nuclei are activated at the same time, $t = 0$. However, in terms of physical realities, the simple possibilities are not necessarily the correct ones.

4.5 Johnson-Mehl-Avrami-Kohlmogorov (JMAK) Theory

The theories for transformation kinetics before JMAK, lack the mechanism for initiation and it was also clear that some mechanism for cessation should also be introduced into the analysis. The mutual interference of growing regions that originate from separate nuclei needs to be taken into account. In a liquid-crystal type transformation when two such regions impinge upon one another, a common interface develops. All growth will cease along this interface. This type of impingement is thus a natural mechanism by which crystallite growth can cease. Furthermore, this impingement is independent of the type of nucleation that is operative.⁷⁹ This concept, primarily geometrical in nature, is an important one. The initial treatment of this problem was give by Johnson and Mehl,⁷⁵ Avrami⁵⁻⁷ and Kolmogorov.⁷⁶ In this work, the Avrami equation is discussed in detail, as it has been the one most commonly

applied in recent past and it is also in good agreement with the experimental data that is reported in the later part of this thesis.

4.5.1 Important assumptions

The derivation of the Avrami equation makes a number of significant assumptions and simplifications.⁸¹

- a) Nucleation occurs randomly and homogeneously over the entire untransformed portion of the material.
- b) The growth rate does not depend on the extent of transformation.
- c) Growth occurs at the same rate in all directions i.e. isotropic.

4.5.2 Derivation of Avrami Equation

Avrami introduced the concept of phantom nuclei and the “extended volume” of transformed material that results from such nuclei, in order to address the problem of impingement. Phantom nuclei are the ones that are allowed to develop in the volume that has already been transformed, therefore termed as phantom. The central idea in the derivation of the JMAK equation is to focus on the increment in the fraction transformed and to relate it to the current value of the fraction transformed. The fraction transformed can be measured in almost any conceivable way, such as from micrographs, Electrical resistivity, Optical properties and Calorimetry.⁸² The relationship between volume and transformed fraction is rather a simple one.

$$X = \frac{V}{V_{total}} \quad (4.6)$$

Here ‘ X ’ is the fraction transformed, ‘ V ’ is the volume transformed and ‘ V_{total} ’ is the total volume. Figure 4.5 shows the concept of an extended fraction transformed can be understood by imagining that two spheres of new phase can overlap with one another as they grow, at the same time ignoring the effect of impingement. Where, V_1 and V_2 are the respective volumes of each sphere. In principle, to calculate the true fraction transformed, the actual volume transformed in this case should be given as the union of V_1 and V_2 , as in Eq. (4.8), i.e.

$$X = \frac{(V_1 \cup V_2)}{V_{total}} \quad (4.8)$$

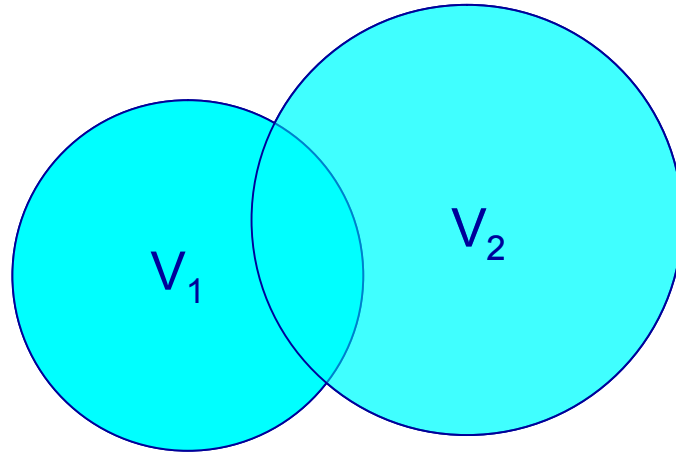


Fig. 4.5: Schematic representation of the overlap between two growing phases (illustrated as spheres).

But the extended fraction transformed ' X_{ext} ' accounts for all the volume, as if no impingement occurs, i.e.

$$dX_{ext} = \frac{d(V_1 + V_2)}{V_{total}} \quad (4.9)$$

During a time interval, t , nucleation and growth can only take place in untransformed material. However, this problem is more easily solved by applying the concept of the extended volume, the volume of the new phase that would form if the entire sample was still untransformed. One of the key assumption in the derivation of the JMAK equation, as already stated in section 4.5.1, is the random distribution of nuclei in space. This assumption allows to make a quantitative relation between the true increment in fraction transformed dX , a fictitious or extended fraction transformed dX_{ext} and the current fraction $(1-X)$.⁷⁷

$$dX = dX_{ext} (1-X) \quad (4.10)$$

Assuming that the probability of the dark blue region falls into the untransformed material (white region as shown in Fig. 4.6), is simply the volume fraction of the untransformed material i.e. $(1-X)$. Then, by multiplying $(1-X)$ with dX_{ext} , one will get the true change in volume fraction i.e. dX . So the R.H.S of Eq.(4.10) i.e. $dX_{ext} (1-X)$, is the probability that any new particle grows in the un-transformed (white) region. As already mentioned, dX_{ext} is the in-correct or the extended change in volume, in-correct in a sense that it ignores any impingement i.e. particles growing through each other or particles growing in already transformed region. The reason why it is needed is that, this extended change in volume, dX_{ext} , is relatively easy to calculate.

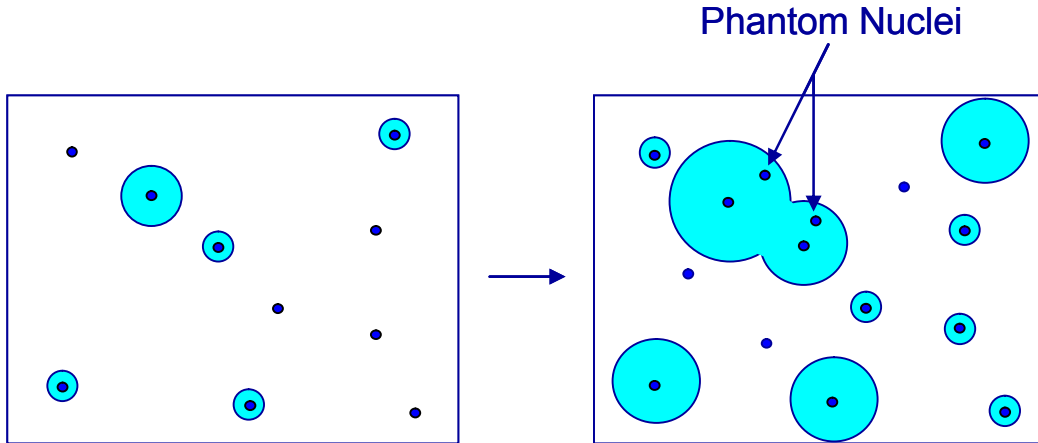


Fig 4.6: The transformation of one phase from another by the growth of nuclei forming randomly in the parent phase.

Assuming that the growth is isotropic i.e. the growth rate is constant, and the particles grow at different times as illustrated in Fig. 4.7. The incubation time τ , is the time before the nucleus grows, will be different for different particles. In a physical sense τ means that the particle does not exist before this time. Since growth is isotropic, constant and unhindered by previously transformed material each nuclei N will grow at a rate G , into a sphere of radius r , where $r=G(t - \tau)$ and so the extended volume of solid phase due to the appearance of nuclei in this time interval will be:

$$V_{\tau} = \frac{4}{3} \pi [G(t - \tau)]^3 = \frac{4}{3} \pi G^3 (t - \tau)^3 \quad (4.11)$$

Of course there is nucleation rate, N' as well and to find the number of particles N , at a given time t , we have to multiply the individual volume by the rate of nucleation N' . The extended fraction increment is then obtained to be;

$$dX_{ext} = \frac{4}{3} \pi G^3 N' (t - \tau)^3 d\tau \quad (4.12)$$

So in between 't' and 't+dt', this is the change in volume. Since this is the in-correct or extended change in the volume, one should change it into correct volume of transformation for solid phase, by simply substituting Eq. 4.12 in Eq.4.10:

$$dX = (1 - X) \frac{4}{3} \pi G^3 N' (t - \tau)^3 d\tau \quad (4.13)$$

or

$$\frac{dX}{(1 - X)} = \frac{4}{3} \pi G^3 N' (t - \tau)^3 d\tau \quad (4.14)$$

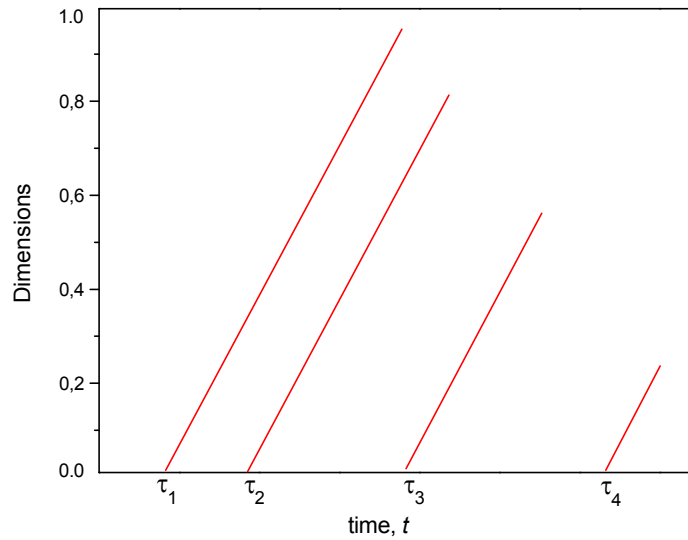


Fig 4.7: The incubation time τ , will be different for the different growing particles (re-constructed image).⁸³

Integrating Eq.4.14, one will get the volume of solid phase in L.H.S and some function of time in R.H.S.,

$$-\ln(1-X) = \frac{4}{3} \pi G^3 N' \int_0^t (t-\tau)^3 d\tau \quad (4.15)$$

or

$$X = 1 - \exp\left\{\frac{-\pi G^3 N' t^4}{3}\right\} \quad (4.16)$$

This can be reduced to the more familiar form of the Avrami (JMAK) equation which gives the fraction of transformed material after a holding time at a given temperature;⁷⁷

$$X = 1 - \exp\{-kt^n\} \quad (4.17)$$

Where, $\pi N' G^3/3$ can be collected into a constant k , which is a function of temperature, specifically together with n , for transformation mechanism, and in this case $n = 4$. Whereas, another derivation (not shown here) indicates that the value of $n = 3$, for the Avrami exponent, when a case of site-saturated, steady-state homogenous nucleation is assumed, with all nuclei present at time, $t = 0$. The shape of the curves obtained from Equations 4.16 and 4.17 should be sigmoidal (as in Fig. 4.3) i.e. starts off slow because particles are small in size, than fast, as

growth rate is fast due to faster volume transformation and finally slow again as it is running out of matrix i.e. running out of parent phase. Therefore, it levels off in the final stages of transformation.

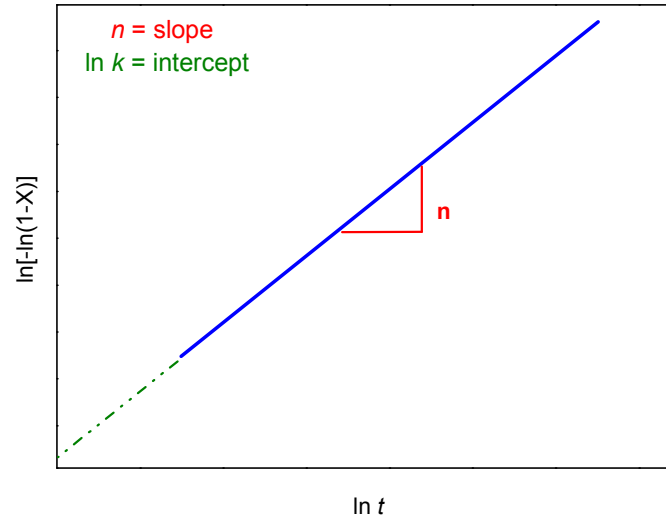


Fig. 4.8: Double logarithmic plots of Eq. 4.18, indicating the Avrami exponent ' n ' and the constant ' k '.

Both Eq. 4.16 and Eq. 4.17 are commonly termed as the Avrami relation. They are very simple and convenient expressions to use and hence their widespread adoption. However, it should be recognized that they are restricted in scope because of the limited nucleation and growth processes that have been considered. Thus, caution must be exercised when interpreting results using these equations. Furthermore, Eq. 4.17 can be re-written in the double logarithmic form as;

$$\ln[-\ln(1-X)] = \ln k + n \ln t \quad (4.18)$$

The advantage of Eq. 4.18 is that, it allows the determination of the constants n and k from a plot of $\ln[-\ln(1-X)]$ vs $\ln t$, as shown in Fig. 4.8. If the transformation follows the Avrami equation, this yields a straight line with gradient n and $\ln k$ is the intercept.

4.5.3 Avrami exponent ' n '

The exponent ' n ' is usually termed as the Avrami exponent. The value of n appropriate to systems with invariant nucleation and growth rates is dependent on the geometry of the growth. The n values for specific geometries for either interface or diffusion controlled

growth are summarized in Table 4.1. It is clear from this summary that even using the derived Avrami expression the exponent n does not define a unique nucleation and growth set.

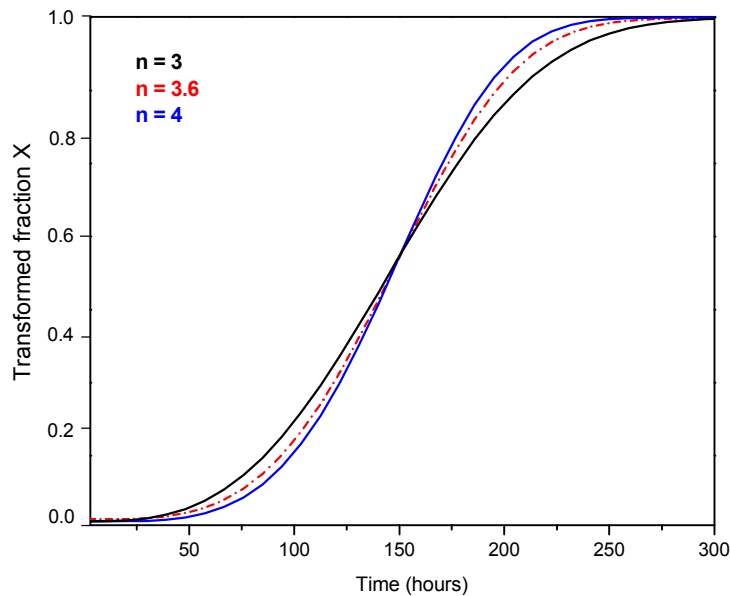


Fig 4.9: Theoretical isotherms based on derived Avrami equation are plotted in Fig.4.8 in accordance with Eq. (4.17) for $n = 3, 3.6$ and 4 .

Figure 4.9 shows the theoretical isotherms based on derived Avrami equation (Eq.4.17) for $n = 3, 3.6$ and 4 . The curves have several important features in common. Their general shape is in accordance with the observations that were described previously i.e. S-shaped. When examined in detail, differences seem to exist that distinguish one curve from another. As n increases from 3 to 4 , the time interval at which transformation is apparent, becomes greater. However, once the transformation develops, the transformation rate becomes greater the higher the value of the exponent n .

All the curves have a common point of intersection at approximately $X = 0.6$. Beyond this point the approach to termination becomes more rapid the larger the value of n . Because of the similarity in shape of the theoretical curves it can be anticipated that in the analysis of experimental data, even when the assumptions made in the derivation are adhered to, it will be a difficult matter to decide between $n = 4$ or 3 . This is particularly true for the early stages of the transformation where the most reliable experimental data are obtained. From purely a mathematical point of view, larger values of n can also be involved. However, the theoretical isotherms for n values of 5 or 6 can scarcely be distinguished by $n = 4$.

Table 4.1. Values of exponent 'n' for various types of nucleation and growth acts⁷⁹

Growth habit	Homogenous nucleation				Heterogeneous nucleation ^a
	Linear growth		Diffusion controlled growth		Linear growth
	Steady state	t = 0 ^b	Steady state	t = 0	
Sheaf-like ^c	6	5	7/2	5/2	5 ≤ n ≤ 6
Three-dimensional	4	3	5/2	3/2	3 ≤ n ≤ 4
Two-dimensional	3	2	2	1	2 ≤ n ≤ 3
One-dimensional	2	1	3/2	1/2	1 ≤ n ≤ 2

^a According to Equation $N = N' \exp(-t)$

^b All nuclei activated at t = 0

^c From L. B. Morgan, Phil. Trans. R. Soc., 247, 13 (1954).

4.6 Time-Temperature Superposition

Once the relevant quantities in the JMAK equation are defined, i.e. the nucleation density, the growth rate and the exponent n as a function of temperature, then the time required to achieve a certain fraction transformed can be calculated. For example, to find the time for a fixed fraction transformed, it can be easily accomplished by manipulation of the basic equation (Eq. 4.17), e.g. for $X = 10\%$.

$$0.1 = 1 - \exp\{-kt^n\} \quad (4.19)$$

$$\Rightarrow -\ln 0.9 = kt^n \quad (4.20)$$

$$\Rightarrow t = \left\{ \frac{-\ln 0.9}{k} \right\}^{\frac{1}{n}} \quad (4.21)$$

Isothermal transformation diagrams also known as time-temperature-transformation or TTT diagrams (see section 5.4 of this thesis as well) are plots of temperature versus time (usually on a logarithmic scale). They are generated from percentage transformation-vs logarithm of time measurements. An isothermal transformation diagram is only valid for one specific composition of material, and only if the temperature is held constant during the transformation, and strictly with rapid cooling to that temperature. Though usually used to represent transformation kinetics for steels, they also can be used to describe the kinetics of crystallization in ceramic materials. Time-temperature-precipitation diagrams and time-

temperature-embrittlement diagrams have also been used to represent kinetic changes in steels.

4.7 Summary of this chapter

In this Chapter the JMAK theory of phase transformation is discussed in detail. Furthermore, a derivation of Avrami equation for the case of continuous nucleation is mentioned, where nuclei are constantly added during transformation. This results in a value of $n = 4$ for the Avrami exponent. Similarly, the value of $n = 3$ is found for the case of site-saturated homogenous nucleation, where all nuclei are present at the start of the transformation (i.e $t = 0$). The hole free volume measured from the PALS and the Tao-Eldrup model, will be used as a measure of the transformed fraction X and the obtained information will be used to discuss the curing kinetics of the one-component epoxy resin formulations, in combination with the JMAK equation. In the next section of this thesis (Chapter 5), the principles of choosing the proper resin and hardener for the formulations are discussed, followed by the results and discussions in Chapter 6, 7 and 8.

5. One-Component Epoxy Resin Formulations

5.1 Epoxy Resins: An Introduction

Epoxy resins are an important class of polymeric materials, characterized by the presence of more than one three-membered ring known as the epoxy, epoxide, oxirane, or ethoxyline group.

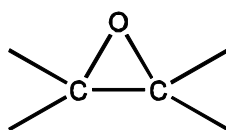


Fig. 5.1: A general schematic showing epoxide group.

The word “epoxy” is derived from the Greek prefix “ep,” which means over and between, and “oxy,” the combining form of oxygen.¹ By strict definition, epoxy resins refer only to non cross-linked monomers or oligomers containing epoxy groups. However, in practice, the term epoxy resin is loosely used to include cured epoxy systems. It should be noted that very high molecular weight epoxy resins and cured epoxy resins contain very little or no epoxide groups. The vast majority of industrially important epoxy resins are bi- or multi-functional epoxides. The mono-functional epoxides are primarily used as reactive diluents, viscosity modifiers, or adhesion promoters. In this chapter the epoxy resins, hardeners, accelerators and fillers used for preparing several one-component epoxy-resin formulations are discussed.

5.1.1 Industrial Applications of Epoxy Resin based formulations

Epoxies are one of the most versatile class of polymers with diverse applications such as metal can coatings, automotive primer, printed circuit boards, semiconductor encapsulants, adhesives, and aerospace composites. Most of the cured epoxy resins provide amorphous thermosets with excellent mechanical strength and toughness; outstanding chemical, moisture, and corrosion resistance; good thermal, adhesive, and electrical properties; no volatiles emission and low shrinkage upon cure; and dimensional stability. The unique combination of these properties is generally not found in any other plastic material. These superior performance characteristics, coupled with outstanding formulating versatility and reasonable costs, have gained epoxy resins wide acceptance as materials of choice for a multitude of bonding, structural, and protective coatings applications.¹

The largest use of epoxy resins is in protective coatings (i.e more than 50%), with the remainder being in structural applications such as printed circuit board (PCB) laminates, semiconductor encapsulants, and structural composites; tooling, molding, and casting; flooring; and adhesives. New, growing applications include lithographic inks and photoresists for the electronics industry.⁸⁴

5.2 Current state of Art and Aim of this work

Commercially available one-component epoxy resin formulations at present, have a curing temperature of 140°C, a storage life of 3.months at ambient conditions and a glass transition of approx. 100°C for the cured network.⁸⁵⁻⁸⁶ The aim of the BMBF project in general was to obtain one-component epoxy resin formulations with a lower hardening temperature (approx.120°C) and higher shelf life for the uncured precursor (e.g. > 6.months) and at the same time a higher glass transition temperature for the cured network i.e. greater than 120°C.

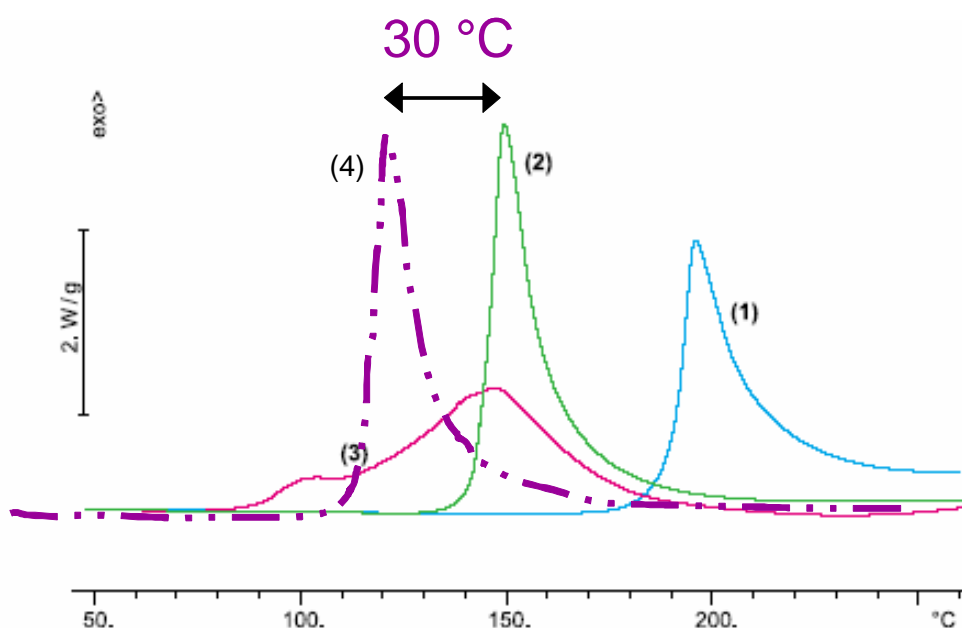


Fig 5.2: DSC curves showing hardening temperatures of different formulations.⁸⁵⁻⁸⁶

Figure 5.2 shows the heat flow with hardening of different Epoxid/Dicyanidamid formulations:

- (1) without accelerator
- (2) with blocked Uron accelerator
- (3) with Imidazol accelerator

(4) with accelerator from multi-functional nano-modules, which as stated earlier was the general motivation for this particular BMBF project.

In particular, the main aim of this work is to characterize epoxy based polymer nano-composites, primarily with PALS technique for both precursor and cured systems. The results which will be discussed in Chapters 6, 7 and 8 of this thesis, proved really important to understand on one hand the curing kinetics of epoxy precursors and on the other the release behaviour of accelerator(encapsulated in micro and nano sized carriers), in the epoxy-hardener matrix.

5.3 Basic principles of formulation

The capability of the highly strained epoxy ring to react with a wide variety of curing agents under diverse conditions and temperatures gives additional versatility to the epoxies. The major industrial utility of epoxy resins is in thermosetting applications. Treatment with curing agents gives insoluble and intractable thermoset polymers.

The most important step in using epoxy resins is to develop the appropriate epoxy formulation since most of them are used as precursors for a three-dimensional cross-linked network. With the exception of the very high M_w phenoxy resins and the epoxy based thermoplastics, epoxy resins are rarely used by themselves. It is usually formulated with modifiers such as fillers and used in composite structures with glass fiber or metal substrates (for coatings). To design a successful epoxy formulation that will give optimum processability and performance, the following factors must be carefully considered:

- Selection of the proper combination of epoxy resins and structures of curing agents.
- Stoichiometric ratio of epoxy and the curing agent.
- Selection of catalyst or accelerator.
- Curing/post-curing processes and conditions.
- Formulation modifiers such as fillers, diluents, toughening agents, etc
- Interactions among the formulation ingredients and with the composite materials (e.g. fibers, metals) on the system chemistry, adhesion, rheology, morphology, and performance.

In order to facilitate processing and to modify cured resin properties, other constituents may be included in the compositions, such as solvents, diluents, plasticizers and tougheners. The development of an epoxy formulation containing a high number of components can be very resource and time-consuming. Techniques such as design of experiments (DOE) are useful tools to facilitate the formulation development process and to obtain optimum performance.⁸⁷ Future developments should include application of high throughput techniques to epoxy formulation development and optimization.

5.3.1 Epoxy resins

Commercial epoxy resins contain aliphatic, cycloaliphatic, or aromatic backbones and are available in a wide range of molecular weights from several hundreds to tens of thousands. The most widely used epoxies are the glycidyl ether derivatives of bisphenol A.⁸⁸ Most commercially important epoxy resins are prepared by the coupling reaction of compounds containing at least two active hydrogen atoms with epichlorohydrin followed by dehydrohalogenation:

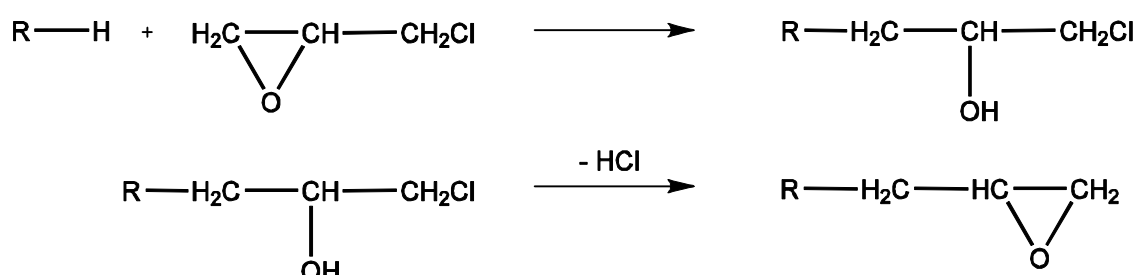


Fig 5.3: Reaction schematic of epichlorohydrin and formation of an epoxy resin.

Table 5.1 U.S. Average Epoxy Resin Prices and Applications (2000)⁸⁹

Resin	\$/kg	Applications
Liquid epoxy resins (Diglycidyl ether of bisphenol A, DGEBA)	2.2	Coatings, castings, tooling, flooring, adhesives, composites
Solid epoxy resins (SER)	2.4	Powder coating; epoxy esters for coatings; can, drum, and maintenance coatings
Bisphenol F epoxy	4.4	Coatings
Multifunctional		
Phenol epoxy novolac	4.8	Castings, coatings, laminates
Cresol epoxy novolac	8.8	Electronics encapsulants, powder coatings, laminates
Other multifunctional epoxies	11-44	Composites, adhesives, laminates, electronics
Cycloaliphatic epoxies	6.6	Electrical castings, coatings, electronics
Brominated epoxies	3.3-5.5	Printed wiring boards, composites
Epoxy vinyl esters	3.3	Composites
Phenoxy resins	11-17	Coatings, laminates, glass sizing
Epoxy diluents	4-11	

These include polyphenolic compounds, mono and diamines, amino phenols, heterocyclic imides and amides, aliphatic diols and polyols, and dimeric fatty acids. Epoxy resins derived from epichlorohydrin are termed glycidyl-based resins. Approximately 75% of the epoxy resins currently used worldwide, are derived from DGEBA.⁸⁹ This market dominance of Bisphenol A based epoxy resins is a result of a combination of their relatively low cost and adequate-to-superior performance in many applications

5.3.1.1 Diglycidyl ether of bisphenol A (DGEBA)

The most important intermediate in epoxy resin technology is the reaction product of epichlorohydrin and Bisphenol A. It is often referred to in the industry as liquid epoxy resin (LER), which can be described as the crude DGEBA where the degree of polymerization, n , is very low ($n \approx 0.2$):

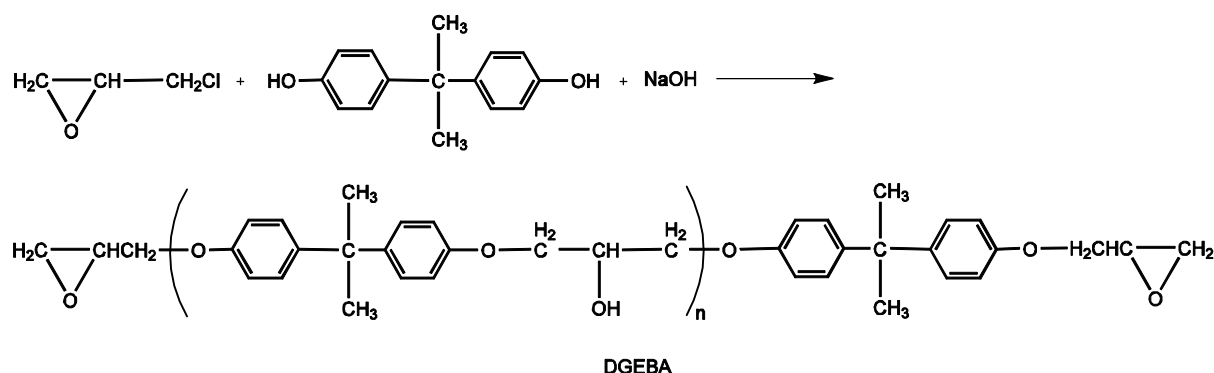


Fig. 5.4: The reaction schematic of Epichlorohydrin and Bisphenol A, leading to formation of DGEBA.

Pure DGEBA is a crystalline solid (mp 43°C) with an epoxide equivalent weight (EEW) of 170. The typical commercial unmodified liquid resins are viscous liquids with viscosities of 11,000–16,000 MPa·s (= cP) at 25°C, and an epoxide equivalent weight of ca 188. They are supercooled liquids with the potential for crystallization, depending on purity and storage conditions. This causes handling problems, particularly for ambient cure applications. Addition of certain reactive diluents and fillers can either accelerate or retard crystallization. Crystallization-resistant, modified resins are available. A crystallized resin can be restored to its liquid form by warming.

The outstanding performance characteristics of the resins are conveyed by the Bisphenol A fraction i.e. toughness, rigidity, and elevated temperature performance, the ether linkages which leads to the chemical resistance, and the hydroxyl and epoxy groups which are

responsible for the adhesive properties and formulation latitude, and reactivity with a wide variety of chemical curing agents.⁸⁹

Table 5.2 DGEBA-Based Epoxy Resins⁸⁹

Resin type	n value ^a	EEW	Mettler softening point, °C	Molecular weight (M_w) ^b	Viscosity at 25°C, MPa.s(=cP)
Low viscosity LER	<0.1	172-176		~350	4,000-6,000
Medium viscosity LER	~0.1	176-185		~370	7,000-10,000
Standard grade LER	~0.2	185-195		~380	11,000-16,000
Type 1 SER	~2	450-560	70-85	~1,500	160-250 ^c
Type 4 SER	~5	800-950	95-110	~3,000	450-600 ^c
Type 7 SER	~15	1,600-2,500	120-140	~10,000	1,500-3,000 ^c
Type 9 SER	~25	2,500-4,000	145-160	~15,000	3,500-10,000 ^c
Type 10 SER	~35	4,000-6,000	150-180	~20,000	10,000-40,000 ^c
Phenoxy resin	~100	>20,000	>200	>40,000	

^a n value is the number-average degree of polymerization which approximates the repeating units and the hydroxyl functionality of the resin.

^bMolecular weight is weight average (M_w) measured by gel-permeation chromatography (GPC) using polystyrene standard.

^cViscosity of SERs is determined by kinematic method using 40% solids in diethylene glycol monobutyl ether solution.

The bisphenol A derived epoxy resins are most frequently cured with anhydrides, aliphatic amines, phenolics, or polyamides, depending on desired end properties. Some of the outstanding properties are superior electrical properties, chemical resistance, heat resistance, and adhesion. Cured Liquid Epoxy Resins (LERs) give tight cross-linked networks having good strength and hardness but have limited flexibility and toughness.

5.3.1.2 Bisphenol F Epoxy Resin

The lowest MW member of the phenol novolacs is bisphenol F, which is prepared with a large excess of phenol to formaldehyde. Epoxidation yields a liquid Bisphenol F epoxy resin with a viscosity of 4000–6000 MPa.s (= cP), an EEW of 165, and $n \approx 0.15$.

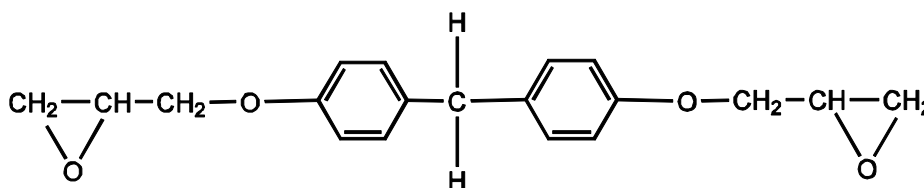


Fig 5.5. Chemical structure showing Diglycidyl ether of Bisphenol F (DGEBF).

This unmodified, low viscosity liquid resin exhibits slightly higher functionality than unmodified bisphenol A liquid resins. Crystallization, often a problem with liquid bisphenol A resins, is reduced with bisphenol F resin. Consequently, noncrystallizing LERs which are blends of DGEBA and Bisphenol F epoxy are available. Epoxy resins based on bisphenol F are used primarily as functional diluents in applications requiring a low viscosity, high performance resin system (eg, solvent-free coatings). Higher filler levels and faster bubble release are possible because of the low viscosity. The higher epoxy content and functionality of Bisphenol F epoxy resins provide improved chemical resistance compared to conventional Bisphenol A epoxies. Bisphenol F epoxy resins are used in high solids, high build systems such as tank and pipe linings, industrial floors, road and bridge deck toppings, structural adhesives, grouts, coatings, and electrical varnishes.⁹⁰

Interestingly, all epoxides contain aromatic rings in their structures. An aromatic ring confers mechanical rigidity and thermal stability to the cross-linked network. It is also worth noting that some of the epoxides in the Tab. 5.2 have two epoxide functional groups, while others have three or four or more. Irrespective of whether a network is developed by mixing the epoxide with a curing agent or is developed from epoxide alone by catalytic homopolymerization, a large number of the molecules in a given formulation must be able to react with more than two other molecules in order to form a cross-linked network instead of merely forming linear chains.⁸⁹ For the sake of clarity, only the experimentally used epoxy resins are discussed in this thesis.

5.3.2 Hardeners (Curing agents)

Epoxide molecules in the pure state at room temperature normally do not react with each other and can stay for years in a dry container without mutual reaction. The types of chemicals added to the epoxide to effect network formation fall into two categories: curing agents and catalysts. Curing agents, sometimes called hardeners, are added in significant amounts (i.e. stoichiometric ratios) to the epoxide and react with it to become a part of the cross-linked network. These curing agents can be aliphatic amines, aromatic amines, or anhydrides. Curing agents are either catalytic or co-reactive. A catalytic curing agent functions as an initiator for epoxy resin homo-polymerization or as an accelerator for other curing agents, whereas the co-reactive curing agent acts as a co-monomer in the polymerization process. The most important groups of co-reactive curing agents are those

with active hydrogen atoms, e.g., primary and secondary amines, phenols, thiols, and carboxylic acids (and their anhydride derivatives). In the following sections, the chemical reactions involved in network formation are discussed. Both when the different curing agents are used i.e. Amine and Anhydride. Since catalytic curing or homo-polymerization are beyond the scope of this work and therefore not discussed here.

5.3.2.1 Amine curing

In amine curing agents, each hydrogen of an amine nitrogen is reactive and can open one epoxide ring to form a covalent bond.⁹¹ When the amine nitrogen contains two hydrogens, each reacts with a different epoxide ring. This scheme is shown in Fig. 5.6, the developing network is evident in this schematic. This scheme applies to both aliphatic and aromatic amine curing agents. The reaction between epoxide and amine produces a C-N bond, whose environmental resistance is good, but whose stability to elevated temperature is highly dependent on the adjacent molecular structure.

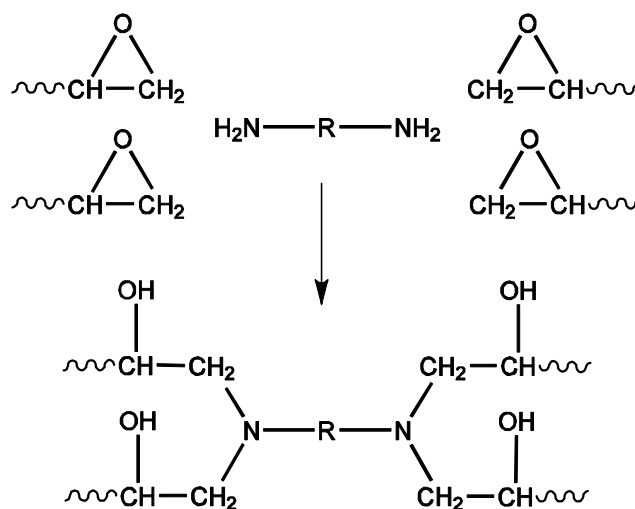


Fig.5.6 Schematic of the reaction between epoxide and an amine curing agent(reconstructed image).⁹²

Each hydrogen reacts with an individual epoxide group. Thus the primary amine group acts bi-functionally and the secondary amine group acts mono-functionally. The epoxide group acts mono-functionally. From the reaction scheme, it is obvious that the correct relative amounts of epoxide and amine curing agent must be used. If there is an imbalance, un-reacted functional groups will be present and the full properties of a complete network will not be attained. The correct amounts for reaction are determined by computing the weight of curing

agent that contains one chemical equivalent of amine hydrogens and matching that with the weight of epoxide that contains one chemical equivalent of epoxide groups.

The temperatures required to achieve cure with amine curing agents fall in a wide range, from 25°C to nearly 200°C, depending on the chemical structure of the amine. The aliphatic amines can cure epoxides at room temperature or only slightly above. Aliphatic amine-cured systems also tend to have low glass transition temperatures, T_g , the temperature at which the mechanical behaviour changes from rigid to rubbery, and cannot be used in composites that will experience high temperature use. Whereas the ring structure of aromatic amines confer solidity and mechanical rigidity. These amine curing agents require elevated temperature cure, but the networks they produce have high glass transition temperatures and are suitable for use in composites that will be exposed to elevated temperatures in service.

5.3.2.1.1 Dicyandiamide (DICY)

Dicyandiamide (DICY) is a solid latent hardener (mp ~208°C). Its latent nature is due to its insolubility in epoxy resins at RT. DICY can be mixed in with epoxy resins to provide a one-package formulation with good stability up to 6 months at ambient temperatures. Cure of epoxies with DICY occurs with heating to 150°C. It is commonly used with accelerators based on tertiary amines, phenol derivatives and imidazoles.⁸⁴ DICY offers the advantage of being latent i.e. it reacts with epoxy resin upon heating and stops reacting temporarily when the heat is removed. This partially cured or “B-staged” state is ideal for prepreg applications. Typically, DICY is used at levels of 5–7 parts per 100 parts of liquid epoxy resins and 3–4 parts per 100 parts of solid epoxy resins.

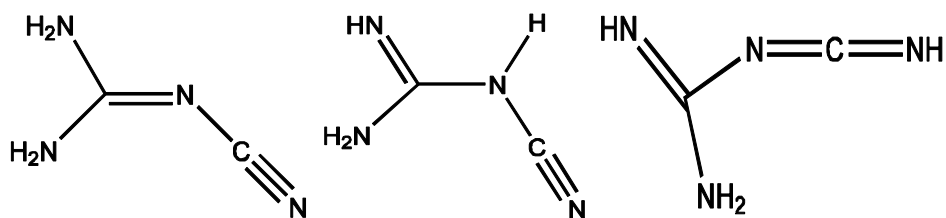


Fig. 5.7: Schematic showing distinct tautomers of Dicyandiamide (DICY).

DICY is one of the first curing agents to be used with epoxy resins. It cures with epoxies to give a highly cross-linked thermoset with good mechanical strength, thermal properties, and chemical resistance, and excellent electrical properties. Because of its latency, low quantity

requirements and excellent balance of properties, DICY is a widely used curing agent in powder coating and electrical laminate applications. These two applications account for 85% of DICY consumption as epoxy curing agent.⁸⁴

To sum up the epoxy–DICY systems offer the following advantages:

- Cost effectiveness (DICY is a low equivalent weight, multifunctional curing agent)
- Stable formulations
- Excellent adhesion to copper and glass
- Good moisture and solder resistance
- Good processability

The primary disadvantage of the standard epoxy–DICY systems is their relatively low thermal performance ($T_g < 140^\circ\text{C}$, $T_d = 300^\circ\text{C}$), which limits their uses in more demanding applications such as the FR-5 boards and other high density circuit boards. Speciality epoxy–DICY systems are available with T_g approaching 190°C , but at higher costs.⁹³

5.3.2.2 Anhydride curing

In anhydride curing agents, the anhydride groups themselves must be cleaved asymmetrically to start the reaction.⁹¹ The initial cleavage, is accomplished with the help of a small amount of accelerator, which is a chemical that functions as a catalyst to speed up the epoxide curing agent reaction. Accelerators will be discussed later in section 5.3.3 of this chapter. Figure 5.8 shows an idealized scheme, where the cleaved anhydride reacts with an epoxide ring carbon, opening the ring in the process. The negatively charged oxygen formed by the opening of the epoxide ring can proceed to react with a different anhydride group, perpetuating the reaction. In this idealized developing network, each anhydride group is bi-functional, i.e. it links to two different epoxide molecules. In practice, the high temperatures required for anhydride cure, plus the presence of accelerator, provides conditions for some extent of epoxide homopolymerization to take place, making the actual curing reaction much more complex than depicted in Fig. 5.8. The reaction between epoxide and anhydride produces primarily ester linkages, which have good stability to elevated temperatures and to most hostile environments except bases.

Not surprisingly, the correct amount of anhydride curing agent relative to the epoxide must be used to obtain a well developed network and the associated good properties. The correct amounts by weight to combine are estimated by examining the reaction scheme and computing the weight of curing agent needed to react completely with a given weight of epoxide.

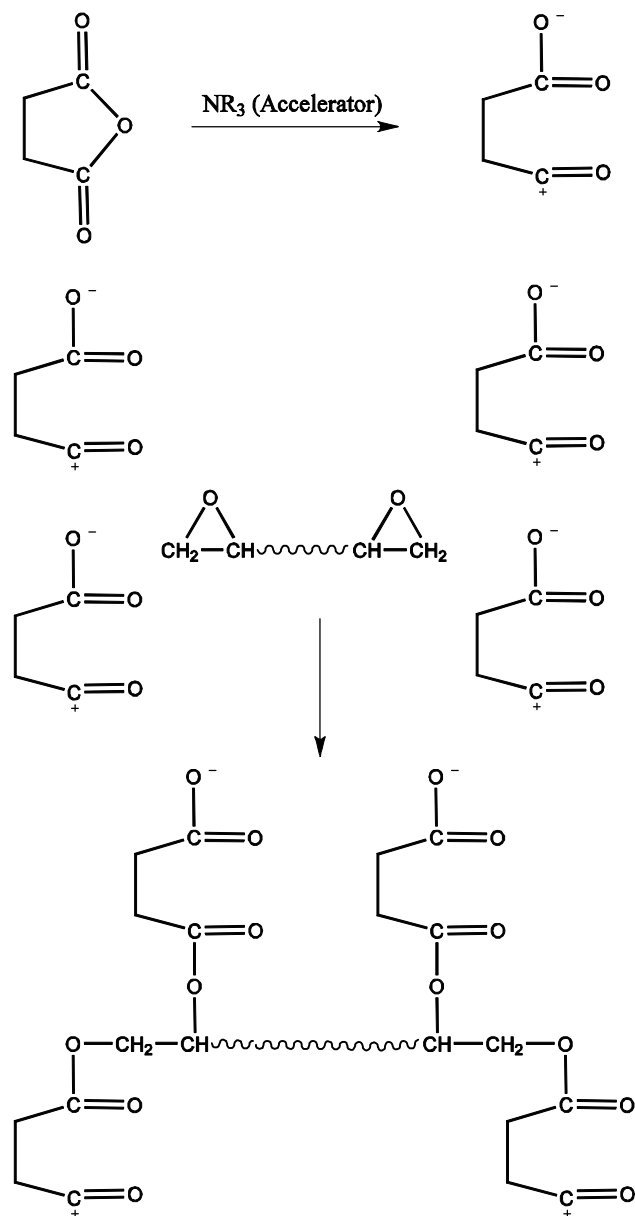


Fig. 5.8 Simplified scheme for the reaction between epoxide and anhydride curing agent(reconstructed image).⁹⁴

The mechanism of anhydride cure is complex and controversial because of the possibility of several competing reactions. The simplified reaction scheme of Fig. 5.8 proposes that one anhydride group reacts with two epoxide groups and one epoxide group reacts with two anhydride groups, making the number of anhydride groups consumed equal to the number of epoxide groups consumed in the reaction. The structures of commonly used anhydride curing

agents vary widely; some are liquid at room temperature whereas others must be heated to liquify. Elevated temperature, typically in the range 100-200°C, is required to achieve cure with anhydride curing agents. The glass transition temperatures of anhydride-cured systems are high.⁹⁴

5.3.2.2.1 Methyl hexahydrophthalic anhydride (MHHPA)

Methylhexahydrophthalic anhydride (MHHPA) is a hardener for hot-cured epoxy resins employed as insulators in the electric industry.⁹⁵ It is produced from methyl tetrahydrophthalic anhydride by catalytic hydrogenation. It is a high-performance product among acid anhydride-type solidifying agents.

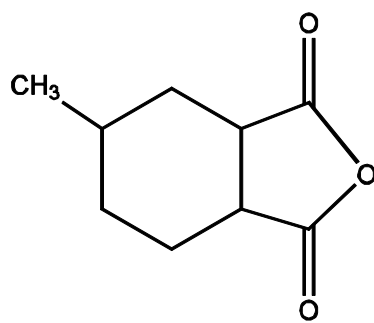


Fig. 5.9: Chemical structure of MHHPA.

MHHPA is heating-solidification type acid anhydride solidifying agent, mainly used in electrical and electronic field, with low melting point, the compounding matter with alicyclic epoxy resin is of low viscosity, long use life, excellent heat resistance and high-temperature electric properties, can be used in dipping of coil of electric apparatus, casting of electric parts and sealing of semiconductor. As an adhesive, the alicyclic epoxy adhesive made from MHHPA has similar refractive index as optical glass, low internal stress after solidifying, high adhesion strength, unchangeable colour, resistance to aging and applications for cohering large-area optical parts.

5.3.3 Accelerators

Accelerators are commonly added to epoxy systems to speed up curing. This term should be used to describe compounds which increase the rate of catalyzed reactions but which by themselves are not catalysts. However, the term accelerator is often used synonymously with catalyst in some of the literature. Accelerators for dicyandiamide cured epoxy adhesive

formulations include tertiary amines, modified aliphatic amines, imidiazoles, and substituted ureas. All except the substituted ureas can cure epoxy resins by themselves. All these materials provide good latency and excellent adhesive applications. Probably the most effective accelerator for dicyandiamide systems is the substituted ureas because of their synergistic contribution to the performance properties of the adhesive and their exceptionally good latency. It has been shown that adding 10 pph of a substituted urea to 10 pph of dicyandiamide will produce an adhesive system for liquid DGEBA epoxy resins that can cure in only 90 min at 110°C. Yet this adhesive will exhibit a shelf life of 3 to 6 weeks at room temperature.⁸⁹ Cures can be achieved at temperature even down to 60°C if longer cure times are acceptable and as discussed in Chapter 8 of this thesis, several epoxy-resin formulations will be in-situ cured at this temperature to study the curing kinetics and with the help of this data the shelf life at room temperatures is extrapolated for selected systems.

5.3.4 Fillers

Fillers are incorporated in epoxy formulations to enhance or obtain specific desired properties in a system. The type and amount of filler used are determined by the specific properties desired. Fillers can also reduce the cost of epoxy formulations. Inert commercial fillers can be organic or inorganic, and spheroidal, granular, fibrous, or lamellar in shape. Some formulations contain up to 90 wt% fillers. For certain applications, fillers can have significant effects on thermoset morphology, adhesion, and the resulting performance. Fillers can increase pot life and lower exotherm of epoxy systems, they also help to increase thermal shock resistance and to decrease the thermal expansion coefficient of an epoxy system by replacing part of the resin with a material that does not change its volume significantly with temperature variations. Using fillers as a partial replacement for a reactive resin that shrinks on curing can reduce shrinkage of the system. The addition of fillers can increase the machinability and abrasion resistance of an epoxy resin system by increasing the hardness of the thermoset. In certain applications, conducting fillers are added to epoxy formulations to reduce the good insulating properties of the epoxy systems.

5.3.5 Micro and Nano-Encapsulation of Accelerators

A significant amount of development is currently occurring relative to latent catalysts because of interest in their long shelf life, high reactivity, and single-component adhesive formulations. Present technologies involve absorption of acidic or basic catalysts in molecular

sieves, formation of Lewis acid salts or other amine salts, micro-encapsulation of amines, and other novel segregation methods. As will be shown in the results section of this thesis (Chapters 7 and 8), the accelerator used throughout this work is encapsulated in micro and nano-size carriers. But both the accelerator and the carrier used for encapsulation will be treated as classified information, due to the non-disclosure agreements concerning this research.

5.4 Epoxy curing process and TTT diagram

The thermosetting or the curing reaction is the joining of many small molecules by chemical reaction to produce an extended network structure. Although this process is a polymerization, it is distinct from the type of polymerization that forms many individual long chains. The thermosetting reaction unifies all the constituent monomers into a single large molecule extending to the boundaries of the material. Since the epoxy curing process is an important factor affecting the cured epoxy performance. Therefore, it is important to understand the curing process and its kinetics to design the proper cure schedule to obtain optimum structure and performance. Excellent reviews on this topic are available in the literature.⁹⁶

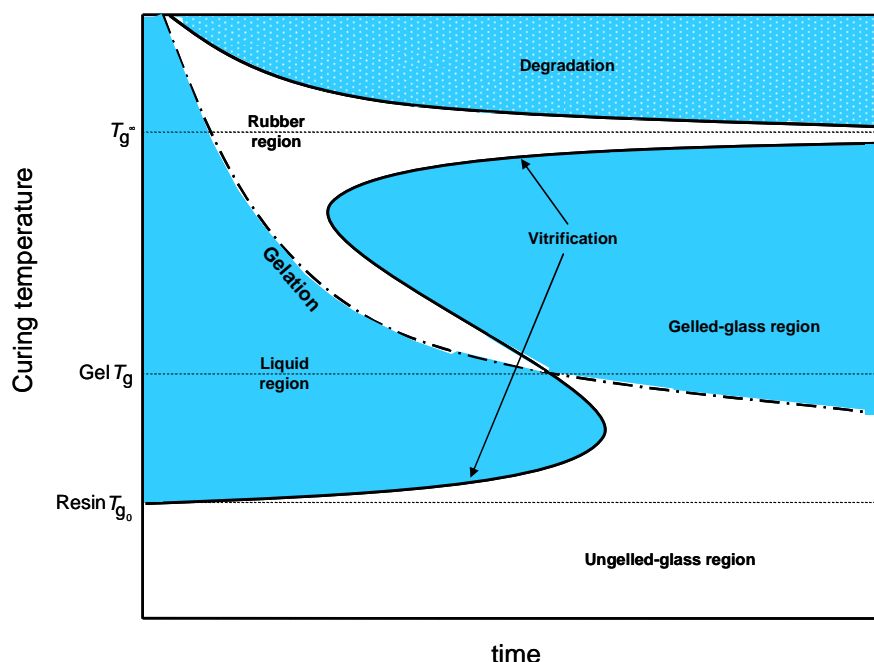


Fig 5.10 : A general schematic of the time-temperature-transformation (TTT diagram) for epoxies(reconstructed image).⁹⁷⁻⁹⁸

The curing of a thermoset epoxy resin can be expressed in terms of a time-temperature-transformation (TTT) diagram as shown in Fig (5.10).⁹⁷⁻⁹⁸ In the TTT diagram, the time to

gelation and vitrification is plotted as a function of isothermal cure temperature. Important features are the gel point and the onset of vitrification. The gel point is defined as the onset of the formation of insoluble, cross-linked polymer i.e. gel fraction in the reaction mixture. However, a portion of the sample may still be soluble i.e. sol fraction. The onset of vitrification is when the glass-transition temperature (T_g) of the curing sample approaches the curing temperature T_c . Ideally, a useful structural thermoset would cure until all monomers are built into the network, resulting in no soluble fraction.

The S-shaped *vitrification curve* and the *gelation curve* divide the time-temperature plot into four distinct states of the thermosetting-cure process i.e. the liquid, gelled rubber, un-gelled glass and the gelled glass. T_g^0 is the glass transition temperature of the unreacted resin mixture; T_g^∞ the glass transition temperature of the unreacted resin mixture and T_g is the point where the vitrification and gelation curves intersect. Post-cure with heat is often required for certain formulations, to release some of the internal stresses and to improve adhesion. However, it must be noted that at temperatures sufficiently above T_g^∞ , onset of network degradation can also be seen if sufficient time is involved, thus one must be careful about potential *over-curing*.

One important application is the management of cure temperatures (T_c) and heating rate i.e. if T is too low, vitrification may occur before gelation and further reactions may not be completed, resulting in an incomplete network structure and poor performance. Furthermore, attention must be paid to the relationship between mixing of reactants and gel point. Epoxy resins and curing agents must be thoroughly mixed prior to the gel point since the rapid viscosity build-up at gel point inhibits homogeneous mixing of reactants, resulting in potential network and morphological in-homogeneities and defects.⁹⁹

5.5 Characterization of Epoxy curing and cured epoxy networks

The TTT diagram is useful in understanding the cure kinetics, conversion, gelation, and vitrification of the curing thermoset. Some techniques have been developed using rheological and dynamic mechanical analysis instruments to determine the gel point and vitrification.¹⁰⁰⁻

¹⁰¹ Understanding the gelation and vitrification characteristics of an epoxy in combination with the curing agent system is critical in developing the proper cure schedule and process to achieve optimum performance.

The degree of cure can be defined in terms of any one of a large number of chemical or physical (including mechanical) properties that change continuously during the curing reaction and reach a constant value at end of the cure. Evaluation of the degree of cure is usually based on one of these properties and full cure is then defined as the point at which this selected property reaches a constant value.

5.5.1 Traditional off-line methods

Intermittent off-line methods include chemical titration of the unreacted epoxide groups present,¹⁰² specific gravity to measure densification¹⁰³ and differential scanning calorimetry (DSC) to measure the residual cure exotherm.¹⁰⁴ Continuous off-line methods include infrared spectroscopy (IR),¹⁰⁵ parallel plate-type bulk dielectrometry¹⁰⁶ and dynamic mechanical analysis (DMA).⁹⁷ The off-line methods, real time or not, are useful for developing a cure schedule for a new epoxy resin formulation, for optimizing processing variables and for quality control of incoming resins or prepregs. They have also been used successfully for the development of mathematical models of cure kinetics. However, because they are off-line, they cannot be used for process control.

5.5.2 Modern in-situ methods

In-situ methods for cure monitoring are real time methods that require sensors small enough to implant and leave in the composite itself. When the information from in situ monitoring is used as continuous input to an appropriate process model, it can be used in process control loops that adjust the processing conditions automatically.

One example of an in-situ method is low frequency dielectrometry using a very small assembly of inter-digitated electrodes called a fringe field sensor. This technique measures changes in ability of permanent dipoles within the resin chemical structure to align themselves with the applied oscillating electric field and also measures changes in the mobility of ions present as impurities in the resin.¹⁰⁷ Both of these quantities correlate with resin viscosity in the early stages of cure and with mechanical rigidity in the later stages of cure.¹⁰⁸

Other examples of in-situ monitoring are based on fluorescence spectroscopy of tag molecules in the resin¹⁰⁹ and on infrared¹¹⁰ and Raman¹¹¹ spectroscopies of the resin molecules

themselves. In these methods, optical fibres are the sensors that transmit the appropriate wavelength of light into the curing resin and also transmit the spectral information back out.¹¹² The spectral changes relate directly to the chemical changes that occur as the curing reaction progresses to completion.

5.6 Summary of this Chapter

Positron annihilation lifetime spectroscopy (PALS) is another addition to the in-situ curing measurement techniques, as already discussed in detail in Chapter 2 of this thesis. Although, this technique has been already used to characterize the cured epoxy composites in past. But in this thesis it will be shown that how Johnson-Mehl-Avrami-Kolmogorov (JMAK) or Avrami equation (discussed in Chapter 4) can be used to fit the experimental data observed from PALS and the obtained Avrami parameters gives us information about the curing kinetics of one-component epoxy resin formulations.

6. Shelf life of one-component epoxy-resin formulation

In this section the first results of the state of art benchmark system are discussed, please note that these results are already published.¹¹³ It is shown how PALS can be used to study the curing behavior of epoxy resins of DGEBA with a hardener of dicyandiamide, from the initial viscous state of the formulation to the cured polymer. Isothermal measurements are done in range from 50°C to 80°C, in steps of 10°C. Onset of gelation is indicated by an increase in the *ortho*-positronium (*o*-Ps) intensity and a sharp decrease in the lifetime. Change of *o*-Ps lifetime was used as a measure for the degree of curing i.e. the transformed fraction X . Applying the Johnson-Mehl-Avrami-Kolmogorov approach, these changes can be characterized and the growth exponent ' n ' and the reaction constant ' k ' are determined. Furthermore, the shelf life of this one component epoxy formulation is extrapolated to room temperature with the help of Avrami parameters.

6.1 Introduction

There are numerous choices of epoxy resins and curing agents, presenting a wide variety of structure and functionality. These details are already discussed in Chapter 5, but for the sake of clarity the following sequence of sub-sections will help the reader to understand the link between the curing of one-component epoxy resin formulations and the JMAK theory of curing kinetics, where the transformed fraction is followed by the sub-nanometer level hole free volume measured from the PALS technique.

6.1.1 One-component formulation

The one-component epoxy resin formulation used here is based on the diglycidyl ether of Bisphenol-A (DGEBA), which is cured with Dicyandiamide (DICY). Curing of epoxies with DICY occurs only while heating to temperatures at least 150°C. DICY may react with epoxy resin upon heating and stops reacting temporarily when the heat is removed. The resulting partially cured or "B-staged" state is ideal for prepreg applications.⁸⁴ Typically, DICY is used at levels of 5–7 parts per 100 parts of liquid epoxy resins and 3-4 parts per 100 parts of solid epoxy resins by weight. In order to achieve low temperature curing a block Uron (U500) accelerator is also used.

6.1.2 Shelf-life and the curing mechanism

The epoxy curing process is an important factor affecting the cured epoxy performance. As stated in the earlier Chapters of this thesis, to obtain optimum network structure and performance, it is imperative to understand the curing process and its kinetics to design the proper cure schedule. A good number of reviews on this topic are already available in the literature.^{96,114} However, from the industrial point of view it is still of utmost relevance, to establish reliable means of experimentally predicting the shelf life of new formulations of one-component epoxies, which is usually guessed from accelerated tests at elevated temperatures relying on selected reference measurements. In order to achieve predictability it is important to understand the complete curing mechanism of epoxies, so that the reaction kinetics can be further elaborated in light of available standard models and further extrapolated to shelf life at storage temperatures.

The curing mechanism of DGEBA/DICY and similar systems is rather complex, involving several simultaneous reactions. There are a number of different mechanisms proposed in the literature.¹¹⁵⁻¹¹⁶ Indirect estimation of cure conversion as a function of time is done with a combination of several experimental techniques and the available theoretical models. This work is one step ahead and proposes the use of PALS in combination with the JMAK theory of transformation kinetics.

6.1.3 Transformed fraction and the JMAK theory

As already discussed in the Chapter 4 of this thesis, the Avrami equation, is a widely accepted model to study phase transformations, e.g. crystallization or austenite-to-martensite transformations.⁷⁷ According to this equation¹¹⁷ (Eq. 4.17, Section 4.5.2 of this thesis), for solid-state transformations displaying the kinetic behavior, the fraction of transformation X is a function of time t .¹¹⁷ Where, ' n ' is termed as the Avrami exponent, which is characteristic for the type of transformation e.g. diffusion or reaction controlled, quenched in nuclei or random nucleation or the shape of the particles of the new phase, The constant ' k ' is named the reaction constant, which is in turn temperature dependent, often via a simple Arrhenius law. In such cases, by performing several isothermal experiments at different temperatures, the activation energy E_a of the rate determining step can be extracted by plotting the reaction constant ' k ' on a logarithmic scale as a function of the reciprocal temperature.

Assuming that the type of reaction and the rate determining step do not change with temperature (i.e. the exponent ' n ' stays constant for different temperatures), the Avrami equation can be used to extrapolate the transformation behavior to other temperatures at least in the early stages of transformation, i.e. for transformed fractions $X \leq 0.5$. The boundary conditions underlying the Avrami equation are not fulfilled for the larger fractions. The basic idea of this research is to apply this model to the curing of the epoxide system, i.e. the nucleation period of crystallization is attributed to the initial period of reaction and the diffusional part to the proceeding of the reaction until saturation is reached. This is in contrast to usual reaction kinetic models, which are of first or second order and do not include any incubation time.

Isothermal and non-isothermal curing behaviors of epoxy resins have already been studied in the light of the Avrami equation in past,¹¹⁸⁻¹²² but only for high curing temperatures and neither the growth exponent nor the reaction constant has been interpreted or extrapolated to the storage temperatures. However, this is of major importance for predicting storage stability of the one component formulations at room temperature.

6.1.4 Free Volume and PALS

It is generally accepted that a key property for all amorphous polymers is the available microscopic free volume, which can be detected by several atomic probes and described by molecular dynamic simulations. Positron Annihilation Lifetime Spectroscopy (PALS) is a widely accepted experimental tool to characterize the free volume in amorphous polymers^{12,123-125} and has been used for epoxy resins¹²⁶ and epoxy based polymers as well.^{44,127-128} For details of PALS technique please refer to the Chapter 2 of this thesis.

In order to apply PALS parameters in combination with the JMAK equation to the curing kinetics, several boundary conditions need to be fulfilled. Firstly, it is possible to correlate the PALS parameters (i.e. o -Ps lifetime and intensity) and the cured or the transformed fraction X . Since there is a good correlation between the shrinkage of epoxy during curing,¹²⁸ with the changes in macroscopic volume measured by Pressure-Volume-Temperature measurements (PVT)) and the microscopic free volume measured by PALS. Secondly, in order to make a reliable extrapolation from the experimentally covered temperature range it is necessary that the reaction pathway does not change with temperature. If the growth exponent ' n ' is found to

be independent of temperature, this indicates that the reaction mechanism remains the same in the observed temperature interval. Both conditions are fulfilled here and will be discussed later in Section 6.3.2.

6.2 Experimental

Dicyandiamide (DICY, Dyhard DF 50 EP within an epoxy-based paste used as curing agent, and blocked Urone accelerator (Dyhard UR 500) were supplied by Degussa Evonik GmbH and AlzChem, Diglycidyl ether of bisphenol-A (DGEBA, Araldite GY 250, with epoxy equivalent weight EEW = 187 g/mol) was obtained from Huntsman. For this particular epoxy-hardener pair the mass ratio is approximately seven parts of DICY hardener, in equivalent weight, per hundred parts of resin, i.e., 7 phr. The applied formulation is similar to the one of published technical systems.¹²⁹ Basic chemical structures of DGEBA(as in Fig. 5.4), DICY(as in Fig. 5.7) and Dyhard UR500 are shown in Fig.6.1.

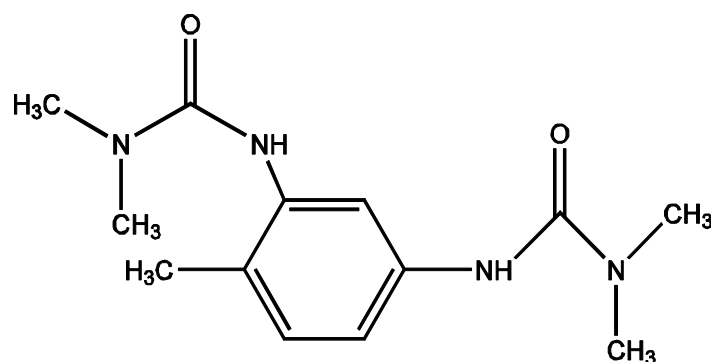


Fig. 6.1: Chemical structures of Dyhard UR500 acclerator.

Positron annihilation lifetime experiments were performed with a fast-fast coincidence setup under high vacuum conditions as described in the Section 2.4.1 of this thesis. The time resolution was 285 ps (FWHM, ²²Na source) and the analyzer channel width was 25.3 ps. The resin, hardener and accelerator are thoroughly mixed at room temperature and after approximately one hour of preparation two identical samples of precursor were sandwiched around a ~1 MBq positron source, prepared by depositing ²²NaCl, between two 7µm-thick Kapton foils.

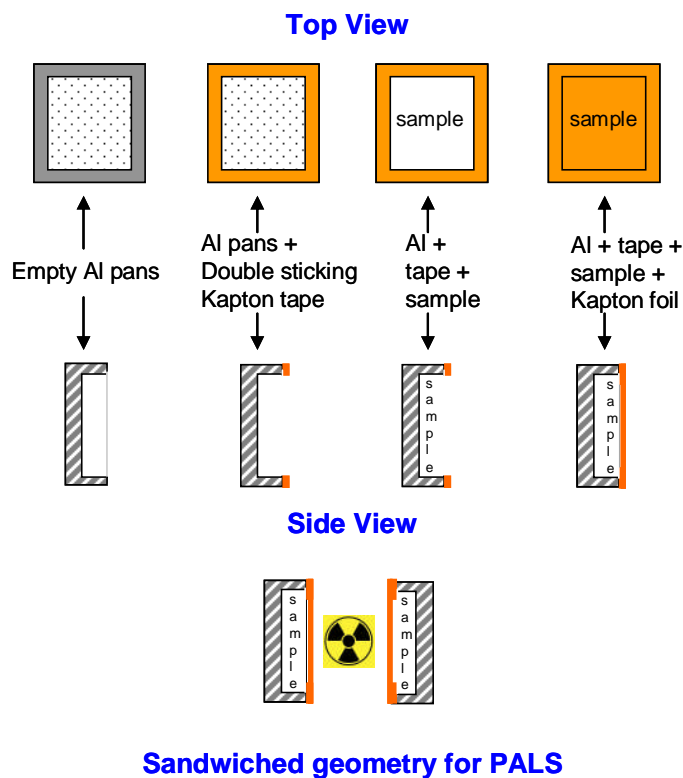


Fig. 6.2. Two identical samples sandwiched around ^{22}Na , for PALS measurement.

To prevent sticking of the source to the samples, each sample was held in an aluminum container of 1 mm width and $8 \times 8 \text{ mm}^2$ area with a window made of foils of $25 \mu\text{m}$ -thick Kapton. Fig. 6.2, shows as an example the general schematic of the sample preparation for measurement with PALS. Several isothermal scans are performed at 50°C , 60°C , 70°C and 80°C (accuracy of $\pm 1 \text{ K}$), for different sets of samples. For each sample the first spectrum was always measured at room temperature (RT) followed by an isothermal run for several hours, at the indicated temperatures. Each measurement lasted 3 hours leading to a lifetime spectrum with a high number of annihilation events ($\sim 5 \times 10^6$).

6.3 Results and Discussions

6.3.1 Analysis of Lifetime Spectra

As already explained in Chapter 2 of this thesis, five million counts per spectrum were necessary to analyze the spectrum with the routine LT9.0 in its distribution mode in order to take into account the distribution of free volume size. The final resolution function used in the spectrum analysis is determined as a sum of two Gaussian curves. The lifetime spectra are deconvoluted into three components: $\tau_1 = 0.15\text{-}0.25 \text{ ps}$, $\tau_2 = 0.45\text{-}0.60 \text{ ns}$ and $\tau_3 = 1.9\text{-}2.6 \text{ ns}$.

Here, τ_1 is the shortest lifetime component, which is attributed to the annihilation of *para*-positronium (*p*-Ps). The intermediate lifetime component τ_2 is attributed to annihilation of *free*-positrons (e^+) and the component τ_3 is attributed to the *ortho*-positronium (*o*-Ps). This is the relevant quantity for the free volume and for the investigation of curing here.

Figure 6.3 shows the most important results obtained from the PALS technique i.e. τ_3 and the I_3 . The plateau of the *o*-Ps lifetime τ_3 observed in the early stages of the lower temperature investigations shows that the mixture is still in its precursor state. The following sharp decrease in *o*-Ps lifetime indicates that the curing sets in. Finally, the cured state is achieved, which is indicated by reaching the saturation limit. One should note that in the course of the process τ_3 is decreasing, reflecting a decrease in hole size, as expected for shrinkage during curing.¹²⁸ The slight reduction in the intensity during curing may be an indication that there are reactive groups inhibiting Ps formation. The half-life of the curing process is also indicated.

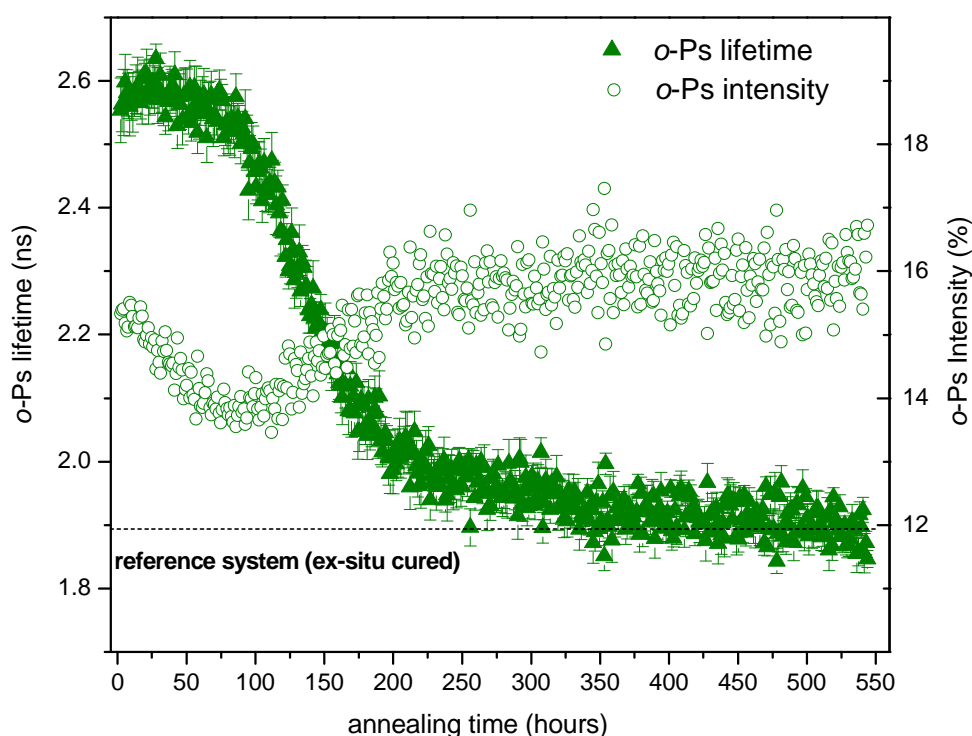


Fig. 6.3: *o*-Ps lifetime, dispersion and intensity as function of curing time at 50 °C. Also shown reference values (ex-situ cured @ 150 °C)

The *o*-Ps lifetime τ_3 as a function of time for different annealing temperatures of 50°C, 60°C, 70°C and 80°C are indicated in Fig. 6.4. It can be observed that the curing time of one-component epoxy resin systems is temperature dependent i.e. the lower the temperature, the longer is the time required for similar stage of curing. The curing times as measured by PALS for the complete temperature range are summed up in Table 6.1. From this table it is also obvious that the higher the curing temperature, the higher the initial τ_0 as expected due to thermal expansion. Please note that the final τ_{∞} is similar for all samples and in the same range as for an externally high temperature cured sample.

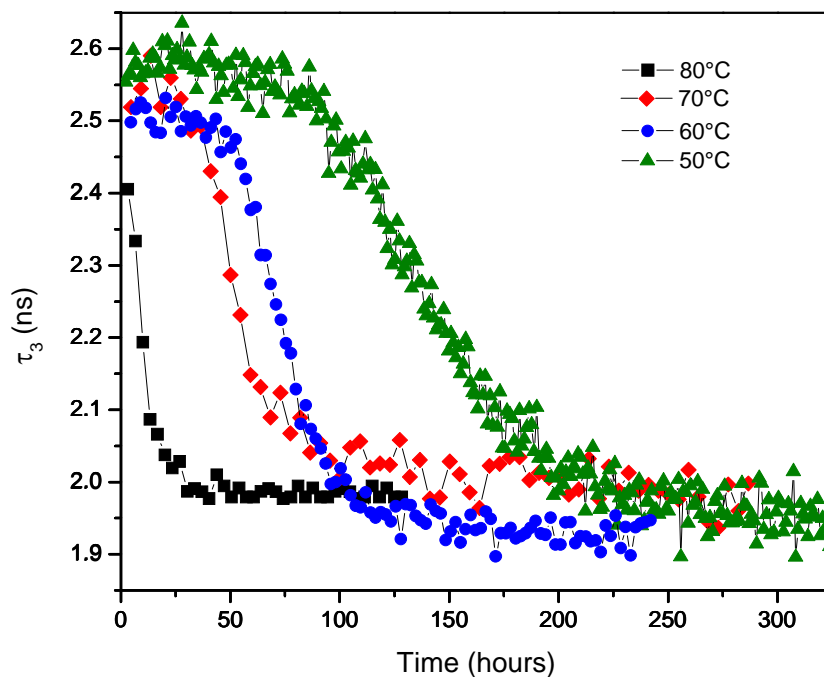


Fig 6.4: The *o*-Ps lifetime as a function of curing time for Epoxy/DICY precursors at 50°C, 60°C, 70°C and 80°C, respectively. Lines between the data points are used as a guide for the eyes.

6.3.2 Curing Kinetics and Avrami equation

As already discussed in the Section 6.1.3, the *o*-Ps lifetime τ_3 is a measure for the degree of transformation X , i.e. the extent of curing. Hence, it is derived from the PALS data;

$$X = \frac{\tau - \tau_0}{\tau_{\infty} - \tau_0} \quad \text{Eq (6.1)}$$

Where τ_0 is the *o*-Ps lifetime of the uncured sample and τ_∞ is the *o*-Ps lifetime of the fully cured sample (see table 6.1). The Avrami approach is limited to a finite fraction of transformed material, which reflects the boundary condition of undisturbed growth of the cross-linked phase being generated. In order to use the appropriate range for fitting to the data for the determination of the Avrami parameter these data are first plotted according to the double logarithmic equation (Eq. 4.18 in Section 4.5.2) and for the sake of clarity only the results of the sample measured at 60°C are shown in Fig. 6.5.

Table 6.1: Calculated Avrami parameters and curing times for the complete series.

$T(^{\circ}\text{C})$	τ_0 (ns)	τ_∞ (ns)	$t_{1/2}$ (hours)	n	k
50	2.59	1.90	140.29	3.60	1.18E-08
60	2.53	1.91	73.33	3.63	1.12E-07
70	2.56	1.96	51.70	3.61	3.84E-07
80	2.41	1.98	6.07	3.67	1.89E-06

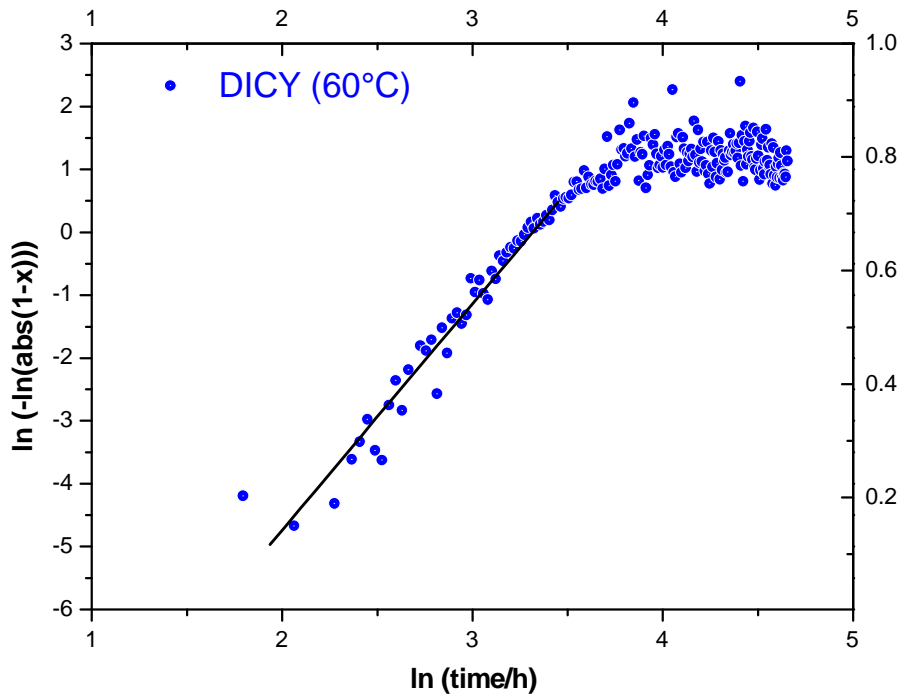


Fig. 6.5: Typical plot of $\ln[-\ln(1-X_i)]$ as a function of $\ln t$, according to Eq. (4.18). The straight line is obtained, where ' n ' is the slope and ' $\ln k$ ' is the intercept is obtained. For clarity reason only the plot of the curing temperature of 60 °C is shown.

As indicated in Fig. 6.5, a straight line was fitted through the linear range. Evaluating the line parameters gives the values of Avrami exponent ' n '. With X_{\max} being the range which yields

a constant value of slope, the value obtained is $n = 3.6$. The maximum for a reasonable fitting range of $X = 0.6$ corresponds to the fact that for more volume transformed, the more nuclei come into contact competing for molecular species to be introduced into the growing polymer grains and the boundary condition of the Avrami equation (undisturbed growth) is not fulfilled any more.

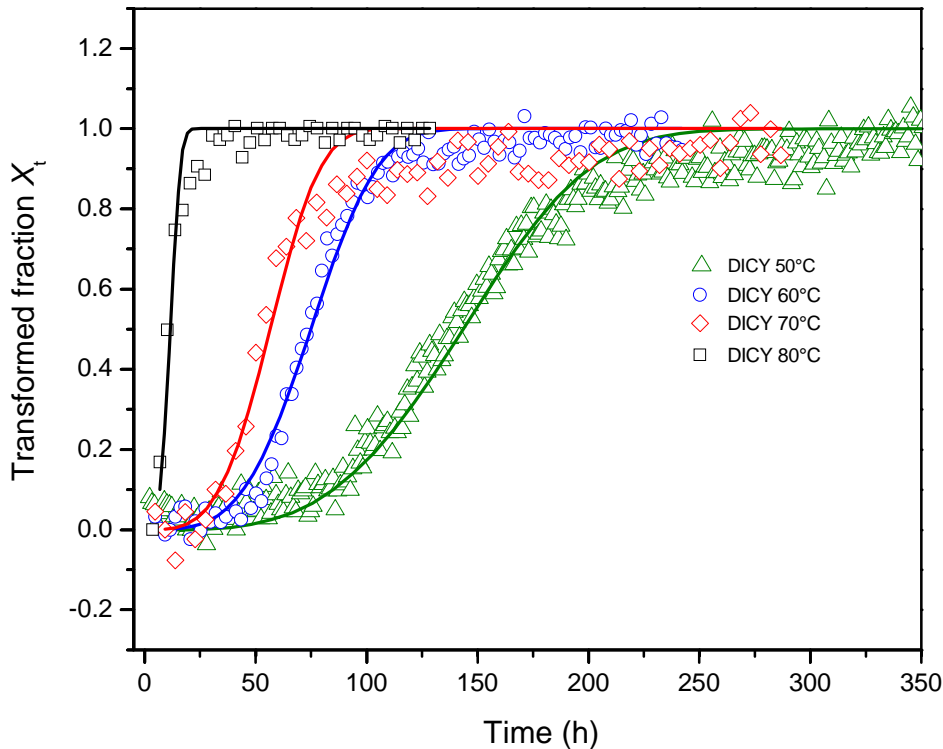


Fig. 6.6: Fit of JMAK kinetics with $n = 3.6$ and appropriate reaction constants to the normalized PALS data. Note the small deviation at higher fractions which is interpreted to be due to the deviations in growth behavior for nuclei/grains in contact.

Figure 6.6 shows as an example the JMAK fits according to Eq. (4.17), to the transformed fraction calculated via Eq. (6.1). In order to take into account the whole set of data, even at the beginning of the experiment, the original data of *o*-Ps lifetime vs. time of storage (see Fig. 6.4) was fitted again with the Eq. (4.17) but only for transformed fraction $X < 0.7$ and with $n = 3.6$ as starting value. In particular for the high temperatures the values for $t = 0$ estimated from room temperature measurements were included in order to get reasonable starting values for τ_0 . For all data measured so far the corresponding parameters are summarized in Table 6.1.

It is found that the growth exponent is always the same within the error margin, indicating that the rate determining step of the curing reaction does not change with temperature, a condition necessary for extrapolation of curing times to lower temperatures. If it is assumed that the crystallization of an amorphous material can be compared with a chemical reaction here (cross-linking of an epoxy from the monomers), then the interpretation from the original derivation can be used. A growth exponent of $n = 4$ has been derived in the original papers under the boundary conditions of random nucleation and diffusional growth, whereas $n = 3$ was derived from quenched in nuclei and diffusional growth.⁷⁷ This is in good accordance with expectations of curing behavior in the present system.

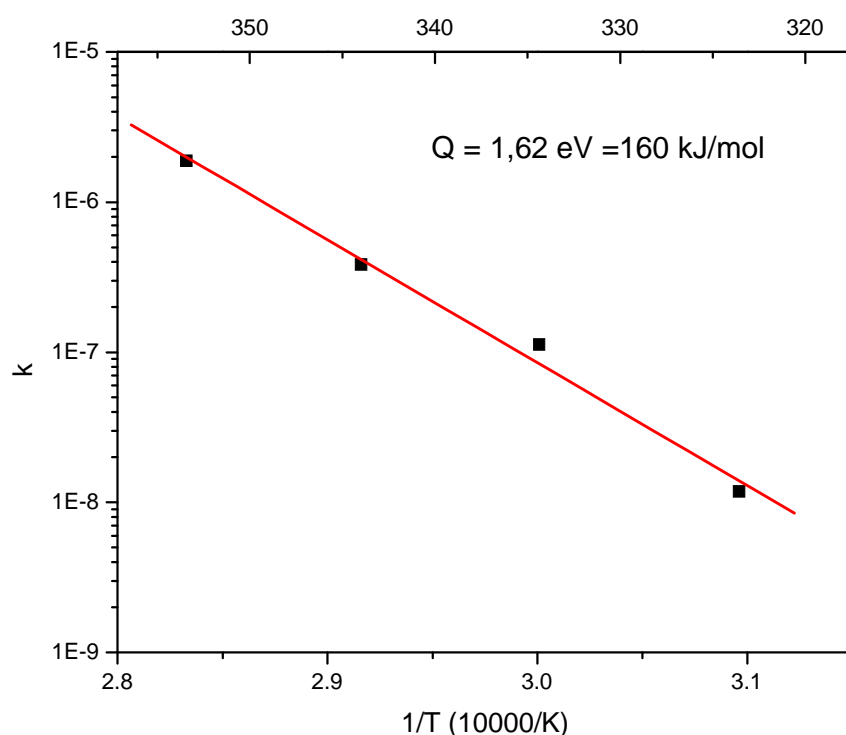


Fig. 6.7: Arrhenius plot of the reaction constant k vs reciprocal temperature demonstrating temperature independent activation energy. It is remarked that k has no reasonable units due to the fractional growth exponent. This plot can be applied for extrapolation of shelf life at a storage temperature of 20 °C or 30 °C.

It may be expected that the random nucleation of cross-linking centers via stimulated nucleation, triggered by action of the accelerator to occur simultaneously. Correspondingly, urone accelerators have been reported to act as initiators of polymerization reactions.¹¹⁶ However, there is not only one molecular mechanism describing the reaction of the urone used in this work. After thermal activation, the comparatively reactive Dyhard® UR 500 accelerator may react in at least three ways. First of all, as an accelerator for the polyaddition

reaction, between DGEBA and DICY. Secondly, as a catalyst for the epoxy homopolymerisation reaction and finally as a curative which is consumed during the polyreaction. The formulation used for the present investigation is not completely optimised with respect to a consumption of all the DICY in the reactive mixture within the curing schedule applied.

Assuming thermally activated behavior, the reaction constant k can reasonably be plotted on a logarithmic scale versus the reciprocal temperature in order to verify an Arrhenius-type activation behavior as shown in Fig. 6.7. The slope directly yields activation energy of approximately 160 kJ/mol. This corresponds to the energy of the rate limiting step of the reaction. This value is distinctly larger than values usually given for the reaction of various epoxides¹³⁰ and the calculated activation energies are termed as model dependent. In this work not only the mere chemical reaction, but also the change in the mobility of molecular species due to increased cross-linking and the transport effects in the system during curing are taken into account.

The chemical reactions occurring during storage at room temperature as compared to curing at temperatures of up to 180°C, it may be expected that according to the latency of the DICY hardener at room temperature its influence on the network forming reaction will increase with increasing temperatures.¹¹⁶ Finally for the present system the shelf life time is extrapolated to storage temperature ($T = 20^\circ\text{C}$) and an upper limit of 850 h ($T = 30^\circ\text{C}$, $t = 500$ h) is estimated, which could be compared to nearly three months (2000 h) of storage of the sample at the same temperature. Hence, the model seems to be useful to give at least lower limits of storage stability.

6.4 Conclusion

PALS have been applied to observe in-situ curing of a typical epoxide with high accuracy and time resolution for the first time. Based on transformed fractions of reactive species calculated from characteristic reference values for *o*-Ps lifetime τ_3 within the reactive system, shrinkage and a decreased molecular mobility within the forming network are monitored, following the chemical reactions limiting the storage stability of the formulations. Applying the Johnson-Mehl-Avrami-Kolmogorov equation to the curing data, appropriate kinetic parameters could be derived. Such proceeding allows extrapolation of the shelf life of one-component epoxy systems at room temperature.

7. Free and encapsulated accelerator formulations

One-component epoxy resin composites are an important class of adhesive materials, especially when it comes to high temperature applications. It is of utmost importance to not only modify the chemical constituents to achieve a higher shelf life of these materials in precursor state, but at the same time making sure that the properties of the cured polymers are not compromised. Even from the product development point of view, it is necessary to study the curing kinetics of these systems and also the characteristic properties of their cured epoxy composites for better understanding and further modification or development. In this section a comparison of IR-spectroscopy and PALS data is presented, which is used to study the effect of free and encapsulated accelerator on the curing times of epoxy precursors at elevated temperature of 60 °C. Furthermore, PALS and differential scanning calorimetry (DSC) are used as the experimental techniques to characterize all together, six different DGEBA–DICY cured epoxy composites. It is remarked that IR-spectroscopy and DSC experiments were performed at the University of Saarland in Saarbrücken and the results are only used for comparison with PALS data.

7.1 Introduction

One-component epoxy resin systems remain the most widely-used adhesives in structural applications,¹³¹ with ease of usage,¹³² good environmental stability,¹³³ and adequate creep resistance.¹³⁴ The storage stability of the one-component epoxy precursors is very important parameter as far as research and development of such formulations is concerned. On one hand a higher shelf life can be obtained by encapsulating the accelerator in a carrier material which delays the reaction with epoxy matrix, increasing the shelf life of one-component epoxy resin formulations and at the same time making sure that hardening temperatures are in acceptable range. But on the other hand, it is also very important not to compromise on the characteristic properties of the cured composites.

Glass-transition temperature T_g , is a critical property of these composites when it comes to high temperature applications. The T_g can change with different combinations of resin, hardener and accelerators and its important to maintain a higher T_g and at the same time having a longer storage life. The properties of epoxy composites are influenced by factors at the molecular level, such as backbone structures of epoxy resin and curing agent; nature of the

covalent bond developed between the epoxy resin and the curing agent during the cross-linking; and the density and the extent of cross-linking i.e. degree of cure.⁸⁹ This class of cured thermosetting polymers are more difficult to analyse as compared to the thermoplastics, as they are insoluble and generally intractable

Free volume is an interesting approach to study not only the precursor state of these epoxies,¹³⁵ but also the T_g and other related properties of their cured composites. In a qualitative sense, free volume may be considered simply as the volume unoccupied by the atomic species of the material. This unoccupied volume has a strong influence on the mobility of segments of polymer molecules, and on the permeability of the polymer to gaseous or liquid penetrants.¹³⁶ The concept of free volume may be considered as rather simplistic in the light of advances in modern polymer physics, but it has the advantage of ease of visualization and, in this particular case, lends itself to quantitative analysis.

Over the past decade Positron annihilation lifetime spectroscopy (PALS) has emerged as one of the entrusted tools to characterize the free volume in amorphous polymers.¹³⁷ The Positron group at the University of Kiel, have used PALS technique to identify changes of free volume in various membranes, nano-composites and low-molecular-weight substances^{124,138-139}. In this study PALS is evaluated as a method to detect free volume in a series of DGEBA-dicyandiamide precursors and their cured epoxy composites, which differs in terms of their chemical constituents.

As shown in Chapter 6 of this thesis, JMAK fits are applied to the experimental data measured by PALS technique. This is helpful to understand the reaction kinetics of the formulations with micro and nano-encapsulated accelerator, in comparison to the system with free accelerator. In this section it is shown that not only the curing times observed by PALS are in good agreement with the IR-spectroscopy data, but at the same time PALS is also suitable for the investigation of holes of sub-nanometre size in their cured composites. The temperature dependence of the hole free volumes, calculated using the Tao-Eldrup model,³⁻⁴ will be presented for the complete series of samples. Apart from that the glass-transition temperatures, T_g and the temperature at which the extrapolated free volume goes to zero, T_0 , and the thermal expansion coefficients of the glassy (α_g) and the rubbery (α_r) phases are also compared. Furthermore, the glass-transition temperatures calculated from the PALS and DSC experiments are compared and discussed.

7.2. Experimental

7.2.1 Preparation of the epoxies

The EP consists of diglycidylether of bisphenol A (DGEBA, CAS-Nr. 1675-54-3; DOW, DER 332) and dicyandiamide (DICY, Dyhard[®]100SF, CAS-Nr. 461-58-5, Alzchem Trostberg GmbH, Germany) in the mass ratio 100 : 6.7. In order to avoid sedimentation of the solid DICY particles, the mixture is pre-cured at 150 °C for 1 h. This step partially dissolves the DICY and increases viscosity due to the formation of oligomers. The corresponding IR spectroscopic oxirane conversion is 15 %. This pre-polymer is degassed in vacuum and homogenised (3200 min⁻¹, 2 x 30 s) by a Speedmixer[®] (Hauschild Engineering, DAC 150 FV, Germany) in normal air at 40 °C. EP_{accel} is made of the pre-polymer and the accelerator (0.5 weight-%, substance not revealed for proprietary reasons) by mixing in the Speedmixer under the same conditions. In a similar manner, EP_{μ-zeolite}, EP_{n-zeolite}, EP_{μ-filler} and EP_{n-filler} are obtained by dispersing the micro-zeolites (2.4 weight-%), the nano-zeolites (2.4 weight-%), the loaded micro-zeolite fillers (2.9 weight-%, corresponding to 0.5 weight-% of accelerator) or the loaded nano-zeolite fillers (2.9 weight-%, corresponding to 0.5 weight-% of accelerator) in the pre-polymer.

For the sake of clarity the six different samples are abbreviated as follow;

BK1 = Pre-polymerized DGEBA and DICY system with a stoichiometric ratio of 100:6.7

BK2 = BK1 + Accelerator (0.5 wt%)

BK3 = BK1 + unloaded μ-Zeolite

BK4 = BK1 + micromodule (0.5 wt% Accelerator encapsulated in μ-Zeolite)

BK5 = BK1 + unloaded n-Zeolite

BK6 = BK1 + nanomodule (0.5 wt% Accelerator encapsulated in nano-Zeolite)

7.2.2 Modulated DSC

MDSC investigations done by the calorimeter Q100 (TA Instruments) at a heating rate of $\beta = 10 \text{ K min}^{-1}$ are carried out with sinusoidal modulation at $f = 1 / 60 \text{ Hz}$ and a temperature amplitude of $\Delta T = \pm 1 \text{ K}$. The measuring cycle for network formation starts by heating the

samples (6 mg in Au-coated Al pans) with $\beta = 10 \text{ K min}^{-1}$ from $5 \text{ }^\circ\text{C}$ to $170 \text{ }^\circ\text{C}$. Then, isothermal curing follows for 240 min for EP, EP $_{\mu\text{-zeolite}}$ and EP $_{\text{n-zeolite}}$, and for 45 min for EP $_{\text{accel}}$, EP $_{\mu\text{-filler}}$ and EP $_{\text{n-filler}}$. The cycle is finished by cooling down to $25 \text{ }^\circ\text{C}$ with $\beta = 10 \text{ K / min}$. The glass transition of the network is deduced from the specific reversible heat flow as measured on the cured samples during heating from $25 \text{ }^\circ\text{C}$ to $225 \text{ }^\circ\text{C}$ with $\beta = 10 \text{ K / min}$ and the same modulation parameters.

7.2.3 IR Spectroscopy

The measurements are done by ATR-FTIR spectroscopy (attenuated total reflection) using a ZnSe hemisphere and p-polarised light at an incident angle 65° and by μ -ATR-FTIR spectroscopy (microscopic ATR; Ge crystal) providing a lateral resolution of $80 \text{ }\mu\text{m}$ and an information depth of approx. $2 \text{ }\mu\text{m}$. The IR-investigation allows to evaluate the chemical modifications due to storage at $25 \text{ }^\circ\text{C}$ and the consumption of epoxy (915 cm^{-1}), primary amine ($\delta (-\text{NH}_2) = 1575 \text{ cm}^{-1}$) and nitrile groups ($\nu (-\text{C}\equiv\text{N}) = 2172 \text{ cm}^{-1}$) during curing. Therefore, the band intensities are divided by the intensity of the phenyl band at 1510 cm^{-1} as internal standard.

7.2.4 PALS

Positron annihilation lifetime experiments have been performed with a conventional fast-fast coincidence setup^{32,140} using a home made temperature-controllable sample holder under high vacuum conditions as described in more detail in a recent work.(J. Kruse 2004) The time resolution was 285 ps (FWHM, ^{22}Na source) and the analyzer channel width amounted to 25.3 ps . All the samples were sandwiched around a $\sim 1 \text{ MBq}$ positron source: $^{22}\text{NaCl}$, deposited between two $7 \text{ }\mu\text{m}$ thick Kapton foils. The samples were cured in aluminum pans and then covered by Kapton foils with the help of double sticking Kapton tape (on the edges of the aluminum pans). The PALS measurements were done at RT (303 K), followed by a measurement at 373 K , which was done for the in-situ conditioning of the material and subsequently quickly cooled down to room temperature. A complete temperature scan was then performed between 103 K and 473 K in steps of 10 K (accuracy of $\pm 1 \text{ K}$). The final resolution function used in the spectrum analysis was determined as a sum of two Gaussian curves. Each measurement lasted 2 hours leading to a lifetime spectrum with the high number

of $\sim 5 \times 10^6$ annihilation events which is sufficiently high to be analyzed with the routine LifeTime (LT9.0) in its distribution mode.

7.3 Results and Discussions

7.3.1 Part I: Precursor series (IR, PALS and JMAK)

7.3.1.1 Shelf life calculated by IR Spectroscopy and PALS data at 60°C

For testing the shelf life with IR spectroscopy the samples were stored at 60°C under atmospheric conditions and measured at selected time intervals. The decreasing epoxy band at 915 cm^{-1} and the increase of an ether band at 1105 cm^{-1} were observed, as shown in Fig. (7.1). Which is due to the formation of polyether chains via anionic polymerization initiated by the accelerator-epoxy zwitterionic adduct.¹¹⁴ The shelf life is defined here as the storage time before the adhesive exceeds the viscosity limit for appropriate handling in the laboratory.

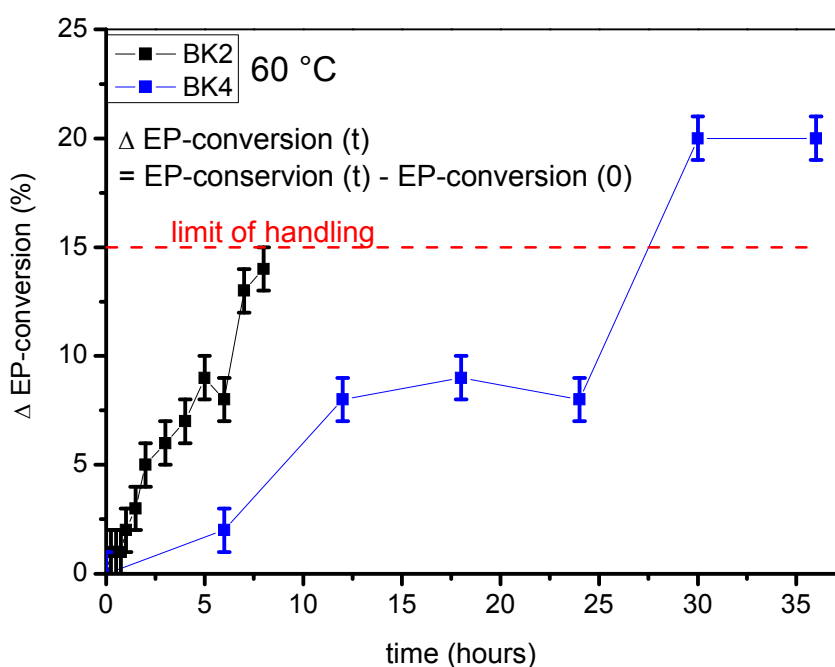


Fig 7.1: IR spectroscopy data for the BK2 and BK4 systems, where the dotted red line indicating the limit of handling for the BK2 formulation (with free accelerator).

The plateau of the *o*-Ps lifetime τ_3 observed in the early stages of the lower temperature investigations shows that the mixture is still in its precursor state. The following sharp decrease in *o*-Ps lifetime indicates that the curing sets in. Finally, the cured state is achieved, which is indicated by reaching the saturation limit. One should note that in the course of the process τ_3 is decreasing, reflecting a decrease in hole size, as expected for free volume

shrinkage due to the curing.¹²⁸ The slight reduction in the *o*-Ps intensity (not shown), during curing may be an indication that there are reactive groups inhibiting Ps formation. Furthermore, the half-life of the curing process is also indicated and is in good agreement with IR spectroscopy data.

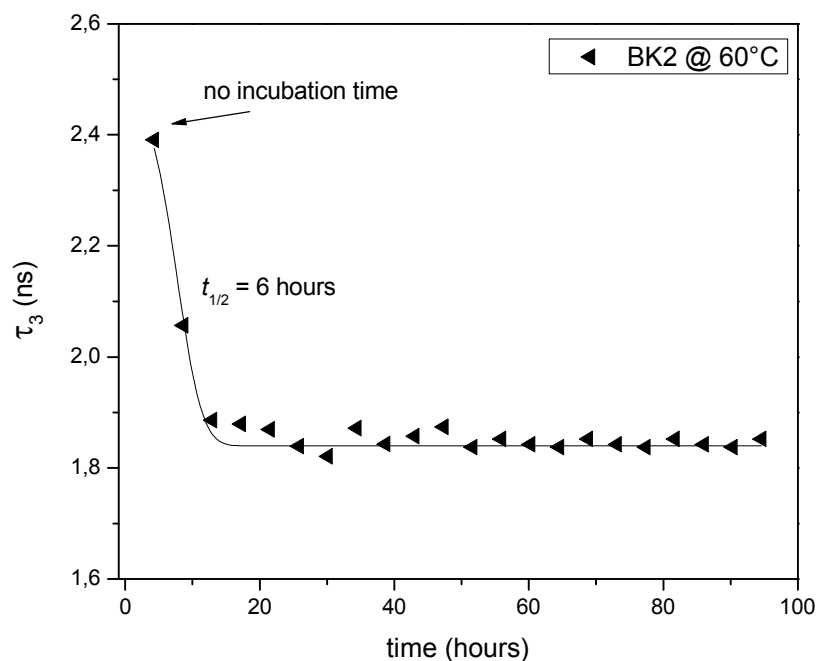


Fig 7.2: PALS data for BK2 sample measured at 60 °C, the storage time ($t_{1/2}$) calculated by PALS are in good agreement with the one measured by the IR.

7.3.1.2 JMAK fits to PALS data

As discussed in Chapter 6, Johnson-Mehl-Avrami (JMAK) or Avrami equation is a widely accepted model to study the phase transformations, e.g. crystallization or austenite to martensite transformations.⁷⁷ According to the Avrami equation (Eq. 4.17), for solid-state transformations displaying the kinetic behaviour, the fraction of transformation X is a function of time t .¹¹⁷ Where ' n ' is the Avrami exponent, a parameter that indicates the dimensionality of growth together with nucleation type,¹⁴¹ a detailed overview is given e.g. in reference^{77,128}. The overall relative transformation rate constant is denoted as ' k ' (its value include contributions from both nucleation and growth), which is in turn temperature dependent via a simple Arrhenius law. The *o*-Ps lifetime τ_3 is a measure for the degree of transformation X , i.e. the degree of curing and can be calculated using Eq. 6.1

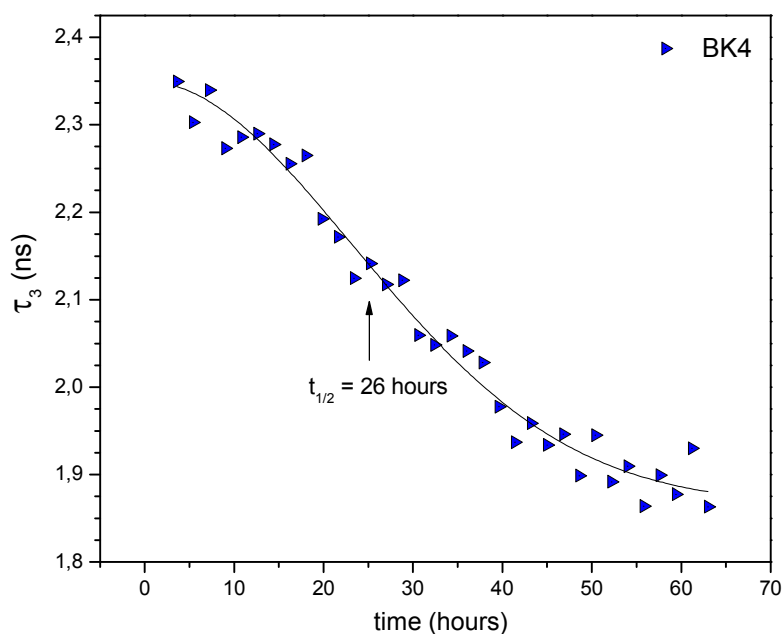


Fig. 7.3: JMAK fits with $n \approx 2$ and corresponding reaction constant to the PALS data for BK4 sample (micro-encapsulated accelerator).

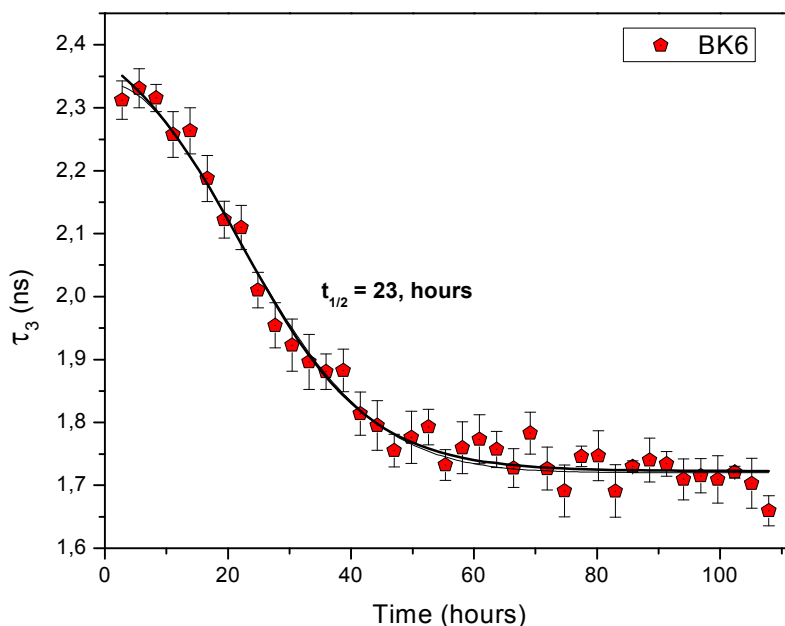


Fig. 7.4: Fit of JMAK kinetics with $n \approx 2$ and corresponding reaction constant to the PALS data for BK6 sample (accelerator encapsulated in nano-sized carrier).

Figures 7.2, 7.3 and 7.4 shows the JMAK fits to the PALS data respectively for the BK2 (system with free accelerator), BK4 (micro-encapsulated accelerator) and BK6 (nano-encapsulated accelerator). Here it is remarked that measurements for the remaining precursor

systems were also done for the BK1 and BK3, but since these systems were without accelerator, which resulted in longer curing times and therefore not reported here. The JMAK fitting analyses indicate almost similar values of the reaction constant ‘ k ’ for all the systems. Whereas an approximate value of $n = 3$, which according to the Ref. ⁷⁹, refers to the three-dimensional linear growth for steady state homogenous nucleation i.e. all nuclei activated at time, $t = 0$. Furthermore, an approximate value of $n = 2$ was obtained for both micro-encapsulated (BK4) and nano-encapsulated (BK6) systems. A value of $n = 2$, refers to two-dimensional linear growth for steady state homogenous nucleation, with all nuclei activated at time, $t = 0$.⁷⁹

The Avrami equation was originally obtained by statistical geometrical considerations dealing with the problem of how a sample volume gets covered by growing objects of a certain shape. Thereby it is assumed that these start at random points, either all at once or at random times. It is the objective of the Avrami treatment to relate the Avrami exponent ‘ n ’ and the rate coefficient k to the shape of the particles, their growth rate, and the time distribution of the nucleation events.

Table 7.1: List of the calculated Avrami parameters and curing times for the complete series of measurements.

Sample	τ_0 (ns)	τ_∞ (ns)	$\Delta\tau$ (ns)	n	k	$t_{1/2}$ (h) PALS	t_{storage} (h) IR
BK1	-	-	-	-	-	> 3 weeks	> 3 weeks
BK2	2.44	1.84	0.6	3.08	1.28E-03	6.	10.
BK3	-	-	-	-	-	> 3 weeks	> 3 weeks
BK4	2.35	1.87	0.48	1.96	1.03E-03	26.	30.
BK6	2.34	1.72	0.62	1.96	1.23E-03	23.	30.

The values of $n = 2$ for the micro and the nano-encapsulated systems indicate that the curing kinetics remains the same for the two systems and are independent of the size of carrier material. So a possible explanation of the two-dimensional linear growth can be due to some of the material curing on the surface of carrier openings, in the early stages of transformation, thus blocking the release of accelerator and delaying its subsequent reaction with the epoxy matrix. Whereas, the coefficient $n = 3$ indicates growth of a constant number density of spheres with a constant rate, so in the free accelerator system (BK2), the accelerator is free to react with the epoxy matrix in all the possible directions and therefore resulting in a three-dimensional linear growth.

7.3.2 Part II: Cured series (PALS, DSC)

7.3.2.1 Analysis of the Positron Lifetime Spectra.

The positron decay in amorphous polymers usually shows three decay channels which are attributed to the annihilation of *p*-Ps (τ_1), free (not Ps) positrons (e^+ , τ_2), and *o*-Ps (τ_3 ; $\tau_1 < \tau_2 < \tau_3$).¹⁴² The routine LT9.0 software² assumes that the annihilation rate distributions $\alpha_i(\lambda)$ follow a log normal function. For reducing the number of fitting parameters the short *p*-Ps and e^+ lifetimes were assumed to appear discrete ($\sigma_1 = \sigma_2 = 0$). The experimentally obtained spectrum is convoluted with the resolution function and fitted with a non-linear least-squares method to the data. The reduced chi-squares of the fits, χ^2/df , were in the acceptable range (1.0 to 1.1), showing the high quality of the fit.

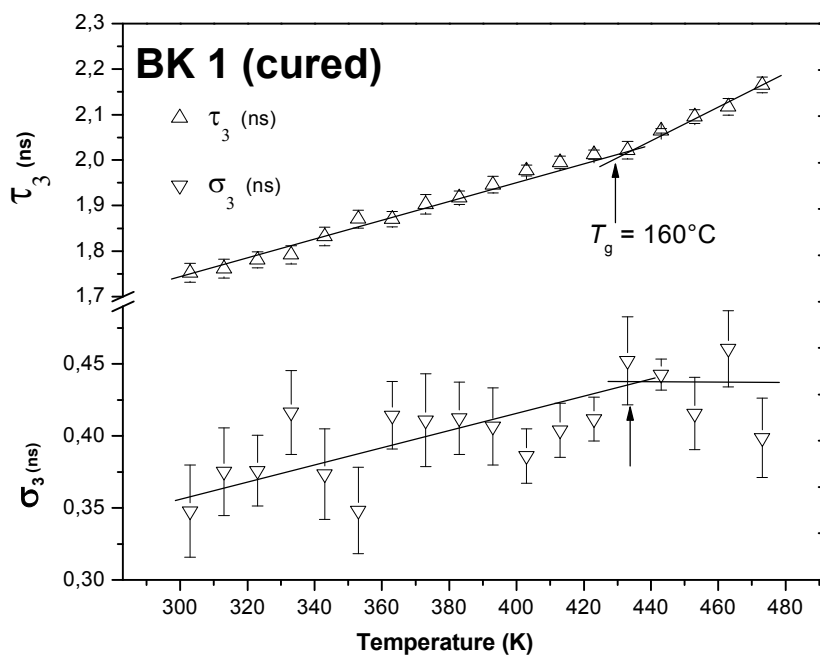


Fig. 7.5: Temperature dependence of *ortho*-positronium lifetime and its distribution for the epoxy composite systems without accelerator (BK1) are shown here.

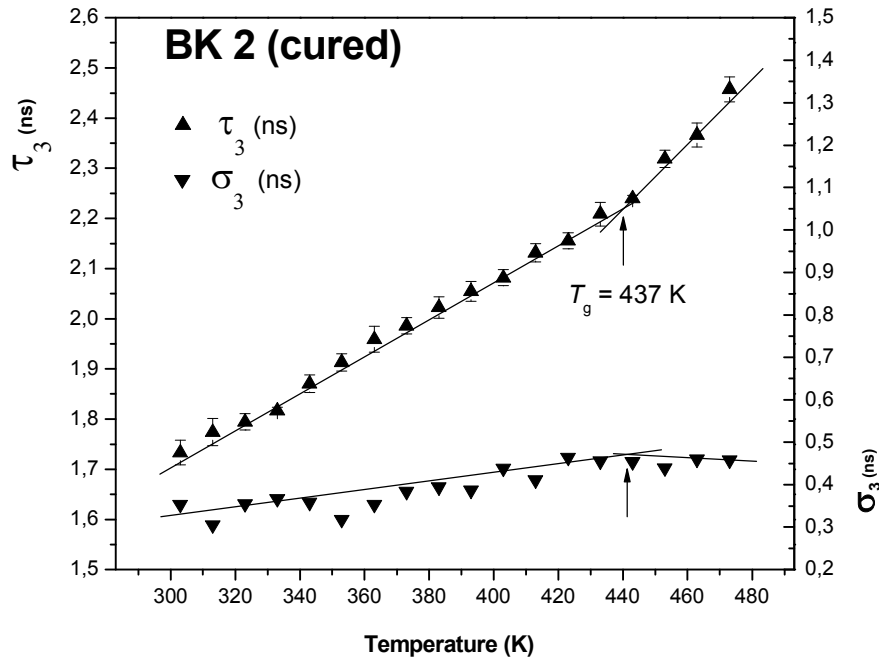


Fig. 7.6: Temperature dependence of *ortho*-positronium lifetime and its distribution for the epoxy composites system with free accelerator (BK2).

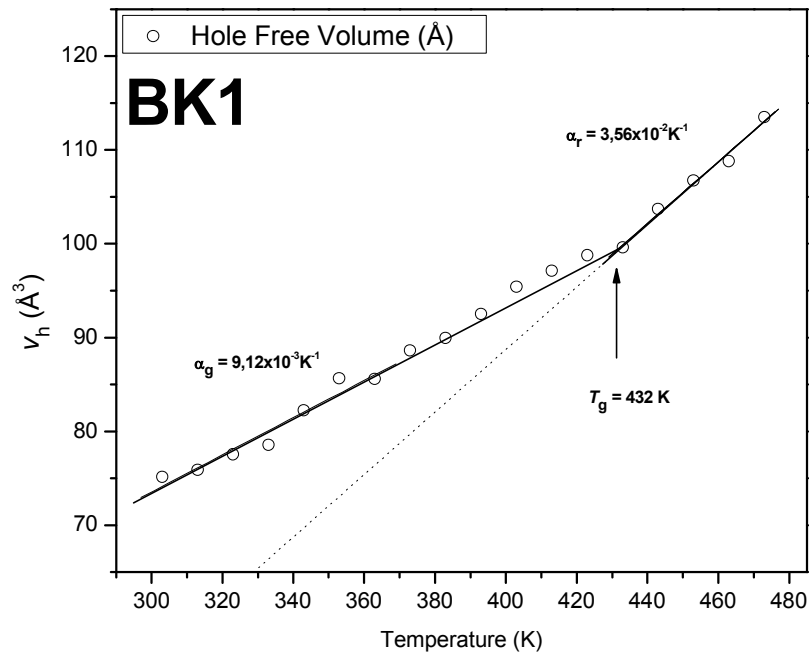


Fig. 7.7: Hole free volume V_h , for the BK 1 system, calculated with the help of Tao-Eldrup model, assuming spherical holes.

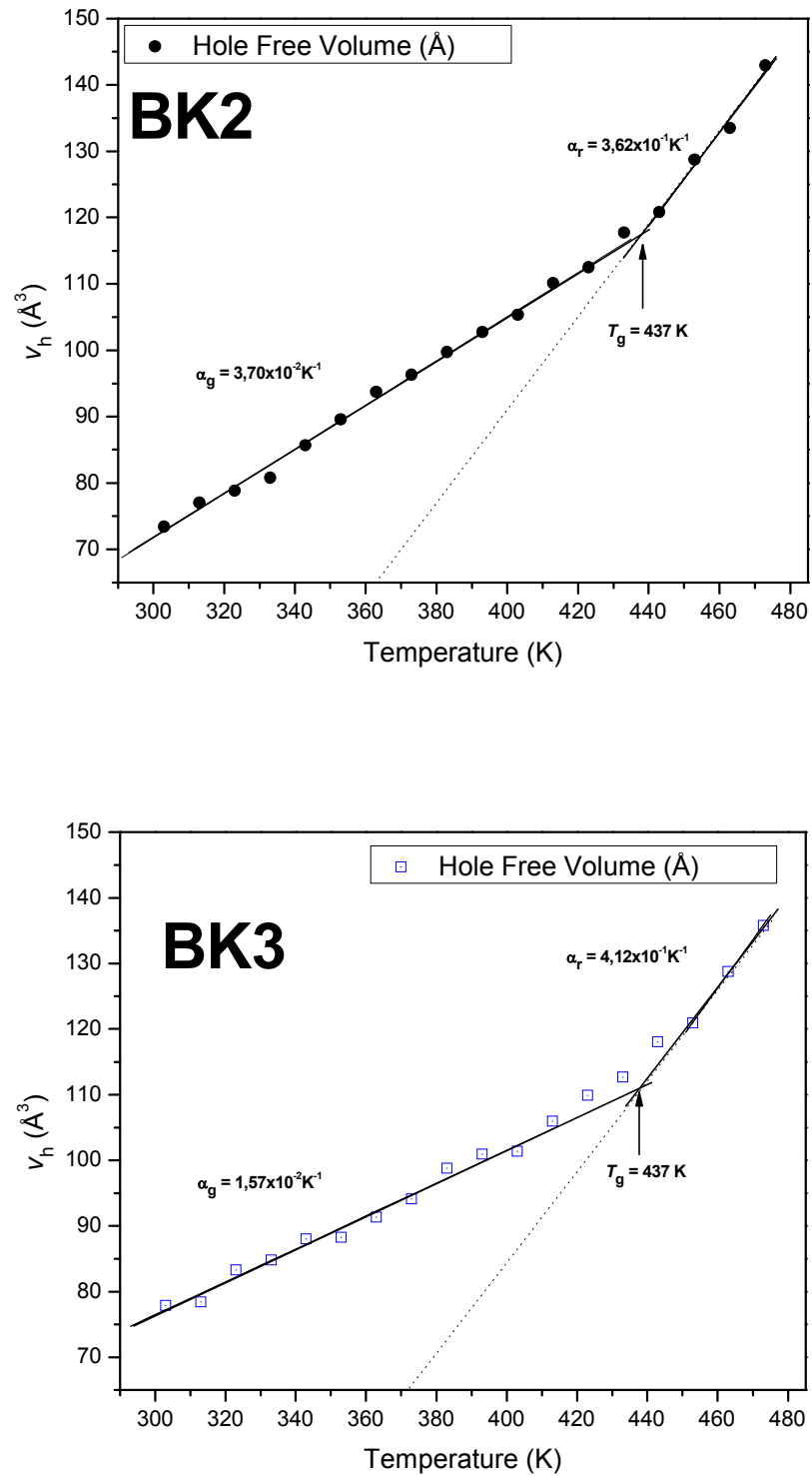


Fig. 7.8: Hole free volume V_h , (a) for the BK2 and (b) for the BK3 systems, calculated with the help of Tao-Eldrup model, assuming spherical holes.

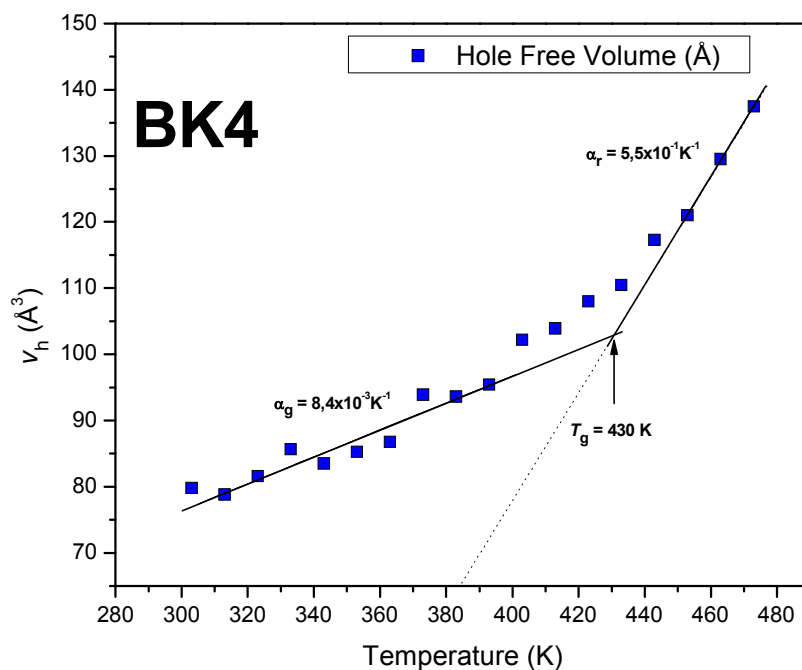


Fig. 7.9: Hole free volume V_h , for the BK4 system, calculated with the help of Tao-Eldrup model, assuming spherical holes.

7.3.2.2 Micro-volumetric T_g and the coefficient of thermal expansion

One of the most suitable approximations for analyzing the glass transition concerns the free volume. The free volume is sensitive to the changes in temperature, thus the thermal expansion of the solid or molten polymer can be explained by a change in free volume. Table 7.2 indicates the list of parameters evaluated with the help of PALS and DSC data for the cured series. Here α_g and α_r are the thermal expansion coefficients for the glass and rubbery phases respectively. Whereas, T_0 being the temperature at which the extrapolated free volume goes to zero.

Tab. 7.2: List of all the parameters evaluated with the help of PALS and DSC data for cured series

Sample	V_h at RT (\AA^3)	V_h at T_g (\AA^3)	T_g^{PALS} (± 5 K)	α_g (K^{-1})	α_r (K^{-1})	T_0 (± 10 K)	T_g^{DSC} (± 5 K)
BK1	74	99.5	432	2.7×10^{-3}	3.4×10^{-3}	329	460
BK2	72	117.1	437	4.6×10^{-3}	6.0×10^{-3}	364	445
BK3	76	110.8	437	3.3×10^{-3}	6.3×10^{-3}	372	455
BK4	76	103.0	430	2.7×10^{-3}	7.8×10^{-3}	384	448
BK5	80	102.4	431	2.1×10^{-3}	5.7×10^{-3}	358	-
BK6	74	105.8	423	2.7×10^{-3}	8.9×10^{-3}	376	-

Figures 7.5 and 7.6 shows the most important results, the mean $\tau_3 \equiv \langle \tau_3 \rangle$ ($\langle \tau_i \rangle = \int \tau \alpha_i(\tau) d\tau$) and the mean dispersion σ_3 (square-root of the variance $\sigma_i^2 = \int (\tau - \langle \tau_i \rangle)^2 \alpha_i(\tau) d\tau$) of the *o*-Ps lifetime distribution $\alpha_3(\tau) = \alpha_3(\lambda)\lambda^2$, where α_3 is the annihilation rate distribution and τ_3 varies between 1.8 ns and 2.5 ns for all the samples and shows a typical glass transition behavior, with a distinct increase in its slope at T_g , which is closely followed by σ_3 . The intensity of the *o*-Ps component (Fig. 7.10) for all the cured samples slightly increases with temperature from 16 % to 23 %, with no change in slope at T_g .

7.3.2.3 Fractional hole free volume f_g (at T_g)

The fractional free volume (%) is expressed as an empirically fitted equation as:⁴⁷

$$f_g = A V_h I_3 \quad \text{Eq (7.1)}$$

where the fractional hole free volume is denoted by f_g (at T_g) and V_h (in \AA^3) is the volume of free-volume holes calculated by using the spherical radius (r_h) of Eq (2.11) from τ_3 (in ns), I_3 (in %) is its intensity, and A is empirically determined to be 0.0018 from the specific volume data.⁴⁷

Tab. 7.3: Fractional hole free volume $f_g(T_g)$, calculated using Eq (7.1)

Sample	V_h at T_g (\AA^3)	T_g (± 5 K)	I_3 (± 0.05 %)	f_g (± 0.05 %)
BK1	99.5	432	25.2	4.51
BK2	117.1	437	19.5	4.11
BK3	110.8	437	23.9	4.76
BK4	103.0	430	20.8	3.86
BK5	102.4	431	18.3	3.37
BK6	105.8	423	16.9	3.21

7.3.2.4 Effect of Cross-Linking on T_g

Polymers with strong intermolecular interactions present high glass transition temperatures, because great energy is required to separate their chains. Cross-links constitute the strongest intermolecular interactions, since they form real chemical bonds. As indicated in Tab. 7.3, comparing respective systems with and without accelerators i.e. BK1 (4.51 %) with BK2(4.11 %), BK3 (4.76 %) with BK4 (3.86 %) and finally BK5(3.37 %) with BK6(3.21 %), it can be

seen that every time the accelerator is introduced in the epoxy resin formulation, the *ortho*-Positronium intensity (I_3) and eventually the fractional hole free volume at T_g is also decreased. This can be attributed to the effect of highly reactive accelerator, resulting in higher degree of cross-linking and therefore a lower fractional hole free volume, as compared to the systems without accelerator. It is known that if the cross-link density increases, then the free volume should decrease, and this consequently gives rise to the T_g , because the molecular mobility is more hindered.¹⁴³ However, only the comparison of BK1 and BK2 agrees with this theoretical interpretation and it is not clear as to why the systems with encapsulated accelerators (i.e. BK4 and BK6) have a lower T_g , although they have lower values of the fractional hole free volumes. For the complete series of cured composites the number density of holes is also estimated, by taking certain assumptions into account, but since there was no significant difference observed and therefore these results will not be reported here.

7.3.2.5 No effect of positron irradiation

A minimum in I_3 near T_g has been reported for several polymers and is generally agreed to be the result of cumulative irradiation.¹⁴⁴ The effect of long-term exposure to the positron source during positron annihilation lifetime measurements was explored by monitoring any change in the *o*-Ps intensity (I_3) as a function of exposure time and temperature.

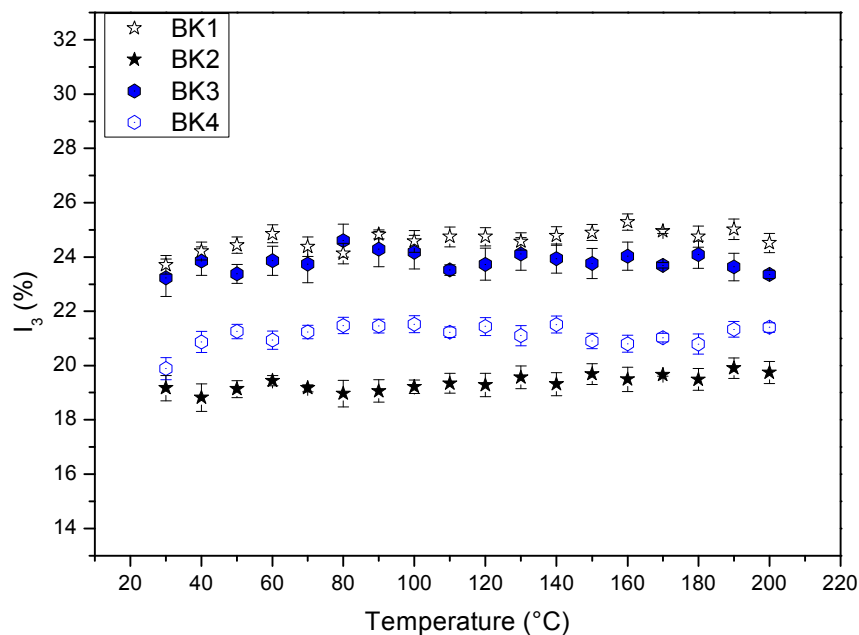


Fig. 7.10: Plots of *ortho*-positronium intensities (I_3) for all the samples, indicating that there is no real temperature dependence, but definitely the intensities of BK1 and BK3 are relatively higher as compared to other samples. For the sake of clarity data for BK5 and BK6 are not shown here.

For the complete series of cured samples, the *o*-Ps intensity within the error bars remains more or less unchanged, which suggest no real irradiation effects. However, as shown in Fig.6, the intensities of BK1 and BK3 are higher as compared to the other samples, for the sake of clarity the intensity data of BK5 and BK6 systems is not shown here.

7.3.2.6 The *ortho*-Positronium Inhibition

Furthermore, it was observed that every time the accelerator is introduced into the formulation, it lowers the intensity of *ortho*-positronium, this effect is attributed to the process of “*ortho*-Positronium inhibition”. Although this interpretation eventually means that the values obtained for the fractional hole free volume, f_h are not reliable, but for the scientific understanding of these results its very important to discuss each and every aspect of the available data. Since the dicyandiamide hardener already have N-atoms in its structure and even the accelerator used here also have Nitrogen in its structure, so due to higher concentration of N-atoms Ps inhibition occurs in the formulations with accelerator, which reduces the intensity of *o*-Ps formation as compared to the systems without accelerators, whereas on the contrary there is no real effect on the *o*-Ps lifetimes.

7.4 Conclusions

An in-depth analysis for the precursor and the cured series of one-component epoxy resin formulations is reported. The shelf-life calculated from PALS is in good agreement with the ones observed by the IR spectroscopy. JMAK fits to the PALS data indicates that the micro (BK4) and the nano-encapsulated (BK6) systems show the same reaction kinetics, with Avrami exponent having an approximate value of $n = 2$, whereas the system with free accelerator (BK2) does not show any incubation time and a higher value of $n = 3$. Furthermore, the cured series of their epoxy composites indicate no real change in the hole free volume at room temperature of 300 K and even other parameters does not indicate any systemic behaviour. The values of T_g calculated by PALS are a bit lower as compared to the ones observed by DSC, which is due to the longer annealing times of PALS technique. However, the *ortho*-Positronium intensity and the fractional hole free volume at the T_g is lowered, every time the accelerator is introduced into the system.

8. The effect of encapsulation on activation energy

It is also very important to investigate the kinetic parameters such as the apparent activation energy (E_a) for understanding the mechanism for the curing of epoxy resins. The E_a determines whether the curing reaction of epoxy resin will be carried out smoothly.¹⁴⁵ By using PALS, an activation energy of 160 kJ/mole is observed for the state of the art dicyandiamide cured 1K-DGEBA benchmark formulation,¹¹³ where block uron is used as an accelerator (see for example Chapter 6 of this thesis). The results presented in this section will show how the activation energy for the 1K formulation with free accelerator vary, as compared to the epoxy-resin formulation with the same accelerator, but encapsulated in a micro-sized Zeolite carrier. The details of the accelerator and the carrier material will be treated as classified.

8.1 Introduction

The relative reaction rates are often expressed in terms of the activation energy, E_a (Arrhenius type relationship). E_a allows comparisons of reaction rates at different temperatures and is influenced by the type of chemical reactions involved in the cure. The epoxy cures are known to involve multiple steps that are likely to have different activation energies. There are two major approaches to kinetic analysis.¹³⁰ Firstly, the reaction complexity can be accounted by using complex models,¹⁴⁶ and secondly, based on fitting of kinetic data to assumed reaction models. In the later, data are fitted to a single-step reaction model that obviously yields a single averaged value of the activation energy for the overall cure process. The resulting value does not reflect changes in the reaction mechanism and kinetics with the temperature and the extent of conversion. However, as the main aim of this work is to predict the shelf-life of 1K epoxy resin formulations with the help of accelerated tests at elevated temperatures, therefore, the JMAK approach used in this work is acceptable.

In the case of hot-curing systems, isothermal kinetics approach is adopted where the reaction kinetics change from being chemically controlled in the liquid state to diffusion controlled in the glassy state as a function of time at a given temperature. The cross-linking reduces molecular mobility and results in the process changing from being kinetically controlled to diffusion controlled.¹⁴⁷ After vitrification, the reaction becomes diffusion controlled and then

practically stops at a maximum conversion, a greater conversion can only be reached by raising the reaction temperature,¹⁴⁸ or increasing time by multiples of 10.

Curing of epoxy resins with phenols or aromatic and aliphatic amines proceeds with fairly low activation energy of 50–58.5 kJ/mol.¹⁴⁹ Activation energies are higher when epoxy compounds having low hydroxyl content are cured alone in the presence of catalysts (92 kJ/mol) or with dicyandiamide (125.5 kJ/mol).¹⁴⁹ Horie et al.¹⁵⁰ reported an activation energy of 53.9 kJ/mol for the system DGEBA-EDA determined by DSC. Gupta et al.¹⁵¹ found a value of 56 kJ/mol, observing that the activation energy hardly changes with the hardener used. Independent of the sample and the technique used for the kinetic analysis, no variation of the activation energy of the epoxy curing reaction was found, which suggests that there are no changes in the mechanism of the reaction along the process.¹⁵²

8.2 Experimental

8.2.1 Material

Diglycidyl ether of bisphenol-A (DGEBA, Araldite GY 250, with epoxy equivalent weight EEW = 187 g/mol) was obtained from Huntsman. Dicyandiamide (DICY, Dyhard DF 50 EP within an epoxy-based paste used as curing agent. For this particular epoxy-hardener pair the mass ratio is approximately seven parts of DICY hardener, in equivalent weight, per hundred parts of resin, i.e. 7 phr. The applied formulation is similar to one of the published technical systems.¹²⁹ As explained earlier the details of accelerator and the carrier material used for micro-encapsulation of the accelerator are treated as classified information and won't be mentioned here.

8.2.2 Analysis and measurement

Positron annihilation lifetime experiments were performed with a fast-fast coincidence setup under high vacuum conditions as described in the Sections (2.4.1 and 6.2) of this thesis. The time resolution was 285 ps (FWHM, ²²Na source) and the analyzer channel width was 25.3 ps. The resin, hardener and accelerator are thoroughly mixed at room temperature and after approximately one hour of preparation two identical samples of precursor were sandwiched around a ~1 MBq positron source, prepared by depositing ²²NaCl, between two 7µm-thick

Kapton foils. Several isothermal scans are performed for different sets of samples at 50°C, 60°C and 70°C for the microencapsulated system and 30 to 60°C for the free accelerator system, in steps of 10°C, with an accuracy of ± 1 K. For each sample the first spectrum is always measured at room temperature (RT) followed by an isothermal run for several hours, at the indicated temperatures. Each measurement lasted approximately 3 hours, leading to a lifetime spectrum with a high number of annihilation events ($\sim 5 \times 10^6$).

8.3 Results and Discussions

8.3.1 The *o*-Ps lifetime and the storage time

The spectrums obtained from PALS are resolved into three lifetime components and in the final fits the (very short) *p*-Ps and the positron lifetime is assumed to be discrete (i.e. standard deviation of lifetime distribution, $\sigma_1 = \sigma_2 = 0$). The *o*-Ps lifetime is allowed to show a distribution ($\sigma_3 > 0$) around its mean value τ_3 . Figures (8.1) and (8.2), shows isothermal annealing plots of the average *o*-Ps lifetime as a function of time, for the 1K formulation with free accelerator and the encapsulated accelerator respectively. The logarithmic axes are used to clearly see the initial stages of curing reaction, especially for the samples at higher temperature, as curing reaction is faster for these samples and not enough data points are available to see the incubation time. The *o*-Ps lifetime values obtained from the first spectrum measured at RT are not shown here for the sake of clarity.

Once again the *o*-Ps lifetime proved to be an excellent probe to follow the in-situ curing of epoxy precursor from its initial liquid state, followed by the onset of gelation and until the solidification state, where the τ_3 values reach the saturation limit. The values obtained for solidification region are in good agreement with the ones obtained for the ex-situ cured samples, at a temperature of 150 °C, of the similar systems. It is remarked, that if the isothermal curing is performed at a temperature above the limiting glass transition temperature, T_g^∞ the system reaches full cure.¹⁵³ This temperature is usually characterized by the maximum value of heat release by DSC technique, which is independent of curing time. When cured at a temperature below T_g^∞ , a system vitrifies before attaining full cure. Therefore the cures performed below this temperature are called incomplete cure. This could be true for the low temperature cures for the system with free accelerator system and will be explained with the help of Avrami parameters in the following sections of this chapter.

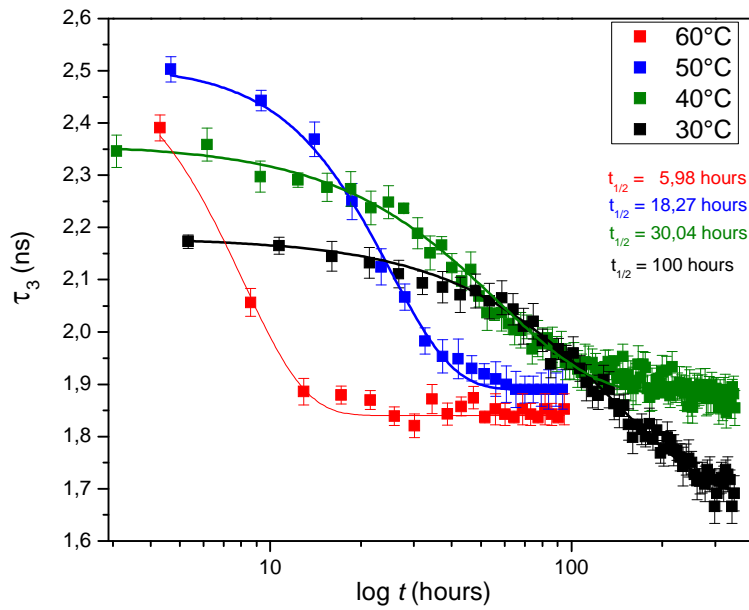


Fig. 8.1: The *ortho*-Positronium lifetime as a function of curing times (logarithmic axes used to clearly see the initial stages of curing), for the 1K formulation with free accelerator. The solid lines indicate the Boltzmann fits to the experimental data to calculate the storage times, $t_{1/2}$.

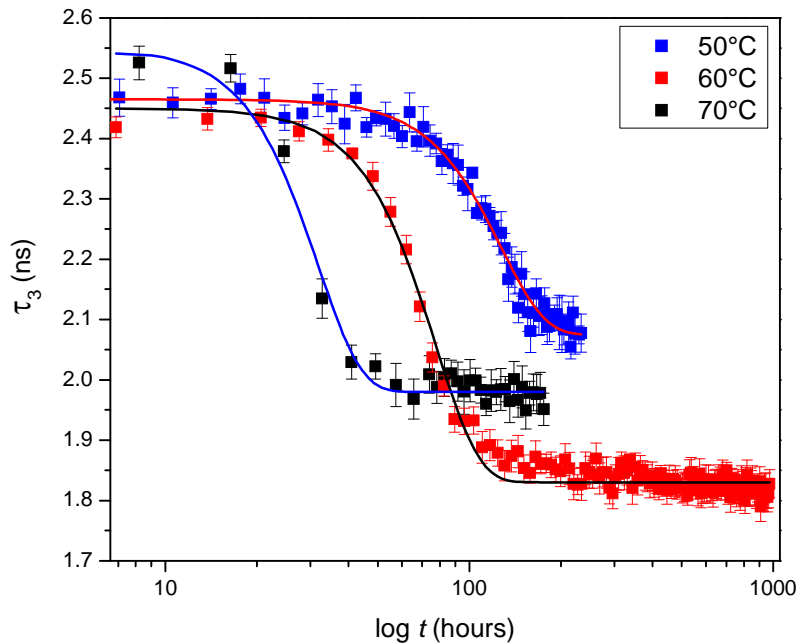


Fig. 8.2: *ortho*-Positronium lifetime as a function of curing times (logarithmic axes used to clearly see the initial stages of curing), for the formulation with micro-encapsulated accelerator. The solid lines indicate the Boltzmann fits to the experimental data to calculate the storage times, $t_{1/2}$.

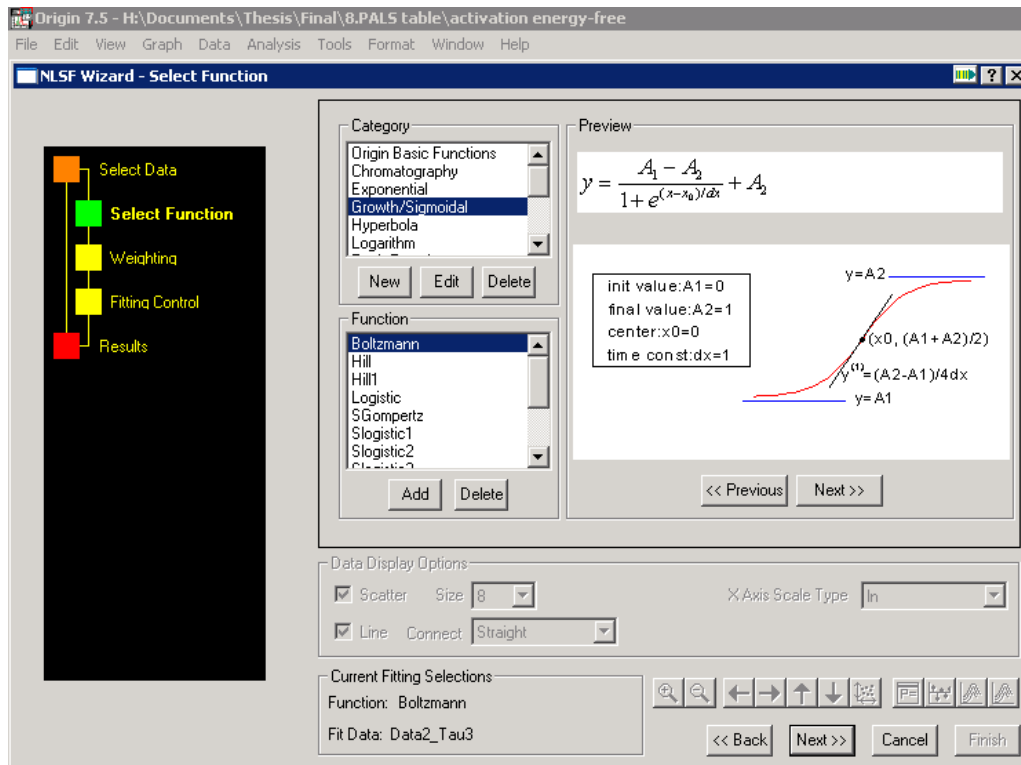


Fig. 8.3: The picture taken during the fitting of *ortho*-Positronium lifetimes with the Boltzmann function, to calculate the storage times, $t_{1/2}$ using Origin 7.5 software.¹⁵⁴

The storage time ($t_{1/2}$) is calculated by using the Boltzmann fitting function, which is available in Origin 7.5 software.¹⁵⁴ Please note that this function has nothing to do with the Boltzmann constant, which is the gas constant R divided by the Avogadro constant N_A , relating energy at the particle level with temperature observed at the bulk level. Here this function assumes τ_0 and τ_∞ as the starting and the end values of the transformation and calculates the storage time $t_{1/2}$ as the middle point, according to the following equation;

$$f(X) = \frac{\tau_0 - \tau_\infty}{1 + e^{(t-t_{1/2})/dt}} + \tau_\infty \quad (8.1)$$

Where $f(X)$ is the Boltzmann function, $\tau_0 = 0$ and $\tau_\infty = 1$, are the initial and the final values respectively. The center, $t_{1/2} = 0$, has the co-ordinates of $(t_{1/2}, (\tau_0 + \tau_\infty)/2)$ and the slope = $(\tau_\infty - \tau_0)/4dt$ and time constant $dt = 1$. Figure (8.3) shows as an example the fitting of *ortho*-Positronium lifetimes with the Boltzmann function, to calculate the storage times, $t_{1/2}$ using Origin 7.5 software.

8.3.2 Transformed fraction and the JMAK fits

As already known, Avrami theory was originally used to describe the kinetic process of polymer crystallization. However, many molecular aggregates (microgels) or high-molecular-

weight particles have been observed during an infinite network formation as a result of crosslinking.¹⁵⁵ Lu et al.¹⁵⁶ considered that in a broad sense, crystallization can be considered as a physical form of cross-linking, and in some aspects the behavior of amorphous cross-linked polymers at a higher degree of curing reaction is similar to that of crystallization. Therefore it is possible to predict the cure process of thermosets using the Avrami equation. Figure 8.4 shows the transformed fraction X as a function of logarithmic time. Where solid lines indicate the JMAK fits according to Eq. (4.17).

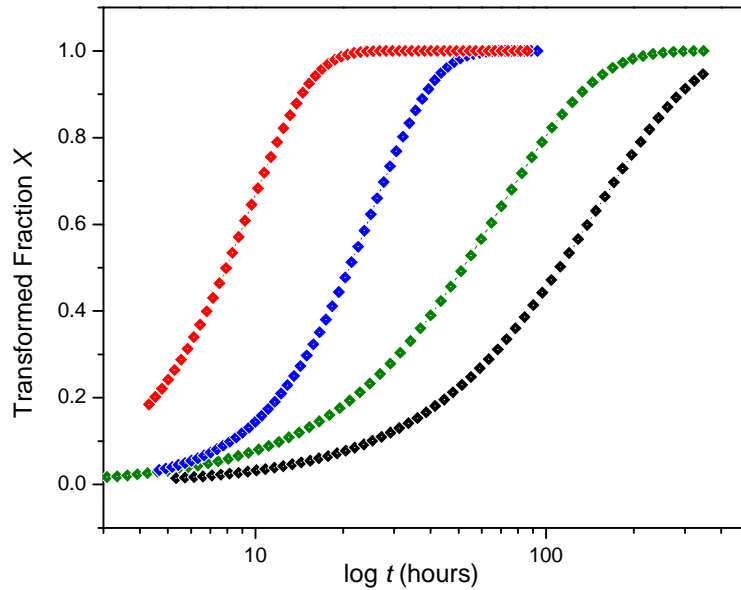


Fig. 8.4: JMAK fits to the transformed fraction X , calculated by Eq. 6.1, for the formulation with free accelerator (for clarity only the JMAK fits are shown here).

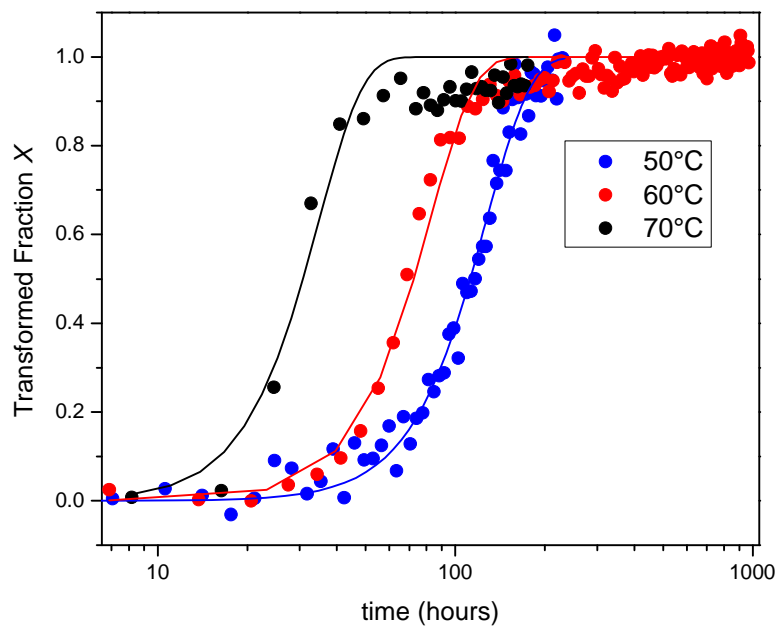


Fig. 8.5: The ρ -Ps lifetimes for the system with encapsulated accelerator, used as a measure of transformed fraction X . The solid lines indicates the JMAK fits to the experimental data

The storage times observed for both series of formulations are summed up in Tables (8.1) and (8.2), respectively for the free and the encapsulated accelerator series. It is clearly evident that the encapsulation of accelerator delays the curing reaction and therefore increases the shelf life of 1K formulation.

Table 8.1: PALS and JMAK parameters for the 1K formulation with free accelerator.

Temp (°C)	τ_0 (ns)	τ_∞ (ns)	$\Delta\tau$ (ns)	n	k	$t_{1/2}$ (h)	T_H^* (°C)	E_a (kJ/mol)
30	2.21	1.68	0.53	1.26	3.30E-03	100,0		
40	2.36	1.88	0.48	1.30	8.96E-03	30,0	124,9	42,5
50	2.51	1.89	0.62	2.10	1.17E-03	18,3		
60	2.45	1.86	0.59	2.02	1.31E-03	5,9		

* T_H values refer to curing temperatures obtained by DSC technique at 20K/min(S. Gramm AWOK, University of Kaiserslautern, *private communication*)

8.3.3 Avrami exponent and the Activation energies

The PALS and JMAK parameters for the system with free accelerator are listed in Table (8.1). The n values of the Avrami exponent were found out to be 1.3 and 2.0 for the temperature ranges of 30 to 40°C and 50 to 60°C, respectively. This suggests that the curing mechanism changes with respect to temperature. However, the Arrhenius plots indicate that the approximate activation energies for both temperature intervals remains the same (i.e $E_a = 42.5$ kJ/mol), irrespective of the change in Avrami exponent and the reaction mechanism.. The value of $n = 2$ is interpreted as a case of 2D-steady state homogenous nucleation with linear growth i.e. the nuclei appearing in constant time intervals.⁷⁹

Table 8.2: PALS and JMAK parameters for the micro-encapsulated accelerator system.

Temp (°C)	τ_0 (ns)	τ_∞ (ns)	$\Delta\tau$ (ns)	n	k	$t_{1/2}$ (h)	T_H (°C)	E_a (kJ/mol)
50	2.47	2.08	0.39	3.03	4.19E-07	113.0		
60	2.45	1.83	0.62	3.03	1.90E-06	67.8	141.9	74.5
70	2.55	1.98	0.57	3.06	3.00E-05	28.6		

* T_H values refer to curing temperatures obtained by DSC technique at 20K/min(S. Gramm AWOK, University of Kaiserslautern, *private communication*)

Whereas, the closest value to understand $n = 1.3$ in Table 4.1 (Section 4.5 of this thesis), is $n = 3/2$ and is known for the case of homogenous nucleation with 3D-diffusion controlled growth, with all nuclei present at time $t = 0$. However, it is still not clear as to why two completely different growth mechanisms have the same activation energy for the rate limiting step. Please note, that for a similar composition with pre-polymerized DGEBA and DICY matrix, as reported in Chapter 7 of this thesis, a value of $n = 3$ was observed at a temperature of 60°C and interpreted as the case of site-saturated homogenous nucleation with 3D-linear growth.

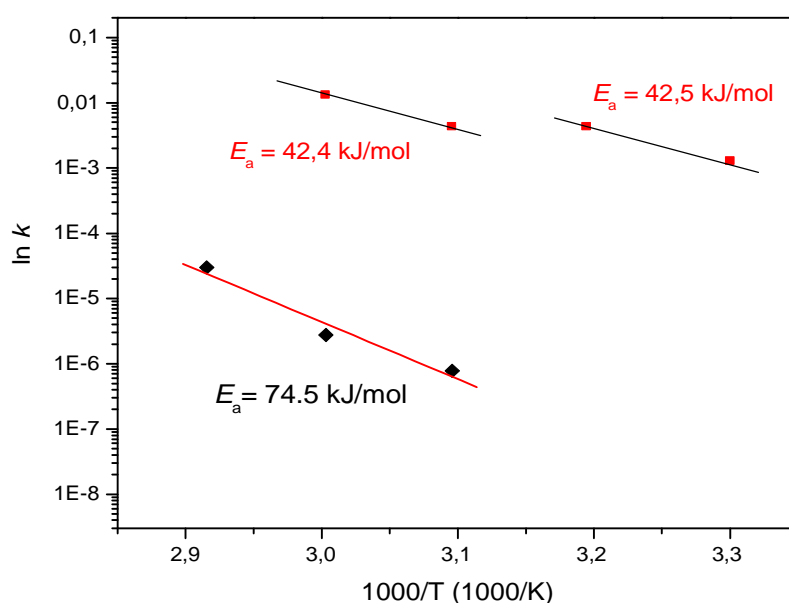


Fig. 8.6: Plots of $\ln k$ as a function of reciprocal temperature, with slope indicating the activation energies for the free (red squares) and encapsulated accelerator systems (black squares).

Table 8.2 shows the PALS and JMAK parameters for the formulation with encapsulated accelerator. The values of the Avrami exponent remain the same for all the measured temperatures i.e $n = 3$, suggesting that the curing mechanism remains the same within this particular temperature range. This value of $n = 3$ refers to a case of 3D- steady state homogenous nucleation. Once again it is remarked that for a similar system with pre-polymerized DGEBA-Dicy matrix a value of $n = 2$ was obtained (as already discussed in Chapter 7 of this thesis). In that case it was speculated as the case of homogenous nucleation with 2D-linear growth due to blocking of pore openings. However, in contrast the systems investigated here, consists of homogeneously distributed μ -Zeolite fillers and this helps with the release of accelerator molecules and the reader is referred to Chapter 9 of this thesis for a detailed understanding of this interpretation. It can be seen that the obtained values of E_a ,

calculated by the Arrhenius plots, for the micro-carrier encapsulated accelerator system is 74.5 kJ/mol. Which is higher than the activation energy of the free accelerator system ($E_a = 42.5$ kJ/mol). Apparently, the activation energy of the rate limiting step for the curing reaction increased when the accelerator is encapsulated, suggesting that it is difficult to react with the dicy-epoxy matrix due to the delay in release of the caged accelerator. Furthermore, an extrapolated shelf-life of this particular 1K-formulation was found to be approximately 400 hours.

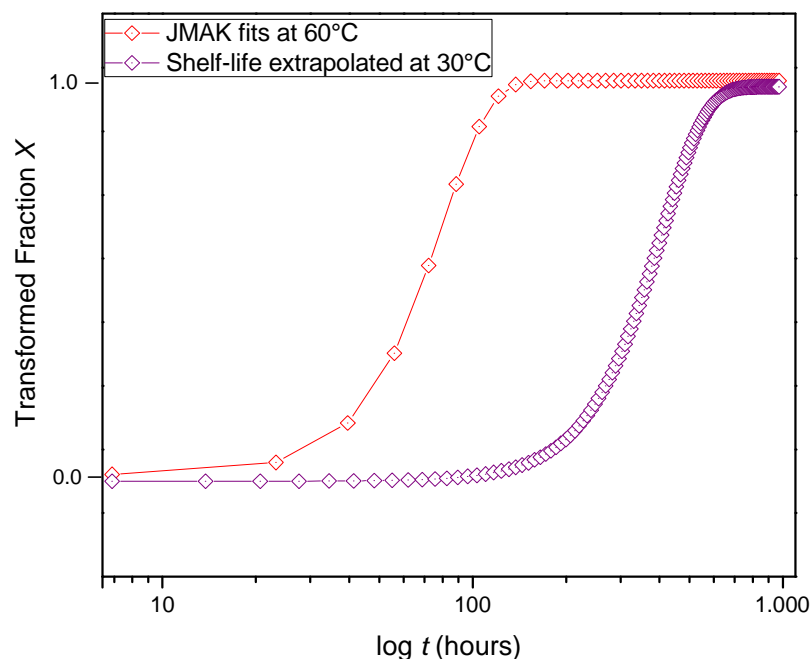


Fig 8.7: Extrapolated shelf life of the formulation with encapsulated accelerator at 30°C, with the help of Avrami parameters ($n = 3$ and $k = 1.08 \times 10^{-8}$).

The apparent rate constant k determines the rates of the nucleation and growth processes that control the curing rate. As seen from Table 8.2, the apparent rate constant k retains a remarkable sensitivity to the cure temperature. Values of k rise with increasing cure temperature, that is, the higher the temperature, the faster the cure rate. Whereas, an increase in the activation energy means that more energy is required for the reaction components to complete the reaction. Figure 8.8 shows the summarized results of extrapolated shelf life ($t_{1/2}$) at RT, hardening temperature (T_H) and the activation energies (E_a), as a function of the avrami exponent (n), for the free accelerator and the encapsulated accelerator systems in comparison to the Benchmark system results (as already discussed in Chapter 6).

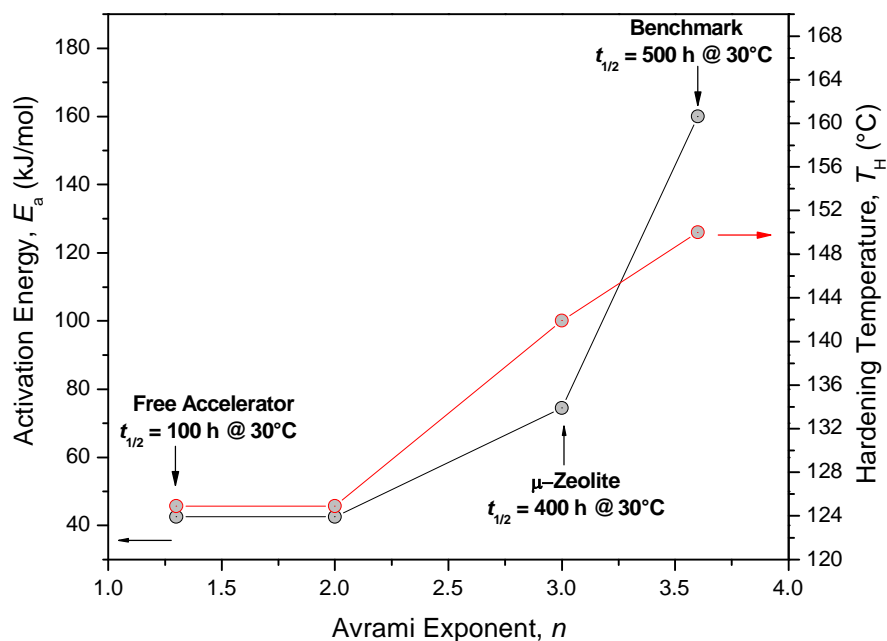


Fig 8.8: Extrapolated shelf life ($t_{1/2}$) at RT, Hardening Temperature (T_H) and Activation Energies (E_a), as a function of the Avrami Exponent (n), for the free accelerator and the encapsulated accelerator systems in comparison to the Benchmark system results (as discussed in Chapter 6).

The Benchmark system have higher activation energy and this might be due to lower reactivity of block uron accelerator (having a melting temperature of 180°C), which might retard the epoxy polymerization process (i.e. the delay in formation of cross-links). Therefore, resulting in a higher shelf life >3 months at RT and a higher curing temperature of approx. 150°C. On the contrary, the accelerator used in this work has a melting temperature lower than 0°C and therefore highly reactive at even at storage temperatures. The system with free accelerator has a shelf-life of approx. 100 hours and the lowest curing temperature of all i.e. $T_H = 124.9$ °C. Finally, it can be seen that encapsulation does help to increase the shelf-life to upto approx. 400 hours and at the same time the results for curing temperature are encouraging i.e. $T_H = 141.9$ °C

8.4 Summary & Conclusion

The isothermal conversion curves show that it takes increasingly longer times for the epoxy resin to fully cure as the temperature is decreased. It is possible to predict the final conversion for the isothermal cure of 1K formulations based on DGEBA-dicyandiamide at any reaction temperatures as long as they show Arrhenius behavior. In other words encapsulation is only possible if the 1K-formulations demonstrates similar reaction kinetics independent of temperature. The combination of PALS and JMAK provides a powerful tool for analyzing

cure and cross-linking reactions associated with thermosetting materials. It provides valuable information on the cure characteristics of 1K formulations, which in turn can be helpful to produce formulations with higher shelf-life and at the same time with lower hardening temperatures. The changes in the quantity or chemical constituents of the epoxy system significantly affect the reaction rate and the degree of cross-linking. Accelerants, retardants, and other additives affect the reaction process as well. This data of curing kinetics provides yet another tool for quantifying parameters of 1K-formulations, such as predicting process rates and estimating product lifetimes. The same approach should be equally useful in characterizing B-stage prepregs and other curing, vulcanizing, and polymerizing reaction systems.

9. Zeolite and Pyrogenic Silica filled Nanocomposites

In the previous sections of this thesis it was shown that how the hole free volume obtained from PALS is used as a measure of the transformed fraction of curing. It is also emphasized that this information can be used to study the curing kinetics of 1K-epoxy formulations with the help of JMAK theory of phase transformation. Now that the PALS is already established as a suitable technique to follow the in-situ curing and the shelf-life prediction of one-component epoxy resin formulations. In this Chapter a brief overview is given on various series of 1K-formulations, studied by PALS and the JMAK. There were three different types of carrier materials proposed for the encapsulation of accelerator i.e. Zeolites, pyrogenic silica and the layered silicates. In the following sections of this thesis only the selected formulations with Zeolites and pyrogenic silica carriers will be discussed, as due to the time constraints it was not possible to do the complete research with the layered silicate carriers within the scope of this PhD thesis. For example, to understand the release behaviour of accelerator, the concentration of accelerator is varied in a μ -Zeolite carrier and the curing kinetics studied for constant accelerator concentrations in DICY/EP formulation. Furthermore, the effect of micro and nano-Zeolite encapsulated accelerator as compared to the similar fillers with multi-stage encapsulation, on the shelf-life at elevated temperatures, the curing kinetics and the hole free volume is discussed. Whereas, for a constant concentration of accelerator encapsulated in an pyrogenic silica carrier, the curing kinetics are studied by varying the concentration of the accelerator in the dicyandiamide cured 1K-formulation.

9.1 Introduction

The term nano-composites means to distribute appropriate amounts of nanoparticles in a polymer matrix.¹⁵⁷ Nanotechnology means that one has to deal with huge surface areas, vast amounts of nano-fillers, and a small distance between them. Polymeric nano-composites can be considered as an important category of organic-inorganic hybrid materials, in which inorganic nanoscale building blocks (e.g., nanoparticles, nanotubes, or nanometer-thick sheets) are dispersed in an organic polymer matrix.¹⁵⁸ They represent the current trend in developing novel nanostructured materials. When compared to conventional composites based on micrometer-sized fillers, the interface between the filler particles and the matrix in a polymer nanocomposite constitutes a much greater area within the bulk material, and hence

influences the composite's properties to a much greater extent, even at rather low concentrations of the filler material.¹⁵⁹

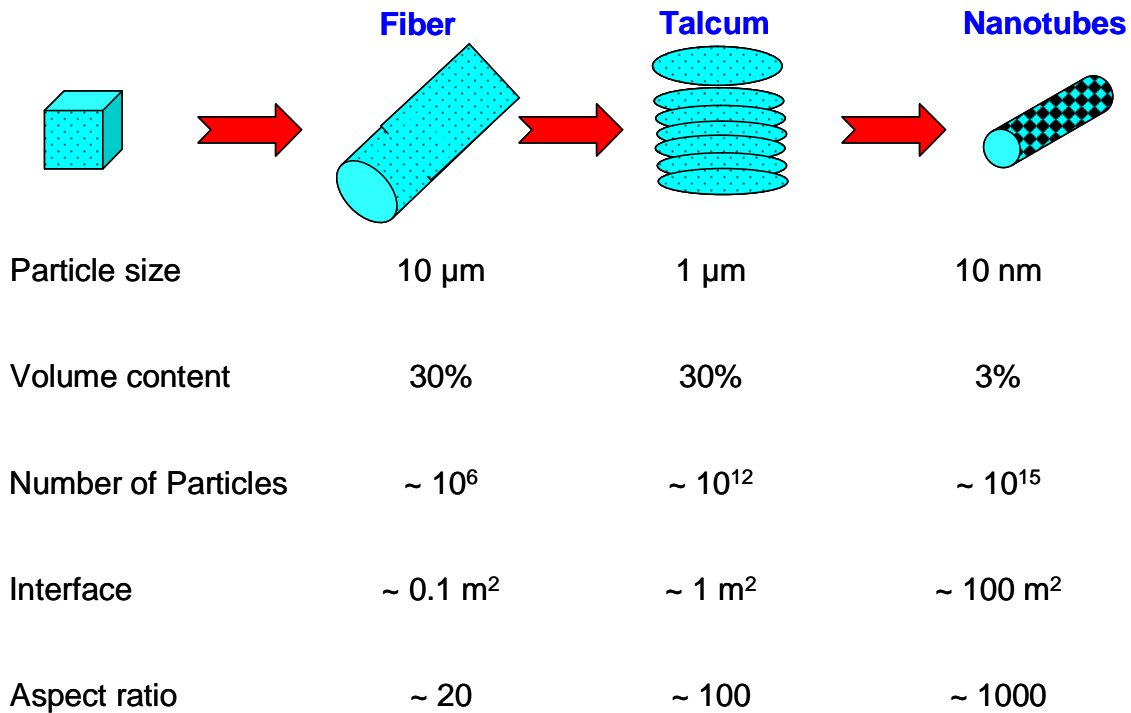


Fig. 9.1: Influence of different particles on the surface area (reconstructed image).¹⁵⁷

On one hand it is important to encapsulated accelerator in nano-sized carriers in order to achieve longer storage times, while on the other hand it is important to have sufficient amount of accelerator concentration in IK-formulations to achieve lower hardening temperatures. It is remarked here that it is extremely problematic to achieve high volume contents of nanotubes in a polymer matrix. All those who report contents in the range of 10% or more might have agglomerates rather than a proper distribution.¹⁵⁷ The key issue of numerous procedures for the preparation techniques of polymer nano-composites is that the geometry, spatial distribution, and volume content of the nano-fillers must be effectively controlled through adjusting the preparation conditions so as to ensure the optimum structural and property requirements of nano-composites.¹⁶⁰ However, in the context of this particular work it is acceptable to have enough filler concentration to have certain amount of accelerator concentration, which can lower the hardening temperatures (T_H) and at the same time prolonging the shelf-life ($t_{1/2}$) of IK-formulations at the storage temperatures. Therefore, to understand the effect of the interaction between the nanoparticles and the epoxy resin, the curing reaction kinetics of the composites have been studied.

9.2 Experimental

9.2.1 Synthesis of Micro and Nano-sized encapsulations

The Zeolite and pyrogenic silica based carrier materials were used for the encapsulation of accelerator. They were developed, optimised with respect to host-guest interactions and characterised with regards to the release and curing behaviour in epoxy adhesive formulations by Fraunhofer IFAM (Bremen, Germany). The nanozeolites (size < 500 nm) as the host system for accelerators were tailored according to computerised simulations by Fraunhofer IFAM (Bremen, Germany), developed by NanoScape (Martinsried, Munich, Germany), loaded with an accelerator and characterised by Fraunhofer IFAM with regard to the release and curing behaviour in epoxy adhesive formulations.¹⁶¹⁻¹⁶² Furthermore, the results discussed in Sections (9.3.2) and (9.3.3), refers to single-step and multi-stage encapsulations for the similar accelerator and carrier combinations, but due to patent reasons the details will not be disclosed here. For an overview of PALS analysis please refer to Chapter 2, 6, 7 and 8 of this thesis.

9.3 Accelerator encapsulation in Zeolite carriers

9.3.1 Effects of varying accelerator concentration in μ -Zeolite carriers

After establishing the combination of PALS data and the JMAK theory of transformation as the state of art technique to follow the in-situ curing in 1K- formulations, the focus of this PhD thesis was shifted towards the understanding of release behavior of the accelerator in the dicyandiamide hardened DGEBA matrix. A series of filler materials were prepared, with varying the concentration of the accelerator in the μ -Zeolite carrier. Whereas, the overall concentration of the accelerator is kept constant in the DICY/EP formulation. As before the PALS data is used to calculate the storage times ($t_{1/2}$) and the curing kinetics were studied by fitting the experimental data with the JMAK model.

Figure 9.2 shows as an example the Zeolite material used in this work, with a total surface area clearly above 300 m²/g. The two Zeolites compared here are a highly loaded one with 25 wt% of accelerator and a lower loaded one with 16 wt% of accelerator, these values were

obtained from the TGA results.¹⁶³ The saturation level or the maximum amount of accelerator concentrations is found out to be at loadings clearly above 20 wt%.¹⁶³

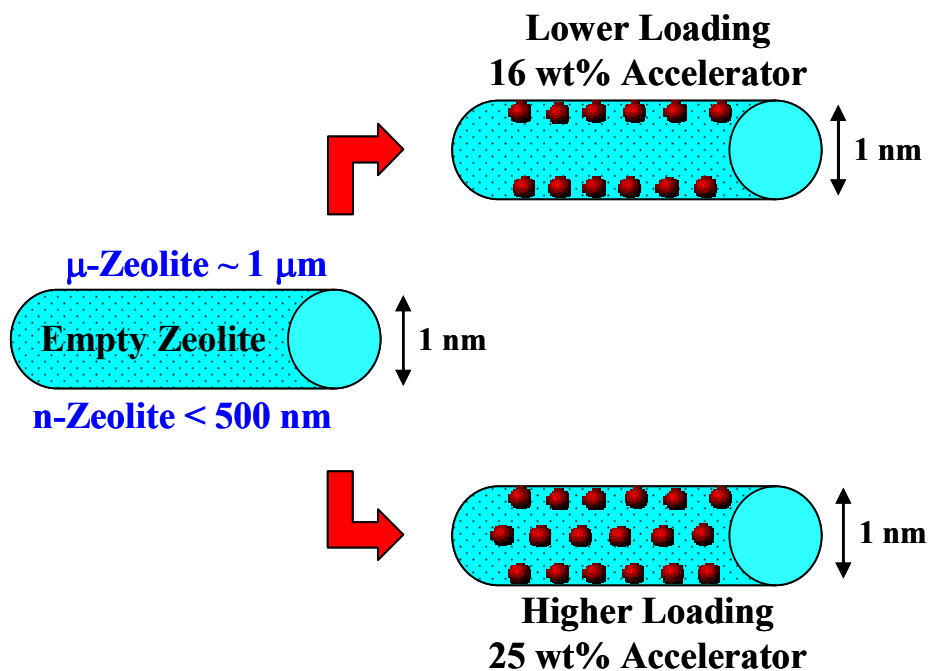


Fig. 9.2: Schematic of the μ -Zeolite carrier before and after loading with the accelerator.

The isothermal plots measured at elevated temperatures of 60°C for the formulations with lower and the highly loaded μ -Zeolite carriers are indicated in Fig.9.3, where the *ortho*-Positronium lifetimes are plotted as a function of logarithmic annealing times. The overall concentration of the accelerator in DICY/EP formulation was varied at 0.15 and 0.5 wt%. The parameters obtained from PALS and JMAK are listed in Tab. (9.1). It can be clearly seen that with increasing accelerator concentration from 16 to 25 wt%, the shelf-life of 1K-formulations is directly affected. The Avrami exponent for the formulations with 0.15 wt% accelerator was found out to be $n = 3.2$ and is approximately the same as compared to the 0.5 wt% accelerator formulations with $n = 3.3$. This on one hand indicates that the reaction mechanism remains the same if similar concentrations of accelerator is used in DICY/EP formulations and is independent of the accelerator concentration in the μ -Zeolite carrier.

Furthermore, the values of $\Delta\tau$ for the highly loaded systems is slightly greater than the lower concentration filler systems, suggesting a higher degree of cross-linking due to the presence of excess amounts of accelerator molecules in the highly loaded carriers. The surface to volume ratio is a key parameter here, as lower the concentration of accelerator the higher the possibility of accelerator molecules to find preferential binding sites with high binding

energies, within the carrier material. As for the case of highly loaded Zeolite carrier with 25 wt% of accelerator concentration, the excess molecules of accelerator are free to react with the DICY/EP matrix once the filler material is dispersed in the matrix. This has two disadvantages, firstly there is no controlled release and secondly this will reduced the shelf-life of the 1K-formulations, as indicated by the results in Tab. 9.1.

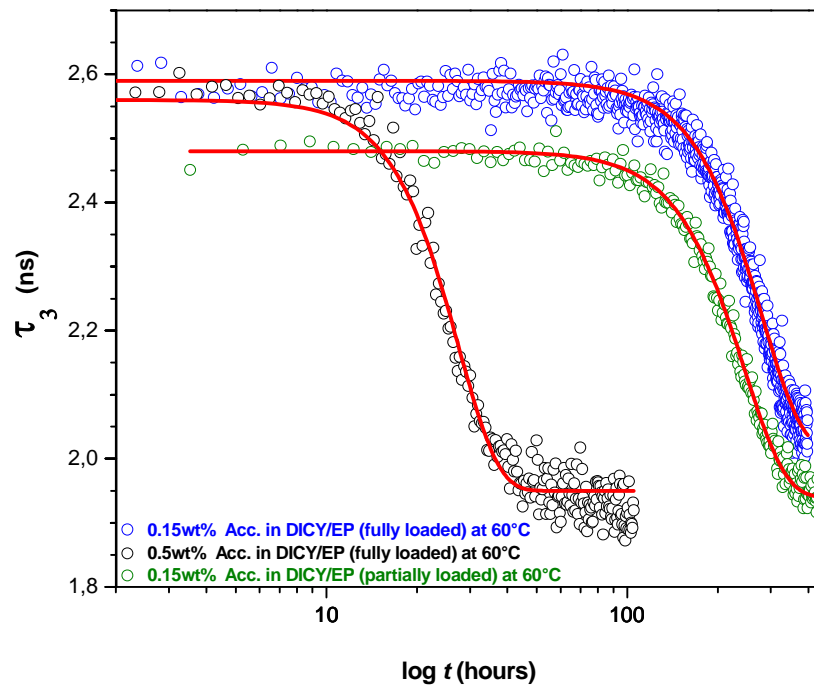


Fig. 9.3: The *ortho*-Positronium lifetime as a function of isothermal annealing time for the partially and the fully loaded accelerator in μ -Zeolite carrier at elevated temperatures of 60 °C.

Table 9.1: PALS and JMAK parameters for the partially and the fully loaded μ -Zeolite carriers.

Accelerator in μ -Zeolite	Accelerator in DICY/EP	τ_0	τ_∞	$\Delta\tau$	n	k	$t_{1/2}$ (h)
16 wt%	0.15 wt%	2.48	1.94	0.54	3.20	2.29E-08	218,
16 wt%	0.5 wt%	2.48	1.95	0.53	3.30	1.35E-08	38,
25 wt%	0.15 wt%	2.59	2.01	0.58	3.21	1.44E-08	243,
25 wt%	0.5 wt%	2.56	1.95	0.61	3.29	2.00E-05	24,

Furthermore, a series of experiments were performed to understand the release behavior of the accelerator with respect to different loading concentrations of accelerator in the μ -Zeolite carrier. Once again isothermal annealing is done at elevated temperature of 60 °C and in order to have a better comparison the concentration of accelerator was kept constant at 0.5 wt% in the DICY/EP formulations. Figure 9.4 shows the *o*-Ps lifetime as a function of annealing time for the complete

series with varying concentration from 11 wt% to 22 wt%. The important parameters obtained are summed up in Tab. 9.2.

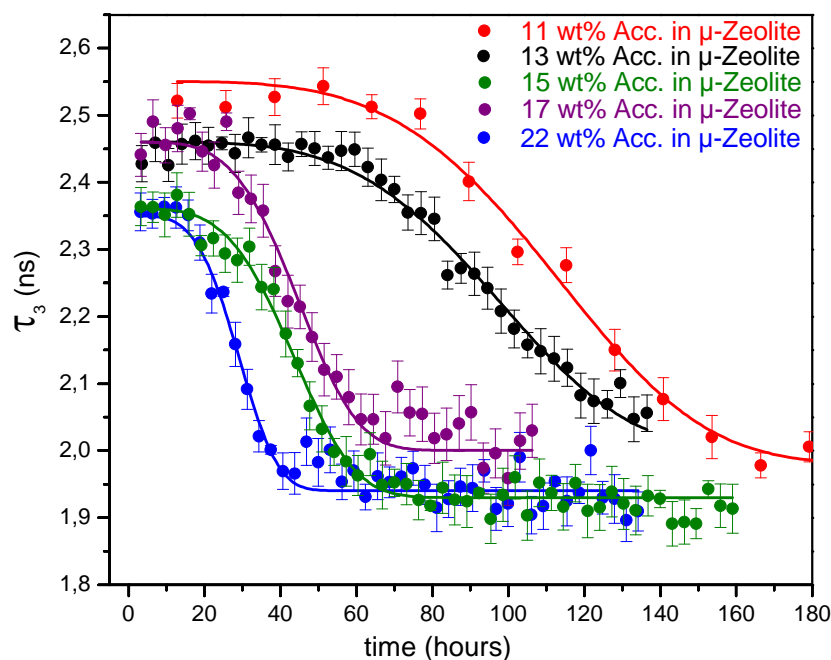


Fig. 9.4: The *ortho*-Positronium lifetime as a function of annealing times for the series of μ -Zeolite encapsulated accelerator at elevated temperatures of 60 °C. The concentration of accelerator was kept constant at 0.5 wt% in the DICY/EP formulations.

Table 9.2: PALS and JMAK parameters for the series with varying concentration of accelerator in μ -Zeolite carriers.

Accelerator in μ -Zeolite	Acc. in DICY/EP	Module (wt%)	τ_0	τ_∞	$\Delta\tau$	n	k	$t_{1/2}$ (h)
11 wt%	0.5 wt%	4.55	2.55	1.98	0.57	3.99	4.75E-09	114,
13 wt%	0.5 wt%	3.85	2.46	2.00	0.46	3.91	1.23E-08	91,
15 wt%	0.5 wt%	3.33	2.36	1.93	0.43	3.79	4.54E-07	43,
17 wt%	0.5 wt%	2.94	2.46	2.00	0.46	3.96	2.10E-07	41,
22 wt%	0.5 wt%	2.27	2.35	1.94	0.41	3.93	1.30E-06	28,

As expected, the increase in accelerator concentration from 11 wt% to 22 wt% reduces the shelf-life at 60 °C from 114 hours to 28 hours. The avrami exponent remains in the range of 3.79 to 3.99 for this series, whereas the reaction constant showed an increase with increasing accelerator concentrations. The value of $\Delta\tau$ is the highest (0.57) for the formulation containing the lowest concentration of accelerator, whereas the rest of the systems have more or less the same value of $\Delta\tau$. In the previous discussion (Page 108, last paragraph), a higher $\Delta\tau$ was presumed as a higher degree of cross-linking due to excess concentration of accelerator. However, here this could be tentatively interpreted as higher degree of cross-linking due to exposure of long annealing times at elevated temperatures.

9.3.2 Single-step micro and nano-sized encapsulations

The results discussed in the previous Section (9.3.1), are for the formulations with μ -sized Zeolite carrier with a particle size of $\sim 1 \mu\text{m}$. In this section a comparison is made to the study the effect of particle size on curing kinetics. As an example the accelerator was encapsulated in micro and nano-sized Zeolite carrier in a single-step, with respective particle size of $\sim 1 \mu\text{m}$ and $< 500 \text{ nm}$. The only difference is that the nano-Zeolite is loaded with 14 wt% accelerator, whereas the concentration of accelerator in micro-sized carrier is 12 wt%. However, the overall concentration of accelerator in both formulations is kept constant at 1.0 wt%. This means more quantity of the micro-sized filler material is required as compared to the formulation with nano-filler. Furthermore, a comparison of hardening temperatures obtained by DSC,¹⁶⁴ as a function of storage times and the varying concentration of accelerator in the nano and μ -Zeolite carriers is done.

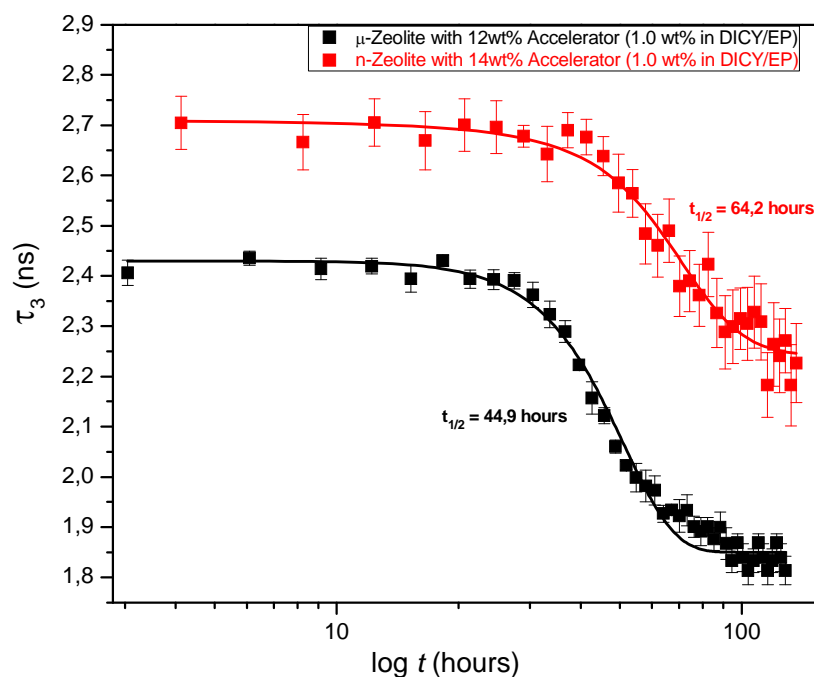


Fig. 9.5: The *ortho*-Positronium lifetime for the accelerator encapsulated by single-step in micro (Black squares) and nano-sized (Red squares) Zeolite carrier formulations, as a function of logarithmic annealing times at elevated temperatures of 60 °C.

Figure 9.5 shows the plots of *o*-Ps lifetime as a function of logarithmic annealing times at elevated temperature of 60 °C. The formulation with accelerator encapsulated in nano-Zeolite has a higher storage life of approx. 64 hours as compared to the one with micro-Zeolite (~ 45 hours). Although the overall concentration of the accelerator in DICY/EP formulation is same

(1.0wt%), but since the μ -Zeolite carrier was loaded with 12 wt % of accelerator, which means more quantity of filler material is present in this formulation i.e 8.33 wt% as compared to the one with nano-Zeolite (7.14 wt%). As indicated in Tab. 9.3, on one hand this high loading concentration of filler material leads to a reduction in $t_{1/2}$ value for the μ -Zeolite formulation i.e. 45 hours as compared to the formulation with nano-Zeolite (64 hours). While on the other hand, it leads to a higher value of hardening temperature ($T_H = 137.7$ °C) for the μ -Zeolite system as compared to the nano-Zeolite formulation ($T_H = 136.1$ °C).

Table 9.3: PALS and JMAK parameters for the formulations with single-step encapsulations with micro and nano-size Zeolite carrier at 60 °C.

Accelerator in Zeolite	Module (wt%)	τ_0	τ_∞	$\Delta\tau$	n	k	$t_{1/2}$ (h)	T_H (°C)
14 wt%								
(n-Zeolite)	7.14	2.71	2.24	0.47	2.90	3.33E-06	64,	136,1
12 wt%								
(μ -Zeolite)	8.33	2.43	1.85	0.58	3.50	1.12E-06	45,	137,7

* T_H values refer to curing temperatures obtained by DSC technique at 20K/min.¹⁶⁴

Although the values of reaction constant k are acceptable given the storage times, but the change in Avrami exponent suggests a different kind of reaction mechanism for the two formulations. Furthermore, the $\Delta\tau$ value for the μ -Zeolite formulation (0.58) is higher as compared to the nano-Zeolite system (0.47), again suggesting a higher degree of cross-linking due to an easy release of accelerator. On the contrary, for the nano-Zeolite encapsulated system, there is a delay in the release of accelerator as the nanoparticles tend to form agglomerates, which might cause a blockage of accelerator exits (see for example Fig. 9.6).

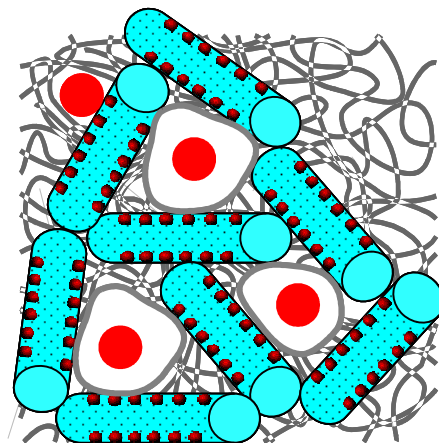


Fig. 9.6: Schematic representation of the possible structures of the cured nanocomposites with agglomerates of nanoparticles (single-step encapsulation), as probed by *o*-Ps.

Interestingly, the τ_0 and τ_∞ values for the system with nano-Zeolite are considerably higher as compared to the formulation with μ -Zeolite. This reconfirms the above-mentioned interpretation, that the nano-filler particles tend to form agglomerates when dispersed in the epoxy matrix and therefore resulting in higher τ_0 and τ_∞ values. It is noteworthy that the problem with dispersive mixing is that the nanoparticles commercially available usually exist in the form of agglomerates, which are difficult to disconnect by the limited shear force during mixing. This is true even when a coupling agent is used,¹⁶⁵ since it can only react with the nanoparticles on the surface of the agglomerates. The latter will maintain their friable structure in the composite and can hardly provide property improvements at all. Even the higher value of storage time $t_{1/2}$, for the nano-Zeolite based formulation as compared to the μ -Zeolite system, agrees with this speculation of agglomerates formation. Since there will be a delay in the release of accelerator due to blockage of pore openings and therefore results in an increased shelf-life.

9.3.3 Multi-stage micro and nano-Zeolite encapsulations

Another possibility of achieving even higher storage life is by closing the pore mouths of the Zeolite carrier with the help of multi-stage encapsulations. Even the positive effects of nanoparticles can be brought into play if nanoparticle agglomerates themselves are reinforced prior to the compounding procedure, since a further promotion of the dispersion by existing methods might be too ideal to be realized. Nanoparticles can be pretreated to introduce grafting polymers onto their surface not only outside but also inside the particle agglomerates. Owing to their low molecular weight, the monomers can penetrate into the agglomerated nanoparticles easily and react with the activated sites of the latter. The interstitial volume inside the nanoparticle agglomerates will be partly filled with grafting macromolecular chains, and the agglomerated nanoparticles will be even closer, therefore reducing the size of big voids between them. In addition, the surface of the nanoparticles will also become "hydrocarbonated" due to an increased hydrophobicity resulting from the grafting polymer. This is beneficial for the filler/matrix miscibility and hence for the ultimate properties.¹⁶⁶ When the pre-grafted nanoparticles are mixed with the melt of a thermoplastic polymer, the filler/matrix interfacial adhesion can be improved by the grafting polymers chemically bonded onto the nanoparticles, in particular by creating entanglements with the matrix molecules

It is well known that cross-linking changes the local molecular packing and leads to a decrease in free volume.¹⁶⁷ A feature of rapid polymerization in cross-linking systems is that the material may not have time to relax to its equilibrium density; hence, more free volume will be available.¹⁶⁸ Generally, all photoinitiated polymerizations and analogous systems will see a competition between cure speed and cure depth; the more rapidly a cross-linking or grafting polymerization proceeds, the less likely it is to give a homogeneous product.

As shown in Fig. 9.7, that multi-stage encapsulation reduces the *o*-Ps lifetimes for the nano-Zeolite encapsulated formulation, which can be interpreted as reduction in the size of agglomerates. In the case of a thermosetting matrix polymer an encapsulation with reactive moieties might lead to the grafting of formed polymer to the surface of the carrier material. The grafted nanoparticles will keep their more stationary suspended state due to the interaction between the grafting polymer and the matrix. After curing such a mixture, the filler/matrix adhesion would also be substantially enhanced by chain entanglement and/or chemical bonding between the grafting polymer and the matrix material. In this context, the desired uniform dispersion of nanoparticles in the matrices on a nanometer level might no longer be critical.

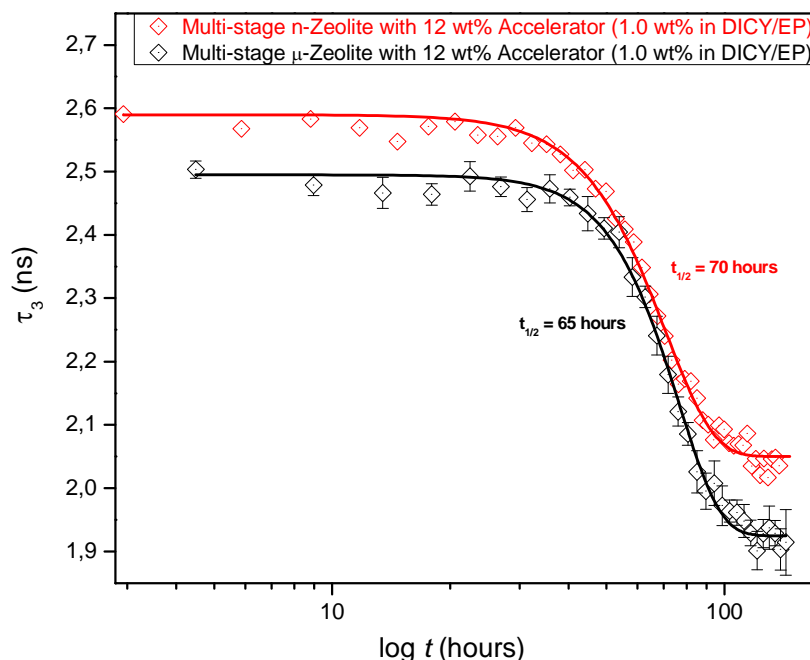


Fig 9.7: The *o*-Ps lifetime as a function of annealing times measured at 60 °C for the 1K-formulations with multi-stage encapsulations with nano(red) and micro-sized(black) carrier.

Table 9.4 shows all the important parameters of the PALS and JMAK analysis for the series of 1K-formulations with multi-stage encapsulation of fillers. It can be seen that for a similar

concentration of filler material for micro and nano-sized carrier systems, the value of $\Delta\tau$ remains almost the same. The change in Avrami exponent again indicating a different kind of reaction mechanism, whereas the reaction constant k is in agreement with the storage times for the two systems i.e. higher the storage time, lower the value of reaction constant.

Table 9.4: PALS and JMAK parameters for the micro and n-Zeolite formulations with multi-stage encapsulations.

Accelerator in Zeolite	Module (wt%)	τ_0	τ_∞	$\Delta\tau$	n	k	$t_{1/2}$ (h)	T_H (°C)
12 wt% (n-Zeolite)	8.33	2,59	2,05	0,54	3,51	3,28E-07	65,	136,3
12 wt% (μ -Zeolite)	8.33	2,50	1,93	0,57	4,09	2,04E-08	70,	141,9

* T_H values refer to curing temperatures obtained by DSC technique at 20K/min.¹⁶⁴

Furthermore, it was observed that multi-stage encapsulation increases the storage time of μ -Zeolite system, from 45 to approximately 70 hours, and even the hardening temperatures increase from 137.7 to 141.9 °C. The hardening temperature for the nano-Zeolite based formulation remains almost the same and seems to be independent of multi-stage encapsulation process. But here it is remarked that the n-Zeolite with single-step encapsulation has almost 14 wt% of accelerator (with 7.14 wt% of filler material in DICY/EP), whereas the multi-stage encapsulation has a concentration of 12 wt% (with 8.33 wt% of filler material in DICY/EP). Therefore, a better comparison can be made if the amounts of concentrations are kept constant for the nano-sized Zeolite carrier, both single and multi-stage encapsulated.

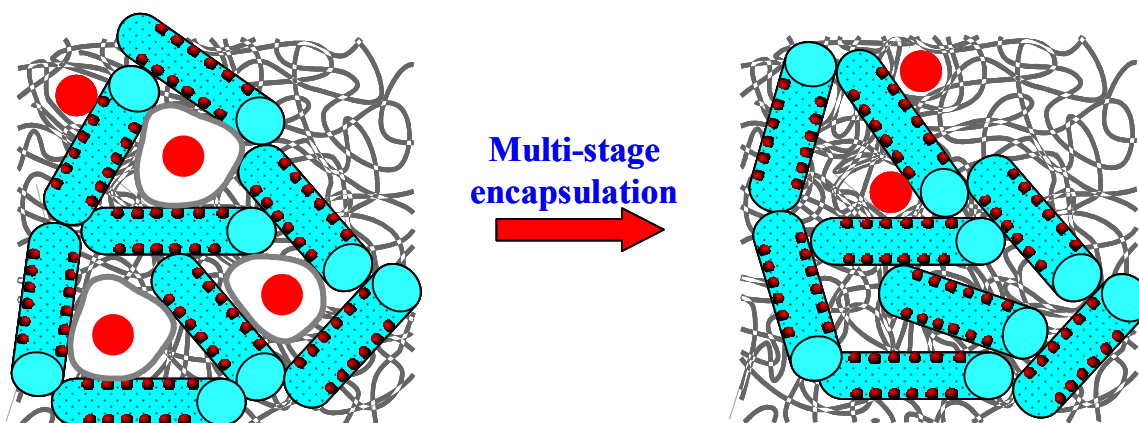


Fig. 9.8: Schematic representation of the possible nanocomposite structures with agglomerates of nanoparticles for both single-step and multi-stage encapsulations, as probed by *o*-Ps.

Another explanation can be due to already cured matrix on the surface of carrier materials, the nano-fillers tend to form an extra free volume around them and therefore resulting in a higher value of the averaged *o*-Ps lifetime for both τ_0 and the τ_∞ .

9.4 Accelerator encapsulation on Pyrogenic Silica carriers

Nanosilica or Pyrogenic silica is a fumed silica product developed in 1942 by Degussa AG (currently Evonik Degussa GmbH) in Germany and also a registered trademark. It is highly dispersed, amorphous, very pure silica that is produced by high-temperature hydrolysis of silicon tetrachloride in an oxyhydrogen gas flame.¹⁶⁹⁻¹⁷⁰ It is a white, fluffy powder consisting of spherically shaped primary particles. The primary particles are spherical and free of pores. They can develop aggregates upon interaction with flame, which join together reversibly to form agglomerates. In contrast to precipitated silicas, Pyrogenic silica does not have a clearly defined agglomerate size. Particle size distribution becomes wider as the average primary particle size increases (see for example Fig. 9.10),¹⁷¹ and the tendency to form agglomerates is reduced. The average diameters of the primary particles are in the range of 12 to 40 nm, whereas, these extremely small particles naturally result in a large specific surface area, ranging from approximately 50 m²/g to 200 m²/g.¹⁷²

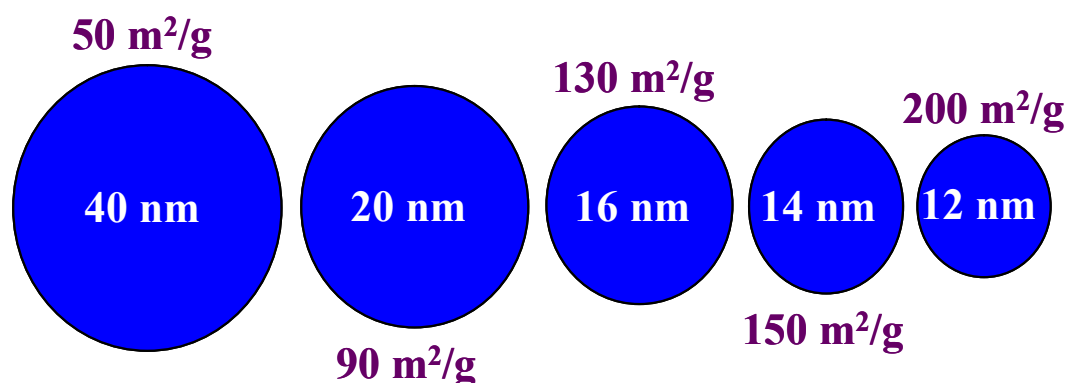


Fig. 9.9: Average primary particle size and their respective surface areas.

Figure 9.9 shows as an example the average particle size and the respective surface areas for the various types of pyrogenic silica fillers investigated during the course of this PhD thesis. Standard hydrophilic products are made of primary particles from 12 nm to 40 nm, and also these products are surface modified to hydrophobic (see for example Fig. 9.11).

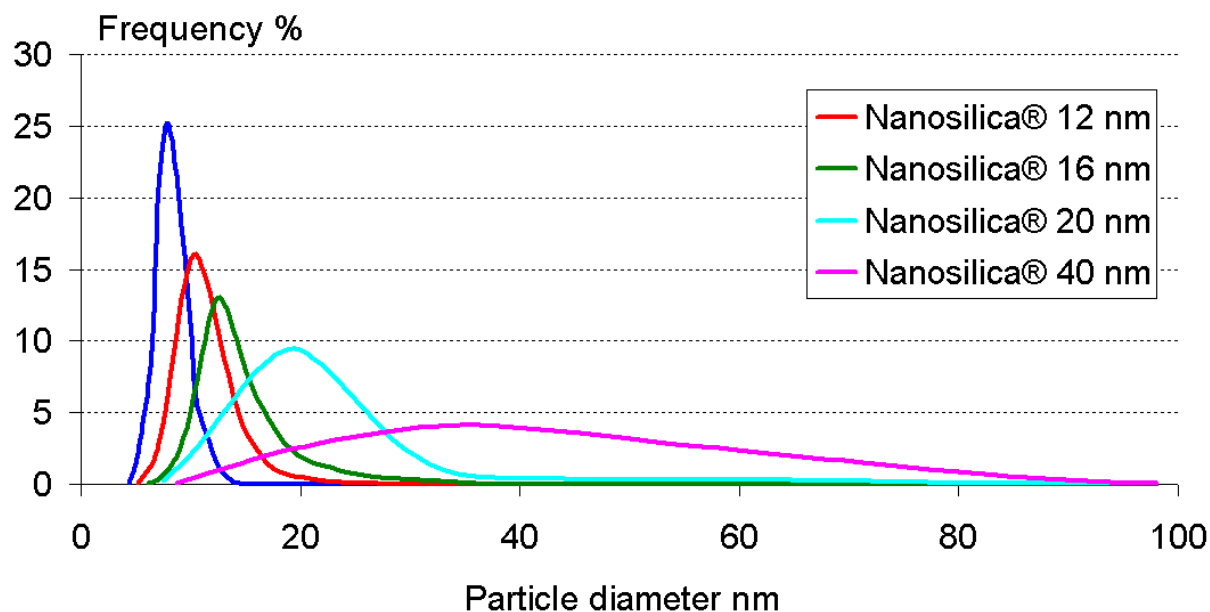


Fig. 9.10: Particle size distributions of various grades of nanosilica. (Courtesy of Evonik Degussa GmbH)¹⁷¹⁻¹⁷²

The size of the surface area is easily illustrated if one considers that approximately 20 g of pyrogenic silica (average primary particle size is 12 nm) has the same surface area as the size of a football field. Pyrogenic silica consists entirely of amorphous silicon dioxide and it starts to sinter and turn into glass above 1200 °C. Crystallization only occurs after heat treatment and pyrogenic silicas are nearly insoluble in water. They are also insoluble in acids, but they do dissolve in strong alkaline media to form silicates. Pyrogenic silica are successfully used in numerous applications such as a reinforcing filler, a thickening and thixotropic agent, as an anti-settling agent or for a free-flow aid. However, within the scope of this PhD thesis the pyrogenic silica are used as a carrier material for the encapsulation of accelerator to obtain higher storage time and lower hardening temperature for 1K-formulations.

9.4.1 Effects of varying accelerator concentration in 1K- formulation

There are different reactive groups such as siloxane or silanol are situated on the surface of the fumed silica particles. The latter are responsible for the hydrophilic behavior of untreated fumed silica. Furthermore, the fumed silica can be surface-modified by the reaction of the silanol groups with suitable compounds. After surface modification, the accelerator can be easily encapsulated on the surface of the pyrogenic silica (as illustrated in Fig. 9.11). In the following sections of this Chapter, the effect of different accelerator concentrations with respect to different particle sizes and different surface areas is discussed. Due to the non-

disclosure agreements related to this research the discussion will be kept simple and the information about the average particle size and the surface area of the nanosilica carriers will not be revealed here. For example, a comparison of low and high surface area nanosilica particles with different loading concentrations is done in the following sections of this Chapter.

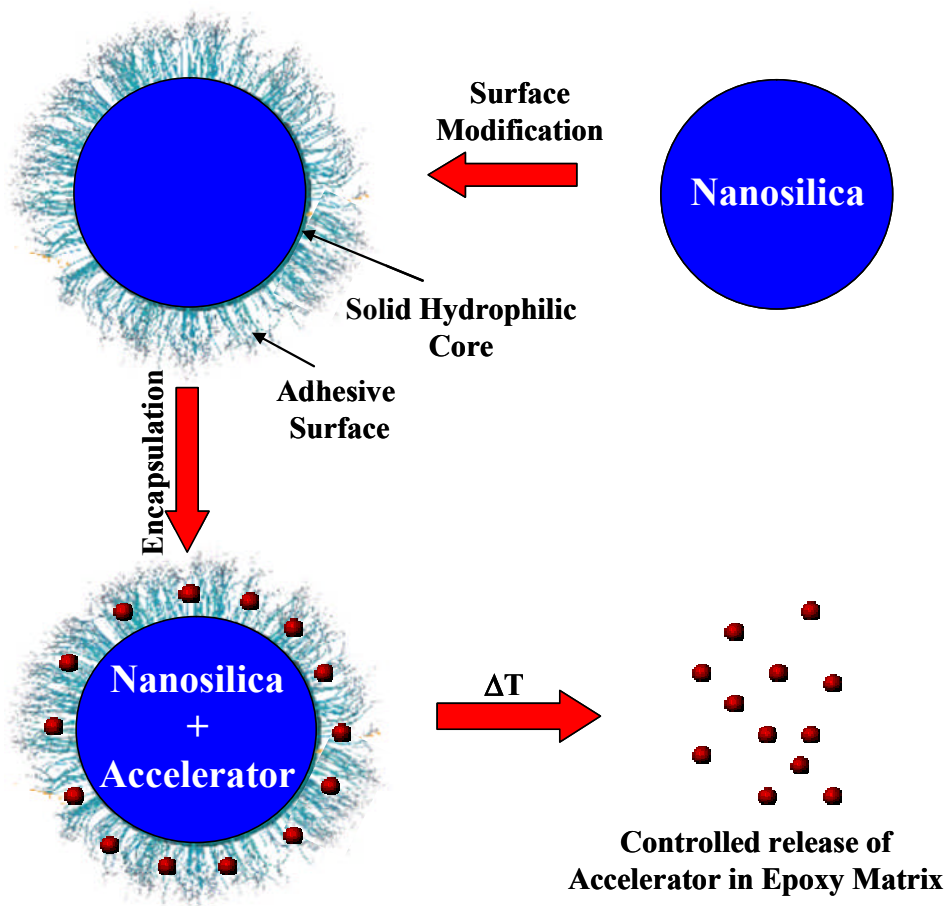


Fig. 9.11: Schematic of accelerator encapsulation on the surface of nano-sized pyrogenic silica carriers, with controlled release in epoxy-resin matrix.

First of all, the series with varying concentration of accelerator in 1K DICY/EP formulation, where a constant accelerator concentration of 5 wt% is encapsulated on the modified surface of a pyrogenic silica with relatively low surface area. Figure 9.12 shows the JMAK fits to the *o*-Ps lifetime as a function of logarithmic annealing times at a temperature of 60 °C. The formulations measured in this series were prepared with the same aerosol filler loaded with an accelerator concentration of 5 wt%. Whereas, the overall concentration of the accelerator in the DICY/EP formulations is varied from 0.15 wt% to 0.8 wt%.

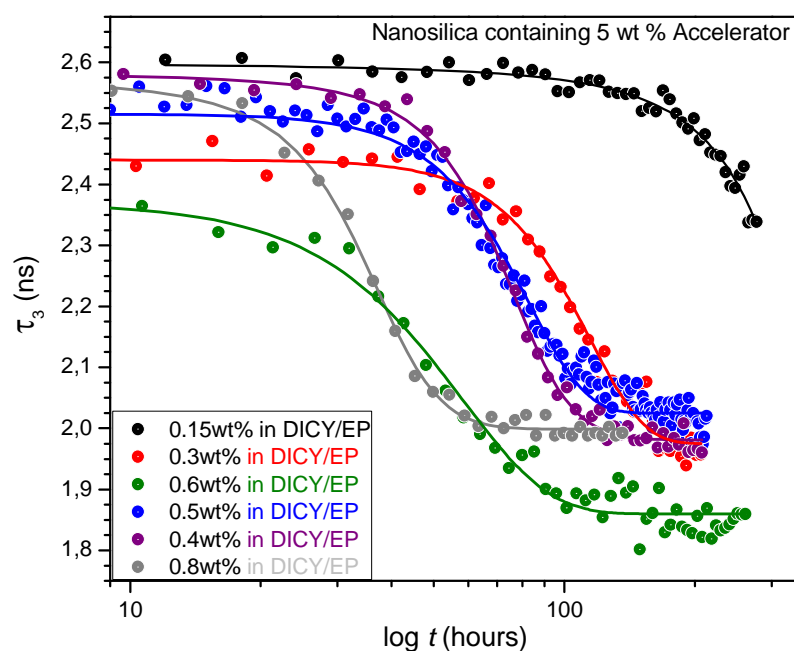


Fig 9.12: JMAK fits to the *o*-Ps lifetime as a function of annealing times measured at 60 °C for the 1K-formulations with different concentration of accelerator. Whereas, the concentration of accelerator was constant at 5 wt% in the nanosilica carrier.

Table 9.5: Important parameters for varying concentration of accelerator in DICY/EP system.

Accelerator in DICY/EP	Module (wt%)	τ_0 (ns)	τ_∞ (ns)	$\Delta\tau$ (ns)	n	k	$t_{1/2}$ (h)	T_H (°C)
0.15 wt%	3	-	-	-	-	-	310,	-
0.3 wt%	6	2.44	1.98	0.46	3.48	6.78E-08	102,	-
0.4 wt%	8	2.58	1.98	0.60	3.49	2.36E-07	70,	-
0.5 wt%	10	2.56	2.02	0.54	2.49	2.00E-05	69,	145,5
0.6 wt%	12	2.37	1.86	0.51	2.17	1.50E-04	42,	143,3
0.8 wt%	16	2.55	2.00	0.55	3.51	2.69E-06	34,	138,4

* T_H values refer to curing temperatures obtained by DSC technique at 20K/min.¹⁶⁴

All the available parameters from PALS and JMAK are listed in Tab. (9.5). The change in Avrami exponent ' n ' at concentrations of 0.5 and 0.6 wt% indicates poor dispersibility due to due to the experimental errors caused during the preparation of these samples. In addition, it should be noted that there is already 4 wt% of another nanosilica filler present in the matrix, with an average particle size of 14 nm and a respective surface area of 150 m²/g.¹⁷¹ Which means that the overall concentration of the nano-filler in the 1K-DICY/EP formulation is approximately 14 and 16 wt%, respectively for the 0.5 and 0.6 wt% of accelerator in DICY/EP.

Although the storage values reflect the expected behaviour i.e. reduction in storage times with increase of accelerator concentrations or vice versa. But particularly these nanosilica encapsulated formulations are difficult to prepare or mix due to high weight concentration of nano-filler(module) material. Therefore, the inconsistency in Avrami parameters reflects poor dispersibility. Ideally, at a constant temperature of comparison, it was expected to have similar values of n , as observed for the systems with Zeolite encapsulated accelerator. In other words, to make a better comparison between the benchmark formulation and the formulation with encapsulated accelerator, it was necessary that the filler material used for benchmark formulation should also be used in the other formulations.

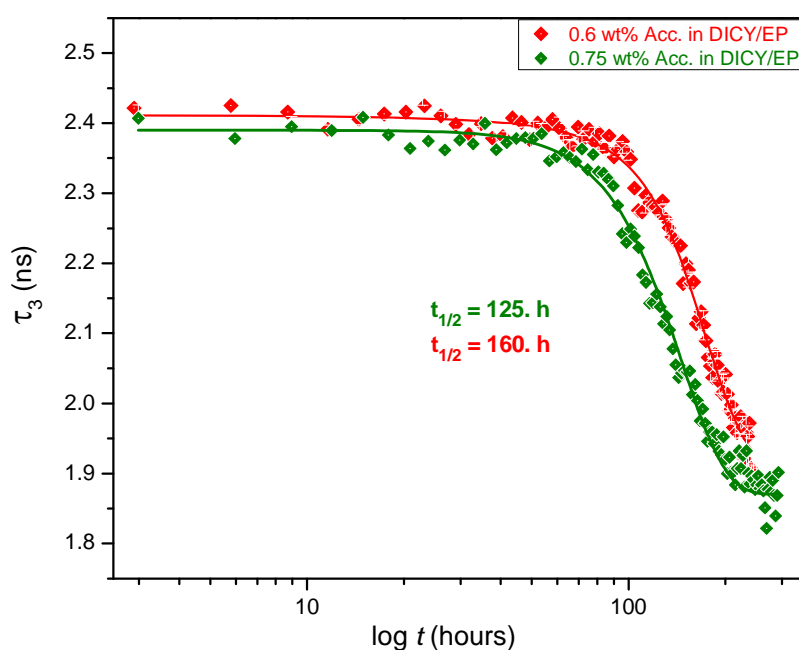


Fig 9.13: JMAK fits to the *o*-Ps lifetime as a function of annealing times measured at 60 °C for the 1K-formulations with different concentration of accelerator. Whereas, the concentration of accelerator was constant at 6.5 wt% in the nanosilica carrier.

Furthermore, isothermal annealing is performed for 1K-formulations with a varying concentration of accelerator in the DICY/EP system. This time the accelerator is encapsulated on the surface of a pyrogenic silica with a high surface area. The concentration of accelerator is fixed at 6.5 wt% in the carrier materials, whereas the overall concentration of accelerator is varied from 0.5 to 1.0 wt% in the 1K-formulation. The *o*-Ps lifetime as a function of logarithmic annealing times and the JMAK fits for selected formulations is shown in Fig. (9.13). Table 9.6 shows the JMAK and PALS parameters for this particular series of formulations. As expected, the storage times decrease with increasing concentration of accelerator in the DICY/EP system. The Avrami exponent remains in the range of 3.2 to 3.4, suggesting that the reaction mechanism reflects the curing transformation in the bulk matrix

and remains independent of the accelerator and the overall nano-filler concentrations in the DICY/EP. Whereas, the reaction constant ' k ' shows a behavior similar to the previous results i.e. higher the storage times, lower the value of reaction constant.

Table 9.6: Important parameters for varying concentration of accelerator in DICY/EP system.

Accelerator in DICY/EP	Filler (wt%)	τ_0 (ns)	τ_∞ (ns)	$\Delta\tau$ (ns)	n	k	$t_{1/2}$ (h)	T_H (°C)
0.5 wt%	7.7	-	-	-	-	-	> 200.	148.
0.6 wt%	9.2	2,41	1,91	0,50	3,40	2,56E-08	160.	153.3
0.75 wt%	11.2	2,39	1,87	0,52	3,20	1,63E-07	125.	149.7
0.8 wt%	12.						60.	149.
1.0 wt%	15.	2,55	2,05	0,55	3,20	1,67E-06	61.	-

* T_H values refer to curing temperatures obtained by DSC technique at 20K/min.¹⁶⁴

The data for the hardening temperatures obtained from DSC experiments does not show any particular trend. The values of $\Delta\tau$ remains more or less constant for all the available formulations. But interestingly, the τ_0 and the τ_∞ values for the system with higher weight concentration are relatively higher as compared to the other formulations. This on one hand can be tentatively interpreted as the formation of agglomerates and therefore results in an increase of the averaged σ -Ps lifetimes, while on the other hand it re-confirms that the Avrami exponent and the $\Delta\tau$ reflects the curing transformation of the bulk matrix alone.

9.5 Summary & Conclusions

It is shown that the combination of PALS and JMAK theory of transformation is a sensitive tool to follow not only the in-situ curing of 1K-formulations, but also to understand the effect of different loading concentrations of the accelerator and the nano-filler on the release behavior. However, as an outlook it would make complete sense if the benchmark system should be dispersed with the same type of nano-filler, which will be used later on for the encapsulation of accelerator. This on one hand will solve the problem of dispersibility due to high concentrations of nano-fillers and on the other hand when compared with the system in which encapsulated accelerator is used, it will only give information about the release behavior of the accelerator in the epoxy matrix. This in turn will be helpful to further tune up the optimum loading concentration of accelerator in the filler material to achieve a higher storage life and at the same time reducing the hardening temperatures.

10. Summary & Outlook

The investigation of the curing kinetics for the state of the art one-component dicyandiamide cured DGEBA formulation, at elevated temperatures is reported for the first time, in terms of the experimental data obtained from the PALS technique combined with the JMAK theory of transformation. It allows to estimate the shelf-life of these formulations at storage temperatures, which otherwise is being done with time consuming methods and techniques. The results are detailed in Chapters 6, 7, 8 and 9 of this thesis, it can be seen that the curing kinetics and storage times at elevated temperatures for a large number of one-component epoxy resin formulations is studied with the help of PALS. The storage times obtained from the PALS data were compared for some of the formulations with the IR-Spectroscopy data, which showed a good correlation.

Furthermore, the accelerator is encapsulated in the micro and nano-carriers to increase the shelf life of epoxy formulations. But at the same time it was important from the industrial applications point of view, to decrease the hardening temperature, so that the energy costs can be reduced. Therefore, to understand the release behavior of the accelerator, firstly the concentration of accelerator in the micro and nano carriers was varied, whereas the concentration of the accelerator in DICY/Epoxy formulations was constant. Secondly, at a constant concentration of the accelerator in the micro and nano-carriers, the curing kinetics are studied by varying the concentration of the accelerator in the DICY/Epoxy formulations. The results indicate that the change in accelerator concentration directly effects the storage time and hardening temperature for the one-component epoxy-resin formulation. Furthermore, it is observed for a series of samples that the avarami exponent is independent of the change in concentration of accelerator and remains the same within the experimental accuracy.

It is also shown that PALS is a very useful technique, when it comes to the characterization of cured epoxy composites. A comparison of PALS with DSC technique was done for a selected series of cured composites, which indicates the glass-transition T_g obtained from the two techniques was in good correlation. Furthermore, with the help of PALS data in combination with the Tao-Eldrup model, the temperature dependence of the hole free volume, the fractional free volume (FFV) and the thermal expansion co-efficients in the glassy and the rubbery phase were also estimated.

During the major part of this work, the main focus was on providing the industrial partners with the shelf-life information for the one-component epoxy-resin formulations, as obtained from PALS data at elevated temperatures. This information was really helpful in developing new synthesis approaches for the encapsulation of accelerator in micro and nano-sized carriers. But as an outlook, purely from the academic research point of view, still there appears to be a lot of open questions. The paragraphs to follow, will be used to throw a light on these topics of purely academic interest.

The effect of the particle size on the storage time and the curing kinetics can be studied by the combination of PALS and the JMAK theory of phase transformation. For example, the DICY is commercially available with particle sizes in the range of 5 to 40 μm and it will be really interesting to see the effect of particle size on the shelf-life and the hardening temperatures of one-component formulations. This will in turn help with the choice of material used in DICY cured one-component formulations. Another possible theme concerning the particle size could be to study the effect of temperature on the final structure of the cured composites. This in turn can be compared with the atomic force microscopy (AFM) or other imaging techniques and these results could be helpful to understand the effect of temperature on the extent of cured fraction and the type of structure formed.

The accelerator used throughout this work for encapsulation purpose, to lower the hardening temperature, has a melting temperature (T_m) of less than 0°C . This makes the accelerator highly reactive not only at the elevated temperatures but even at the storage conditions as well. Since accelerators with melting temperatures higher than storage temperatures are commercially available, so it will be better to use one with T_m above room temperature. It is expected that this will increase the shelf life of the formulation and at the same time it can be useful in achieving low temperature curing. Since no incubation time was observed for the free accelerator systems (as reported in Chapter 7 of this thesis), it will be interesting to study a comparison of free and encapsulated accelerator on the activation energies for such an accelerator (with $T_m > \text{RT}$).

There was already a nanosilica filler material used for all the dicyandiamide cured formulations to control the viscosity, which is acceptable as long as formulations with the free accelerator or the Zeolite encapsulated accelerator are concerned. But the precursor was difficult to prepare or mix, when this nanosilica filler was used in combination with the

accelerator encapsulated on pyrogenic silica based carriers, as the viscosity is apparently affected by high weight concentration of fumed silica particles. Therefore, a benchmark system should be the one containing the same filler material as the one which is later on supposed to be used as the carrier material for accelerator encapsulation. Furthermore, the accelerator was mostly encapsulated in Nanosilica and Zeolite based carriers, it will be interesting to see the effect of other carrier materials (such as layered silicates) e.g., on one hand the curing kinetics of one-component formulations and on the other hand, how it affects the properties of their cured composites.

To the best of knowledge the reaction chemistry of such one-component formulations is not known and even it is impossible to simulate the cured structure of such formulations. Therefore, a comparison of PALS data can be studied in combination with the pressure-volume-temperature (PVT) experiments. This will give complete structural information such as, the temperature dependence of the hole free volume, the specific total, the occupied and the specific free volume along with fractional free volume and the number density of holes. This will enable to calculate the cross-linking density, which will be of great help in simulating such complex structures.

11. Bibliography

- 1 M.A. Clayton. *Epoxy resins: chemistry and technology*. 2nd Edition edn, (Marcel Dekker Inc., 1987).
- 2 J. Kansy. Microcomputer program for analysis of positron annihilation lifetime spectra. *Nuclear Instruments and Methods in Physics Research Section A: Accelerators, Spectrometers, Detectors and Associated Equipment* **374** (2), 1996, 235–244 **374**, 235-244 (1996).
- 3 S. J. Tao. Positronium annihilation in molecular substances. *Journal of Chemical Physics* **56**, 5499–5510 (1972).
- 4 M. Eldrup, D. Lightbody & Sherwood, J. N. The temperature dependence of positron lifetime in solid pivalic acid. *Chemical Physics* **63**, 51-58 (1981).
- 5 M. Avrami. Kinetics of Phase Change. I: General Theory. *J. Chem. Phys.* **7**, 1103 (1939).
- 6 M. Avrami. Kinetics of phase change II. Transformation-time relations for random distribution of nuclei. *J. Chem. Phys.* **8**, 212-224 (1940).
- 7 M. Avrami. Granulation, phase change and microstructure Kinetics of phase change. III. *Journal of Chemical Physics* **9**, 177-184 (1941).
- 8 B.S.S. Daniel *et al.* Free volume evolution in bulk metallic glass during high temperature creep. *MRS Symp. Proc.* **CC 11.16**, 754 (2003).
- 9 C. Nagel *et al.* Free volume changes in the bulk metallic glass $Zr_{47}Ti_8Cu_{7.5}Ni_{10}Be_{27.5}$ and the undercooled liquid. *Phys. Rev. B* **57**, 10224 (1998).
- 10 C. Nagel, K. Rätzke, E. Schmidtke, F. Faupel & Ulfert, W. Positron annihilation studies of free volume changes in the bulk metallic glass $Zr_{65}Al_{7.5}Ni_{10}Cu_{17.5}$ during structural relaxation and at the glass transition. *Phys. Rev. B* **60**, 9212 (1999).
- 11 C. Nagel, K. Rätzke, E. Schmidtke & Faupel, F. Free volume changes in bulk amorphous alloys during structural relaxation and in the supercooled liquid state. *MRS Symp. Proc.* **75**, 554 (1999).
- 12 J. Kruse *et al.* Free Volume in Polyimides: Positron Annihilation Experiments and Molecular Modelling. *Macromolecules* **38**, 9638 (2005).
- 13 J. Kruse *et al.* Free volume in polymeric membranes: Experiment and simulation. *Membrane News* **66**, 51 (2004).
- 14 R.De.Miranda, J. K., K.Rätzke, F.Faupel, D.Fritsch, V.Abetz, P.M.Budd, J.D.Selbie, N.B.McKeown, B S.Ghanem. Unusual temperature dependence of positron lifetime in a polymer of intrinsic microporosity. *Phys. Stat. Sol. Rapid Res. Lett.*, **5**, 190 (2007).
- 15 J.Kanzow, V. Z., H.Nabika, M.Mizuhata, S.Deki, F Faupel,. In-situ investigations on the cross-linking process of the epoxy resin system DGEBA-DETA by means of positron annihilation lifetime spectroscopy in comparison with infrared spectroscopy. *Mat. Sci. Forum* **445-446**, 313 (2004).
- 16 G.Dlubek, M. Q. S., K.Rätzke, F.Faupel, J Pionteck, M. Paluch. The temperature dependence of free volume in phenyl salicylate and its relation to structural dynamics: A positron annihilation lifetime and pressure-volume-temperature study. *J. Chem. Phys.* **130**, 144906 (2009).
- 17 P. A. M. Dirac. in *Proc. Cambridge Phil. Soc.* 361-375.
- 18 C.D. Anderson. The positive electron. *Phys. Rev.* **43**, 491-498 (1933).
- 19 A.E. Ruark. Positronium. *Physical Review* **68**, 278 (1945).
- 20 P. G. Coleman. in *Encyclopedia of Applied Spectroscopy* (ed D. L. Andrews) Ch. 5, (WILEY-VCH Verlag GmbH, 2009).
- 21 J. Kruse. *Freies Volumen in Membranpolymeren – Positronenannihilationslebensdauerspektroskopie an ausgewählten Systemen* PhD thesis, Christian-Albrechts University of Kiel, (2007).
- 22 O.E. Mogensen. (Springer-Verlag, Berlin, Heidelberg, 1995).

- 23 C. Dauwe, B. Van Waeyenberge & N. Balcaen. Positronium formation in poly(methyl methacrylate). *Phys. Rev. B* **68**, 1322021-1322024 (2003).
- 24 T. Hirade, F.H. Maurer & M. Eldrup. Positronium formation at low temperatures: the role of trapped electrons. *Rad. Phys. Chem.* **58**, 465-471 (2000).
- 25 A. Ore. Universitetet i Bergen Arbok, (1949).
- 26 O.Mogensen. in *Springer Series in Chemical Physics* Vol. 58 (Springer-Verlag, 1995).
- 27 S.V.Stepanov, V. M. B. Electric field effect on Ps formation in liquids. *Journal of Chemical Physics* **116**, 6718-6195 (2002).
- 28 W.Brandt, S.Berko & W.W.Walker. Positronium Decay in Molecular Substances. *Physical Review* **120**, 1289 (1960).
- 29 R. Krause-Rehberg & H. S. Leipner. in *Springer series in solid-state sciences* Vol. 127 (Springer, Berlin, 1999).
- 30 S. Thraenert, E. Hassan & R. Krause-Rehberg. Ortho-positronium lifetime measurement – positron source activity and statistics *Nuclear Instruments and Methods in Physics Research Section B: Beam Interactions with Materials and Atoms* **248**, 336–339 (2006).
- 31 C. Nagel. *Freies Volumen und Transporteigenschaften in hochselektiven Polymermembranen und metallischen Massivgläsern*, Christian-Albrechts-Universität zu Kiel, 1999, (1999).
- 32 Y.C. Jean, P. E. Mallon & Schrader, D. M. (World Scientific Publishing Co. Pte. Ltd., Singapore, 2003).
- 33 S. McGuire & D. J. Keeble. Positron lifetime and implantation in Kapton. *Journal of Physics D: Applied Physics* **39**, 3388-3393 (2006).
- 34 P. Kirkegaard, M. Eldrup, O. E. Mogensen & Pedersen, N. J. *Computer Physics Communications* **23**, 307-335 (1981).
- 35 S. W. Provencher. *Computer Physics Communications* **27**, 229-242 (1982).
- 36 A. Shukla, M. Peter & Hoffmann, L. *Nuclear Instruments and Methods A* **335**, 310 (1993).
- 37 H. Cao, G.H. Dai, J.P. Yuan & Jean, Y. C. Reliability of ortho-Positronium Lifetime distribution analysis in Polymers by using CONTIN program. *Materials Science Forum* **255-257**, 238-242 (1997).
- 38 H. Nakanishi, S. Wang & Y.C. Jean. in *Positron Annihilation Studies of Fluids* (ed S. Sharama) 292–298 (World Scientific, 1988).
- 39 G. Ferrante. Annihilation of Positrons from Positronium Negative Ion $e^-e^+e^-$. *Physical Review* **170**, 76 (1968).
- 40 A. Dupasquier, P. De Natale & Rolando, A. Formal calculation of the pick-off annihilation rate for ortho- and parapositronium. *Physical Review B* **43**, 10036 (1991).
- 41 J. Kanzow *et al.* In-situ investigations on the cross-linking process of the epoxy resin system DGEBA-DETA by means of positron annihilation lifetime spectroscopy in comparison with infrared spectroscopy. *Mat. Sci. Forum* **445-446**, 313 (2004).
- 42 T. Suzuki, Y. Oki, M. Numajiri, K. Kondo & Y. Ito. Positron annihilation and polymerization of epoxy resins. *Polymer*, **7**, 1361-1365 (1993).
- 43 T. Suzuki *et al.* Polymerization of bisphenol-A dicyanate studied by positron annihilation. *Materials science forum* **175-178**, 785-788 (1995).
- 44 T. Suzuki, T. Hayashi & Y. Ito. Polymerization of epoxy resins studied by positron annihilation. *Mat. Res. Innovat* **4**, 273-277 (2001).
- 45 W. Salgueiro, J. Ramos, A. Somoza, S. Goyanes & I. Mondragon. Nanohole volume dependence on the cure schedule in epoxy thermosetting networks: A PALS study. *Polymer* **47**, 5066-5070 (2006).
- 46 A.J. MacKinnon, R.A. Pethrick, S.D. Jenkins & P.T. McGrail. Investigation of thermoplastic-modified thermosets: positron annihilation and related studies of an amine-cured epoxy resin. *Polymer* **35**, 5319-5326 (1994).
- 47 Y.Y. Wang, H. Nakanishi & Jean, Y. C. Positron annihilation in amine-cured epoxy polymers - pressure dependence. *Journal of Polymer Science Part B: Polymer Physics* **28**, 1431-1441 (1990).
- 48 J.D.Ferry. (Wiley, New York, 1980).
- 49 W.J.McKnight, J. J. A. a. (Wiley, New York, 1983).
- 50 M.L.Williams, R. F. L., and J.D.Ferry. *J. Am. Chem. Soc.*, **77**, 3701 (1955).

- 51 W.W.Lee. Selection of barrier materials from molecular structure. *Polym. Eng. Sci.* **20**, 65-68 (1980).
- 52 J.D.Vrentas, J. L. D., and J.W.Huang. *Macromolecules* **19**, 1718 (1986).
- 53 W.Brostow & M.A.Macip. *Macromolecules* **22**, 2761 (1989).
- 54 S.Matsuoka. (Hanser, New York, 1992).
- 55 H.Eyring. *J. Chem. Phys.* **4**, 283 (1936).
- 56 J.Liu, Q. D., and Y.C.Jean. *Macromolecules* **26**, 7149 (1993).
- 57 A.Bondi. (John Wiley & Sons, Inc., New York, 1968).
- 58 vanKrevelen, D. W. (Elsevier, Amsterdam, 1990).
- 59 D.N.Theodorou. (ed P. Neogi) 67-142 (Marcel Dekker, New York, 1996).
- 60 M.L. Greenfield & D.N.Theodorou. Geometric analysis of diffusion pathways in glassy and melt atactic polypropylene. *Macromolecules* **36**, 5461-5672 (1993).
- 61 W.L.Mattice, S. M. a. *Macromolecules* **26**, 7274 (1993).
- 62 D.Bamford. PhD thesis, University of Bristol, (2003).
- 63 R.J.Roe, D. R. a. *Macromolecules* **23**, 5312 (1990).
- 64 V.I.Betekhtin, E. L. G., A.G.Kadomtsev, A.Yu.Kipyatkova and O.V.Tolochko. Effect of annealing on the excess free volume and strength of amorphous alloys. *Physics of the Solid State* **42**, 1460-1464 (2000).
- 65 A.Y.Alientiev, V. P. S., T.C.Merkel, V.I.Bondar, B.D.Freeman and Y.P.Yampolski. Gas and vapor sorption, permeation and diffusion in glassy amorphous Teflon AF1600. *Macromolecules* **35**, 9513-9522 (2002).
- 66 B.Nagasaka, T. E., H.Nakayama, N.Nakamura, Y.Ito. Positron annihilation and ^{129}Xe NMR studies of free volume in polymers. *Radiation Physics and Chemistry* **58**, 581-585 (2000).
- 67 H.Vajdlenková, J. B. Spin probe mobility in relation to free volume and relaxation dynamics of glass-formers: A series of spin probes in poly(isobutylene). *Journal of Polymer Science Part B: Polymer Physics* **47**, 1058-1068 (2009).
- 68 J.M.Torkelson, J. S. R. a. Photochromic and fluorescent probe studies in glassy polymer atrices. 5. Effects of physical aging on bisphenol-A polycarbonate and poly(vinyl acetate) as sensed by a size distribution of photochromic probes. *Macromolecules* **25**, 4792-4796 (1992).
- 69 T.S.Chow. *Macrom. Theory Simul.* **4**, 397-404 (1995).
- 70 Y.C.Jean, J.-P. Y., J.LIU, Q.DENG and H.Yang. Correlations between gas permeation and free-volume hole properties probed by positron annihilation spectroscopy. *Journal of Polymer Science: Part B: Polymer Physics* **33**, 2365-2371 (1995).
- 71 R.M.Dammert, S. L. M., F.H.J.Maurer, I.M.Neelow, S.Niemelä, F.Sundholm and C.Wästlund. Free volume and tacticity in polystyrenes. *Macromolecules* **32**, 1930-1938 (1999).
- 72 V.Shantarovich, Y. Y. a. in *Materials Science of Membranes: for Gas and Vapor separation* (ed I.Pinnai and B.D.Freeman Y.Yampolski) (John Wiley & Sons Ltd., UK, 2006).
- 73 R.S.Spencer, R. F. B. a. *J. Appl. Phys.* **15**, 398 (1944).
- 74 F.H.J.Maurer, J.H.M. Palmen & H.C.Booij. Generalized stress relaxation behaviour and physical aging in heterogeneous amorphous polyblends *Rheologica Acta* **24**, 243-249 (1985).
- 75 W.A. Johnson & R.F. Mehl. *Trans. Am. Inst. Min. Metall. Eng.*, **135**, 416 (1939).
- 76 A.N. Kolmogorov. Statistical theory of crystallization of metals.(in russian). *Izvestia Akademia Nauk SSSR Ser. Mathematica* **1**, 355-359 (1937).
- 77 J.W. Christian. *The theory of transformations in metals and alloys. Part I, Equilibrium and general kinetic theory.* (Pergamon, 1975).
- 78 W.D. Callister Jr. *Materials Science and Engineering: An Introduction.* 5th edn, (John Wiley and Sons Inc., 2000).
- 79 L. Mandelkern. *Crystallization of Polymers: Kinetics and Mechanisms, Volume 2.* 2nd edn, Vol. 2 (Cambridge University Press, 2004).
- 80 D.A. Porter & K.E. Easterling. *Phase Transformations in Metals and Alloys.* (Chapman and Hall, 1991).
- 81 A.K. Jena & M.C. Chaturvedi. *Phase Transformations in Materials.* . 243 (Prentice Hall, 1992).
- 82 Prof. A.D. Rollett. *Microstructure Properties II: The KJMA Equation* (Department of Materials Science and Engineering; Carnegie Mellon University Pittsburgh, USA, 2009).
- 83 Prof. H.K.D.H. Bhadesia. *Kinetics and Microstructure Modelling.* (2010).

- 84 E.M. Petrie. *Epoxy Adhesive Formulations*. (MacGraw Hill, 2006).
- 85 Dyhard Booklet. (ed Degussa Fine Chemicals) (March 2003).
- 86 BMBF Projekt. Entwicklung vernetzungssteuernder Nanomodule mit controlled Release-funktion für Polymerharz-Systeme mit erhöhter Lagerstabilität und reduzierter Härtungstemperatur (www.nanomodule.de) (NANOMODULE, 2006).
- 87 G.K. Noren. Cationic UV Curable Formulations Containing Hydroxy Functional Fluoropolymer Resins. *Journal of Coatings Technology* **72**, 53-59 (2000).
- 88 Herman F. Mark. (John Wiley & Sons, 2004).
- 89 H. F. Mark. in *Encyclopedia of polymer science and technology*. Vol. 9, *Epoxy resins*. (John Wiley & Sons, 2004).
- 90 Dow Chemical Company USA. Liquid Epoxy Resin - DGEBA (2010).
- 91 Y. Tanaka. in *Epoxy Resins: Chemistry and Technology* (ed M.A. Clayton) pp.969 (Marcel Dekker Inc., 1988).
- 92 Prof. Dr. Franz Faupel. Lecture notes "Polymer-I". (2010).
- 93 Hexion Speciality Chemicals - USA. Electrical Laminating Resins. (www.hexion.com) (2010).
- 94 L.S. Penn & H. Wang. in *Handbook of Composites* (ed S.T. Peters) (Chapman and Hall, London, 1998).
- 95 P. Pfäffli, M. Hämeilä, R. Riala, J. Tornaues & R. Wirmoila. Exposure to methylhexahydrophthalic anhydride (MHHPA) in two workplaces of the electric industry. *Journal of Environmental Monitoring* **6**, 295-299 (2004).
- 96 J.P. Pascault, H. Sauterau, J. Verdu & R.J.J. Williams. *Thermosetting polymers*. (Marcel Dekker, 2002).
- 97 J.B. Enns & J.K. Gillham. The time-temperature transformation (TTT) cure diagram: modeling the cure behavior of thermosets. *Journal of Applied Polymer Science* **28**, 2567-2591 (1983).
- 98 G. Wisanrakkit & J. K. Gillham. The Glass Transition Temperature (T_g) as an Index of Chemical Conversion for a High- T_g Amine/Epoxy System: Chemical and Diffusion-Controlled Reaction Kinetics. *Journal of Applied Polymer Science* **41**, 2885-2929 (1990).
- 99 K. Dusek. in *Epoxy Resins and Composites III, Advances in Polymer Science* Vol. 78 (ed K. Dusek) pp. 1-59 (Springer-Verlag, Berlin, 1986).
- 100 C. M. Tung & J. P. Dynes. *Journal of Applied Polymer Science* **27**, 569-574 (1982).
- 101 M. E. Smith & H. Ishida. *Journal of Applied Polymer Science* **73**, 593-600 (1999).
- 102 H. Jahn & P. Goetzky. in *Epoxy Resins: Chemistry and Technology*, (ed C.A. May) pp. 1049-1087 (Marcel Dekker, Inc. New York, , 1988).
- 103 C.T. Chou & L.S. Penn. Mechanism by which an orthocarbonate reduces residual stress in a composite. *Journal of Composite Materials* **26**, 171-184 (1992).
- 104 J. Mijovic & H.T. Wang. Cure kinetics of neat and graphite-fiber-reinforced epoxy formulations. *Journal of Applied Polymer Science* **37**, 2661-2673 (1989).
- 105 R. Morgan. Structure-property relations of epoxies used as composite matrices. *Advances in Polymer Science* **72**, 143 (1985).
- 106 S. Yalof & W. Wrasidlo. Crosschecking between dielectric measurements, DTA, and other methods of thermal analysis in research and production. *Journal of Applied Polymer Science* **16**, 2159-2173 (1972).
- 107 S.D. Senturia & N.F. Sheppard. Dielectric analysis of thermoset cure. *Advances in Polymer Science* **80**, 147 (1986).
- 108 P.R. Ciriscioli & G.S. Springer. Dielectric cure monitoring - a critical review. *SAMPE J.* **25**, 3542 (1989).
- 109 C.S.P. Sung & R. Mathisen. Cure characterization of an epoxy network by fluorescence behavior of trans-diaminostilbene. *Polymer* **28**, 941-945 (1987).
- 110 P.R. Young, M.A. Drury, W.A. Stevenson & D.A. Compton. In-situ composite monitoring using infrared-transmitting optical fibers. *SAMPE J.* **25**, 11-16 (1989).
- 111 M.L. Myrick, S.M. Angel, R.E. Lyon & T.M. Vess. Epoxy cure monitoring using fiber-optic Raman spectroscopy. *SAMPE J.* **28**, 3742 (1992).
- 112 J. Mijovic, J.M. Kenny, L. Nicolais & S. Pejanovic. Present and future trends in insitu monitoring of processing of advanced composites. *SAMPE J.* **28**, 3946 (1992).

- 113 K. Raetzke, M.Q. Shaikh, F. Faupel & P.-L.M. Noeske. Shelf stability of reactive adhesive formulations: A case study for dicyandiamide-cured epoxy systems *International Journal of Adhesion and Adhesives* **30**, 105-110 (2010).
- 114 B. Ellis. *Chemistry and Technology of Epoxy Resins*. 1st ed. edn, 72, 116 (Blackie Academic & Professional, 1993).
- 115 J. Kanzow *et al.* *Applied Surface Science* **239**, 227 (2005).
- 116 S.A. Zahir. in *Advances in Organic Coatings Science and Technology, Vol. IV: Sixth International Conference in Organic Coatings Science and Technology* Vol. 4 eds G.D. Parfitt & A. V. Patsis pp.83 (Technomic Publishing Co. Inc., 1982).
- 117 L.H. Sperling. *Introduction to Physical Polymer Science*. (Wiley, 2005).
- 118 M. Cao *et al.* *Journal of Applied Polymer Science* **85**, 873 (2002).
- 119 M. Pollard & J.L. Kardos. *Polymer Engineering and Science*, **27**, 829 (1987).
- 120 M.G. Lu, M.J. Shim & S.W. Kim. *Journal Thermal Analysis and Calorimetry* **58**, 701 (1999).
- 121 D.Z. Chen, P.S. He & L.J. Pan. *Polymer Testing* **22**, 689 (2003).
- 122 X.H. Zhang, Y.Q. Min, H. Zhao, H.M. Wan & G.R. Qi. *Journal of Applied Polymer Science* **100**, 3483 (2006).
- 123 R.De. Miranda *et al.* Unusual temperature dependence of positron lifetime in a polymer of intrinsic microporosity. *Phys. Stat. Sol. Rapid Res. Lett.*, **5**, 190 (2007).
- 124 J. Kruse *et al.* Free volume in C-60 modified PPO polymer membranes by positron annihilation lifetime spectroscopy. *J Phys Chem B* **111**, pp. 13914–13918. (2007).
- 125 G. Dlubek, J. Pionteck, M.Q. Shaikh, E.M. Hassan & R. Krause-Rehberg. *Physical Review E* **75**, 021802 (2007).
- 126 G. Dlubek, M.Q. Shaikh, R. Krause-Rehberg & M. Paluch. *J. Chem. Phys.* **126**, 024906 (2007).
- 127 J. Kanzow *et al.* in *Adhesion - Current research and applications* (ed W. Possart) 465 (Wiley-VCH, 2005).
- 128 A. Somoza, W. Salgueiro, S. Goyanes, J. Ramos & Mondragon, I. Volume changes at macro- and nano-scale in epoxy resins studied by PALS and PVT experimental techniques *Radiation Physics and Chemistry* **76**, 118-122 (2007).
- 129 Dyhard Booklet. (ed by Degussa Fine Chemicals) (2005).
- 130 S. Vyazovkin & N. Sbirrazzuoli. *Macromol. Chem. Phys.* **200**, 2294-2303 (1999).
- 131 T. M. Goulding. *Handbook of Adhesive Technology*. 2nd Ed. edn, (Marcel Dekker, Inc., 2003).
- 132 G. Webster. *Chemistry & Technology of UV & EB Formulation for Coatings, Inks & Paints*. Vol. 2 (John Wiley & Sons, Inc., 1997).
- 133 E.W. Flick. *Contemporary Industrial Coatings, Environmentally Safe Formulations*. (Noyes Publishers, 1985).
- 134 W.K. Goertzen & Kessler, M. R. Creep behavior of carbon fiber/epoxy matrix composites. *Materials Science and Engineering: A*. **421**, 217-225 (2006).
- 135 G. Dlubek, J. Pionteck, M.Q. Shaikh, E. M. Hassan & Krause-Rehberg, R. Free volume of an oligomeric epoxy resin and its relation to structural relaxation: Evidence from positron lifetime and pressure-volume-temperature experiments. *Phys. Rev. E* **75**, 021802-02180213 (2007).
- 136 M. Rudel *et al.* Temperature dependence of positron annihilation lifetimes in high permeability polymers: amorphous Teflons AF. *Macromolecules* **41**, 788 (2008).
- 137 G. Dlubek *et al.* The free volume in two untreated, pressure-densified, and CO₂ gas exposed polymers from positron lifetime and pressure-volume-temperature experiments. *e-Polymers* **108**, 1 (2007).
- 138 M. Rudel *et al.* Temperature dependence of positron annihilation lifetimes in high permeability polymers: amorphous Teflons AF. *Macromolecules* **41**, 788 (2008).
- 139 G. Dlubek *et al.* The temperature dependence of free volume in phenyl salicylate and its relation to structural dynamics: A positron annihilation lifetime and pressure-volume-temperature study. *J. Chem. Phys.* **130**, 144906 (2009).
- 140 O. Mogensen. in *Springer Series in Chemical Physics* Vol. 58 (Springer-Verlag, 1995).
- 141 V. Abetz. *Advances in Polymer Science. Block Copolymers II*. (Springer-Verlag, 2005).

- 142 G. Dlubek, M.Q. Shaikh, R. Krause-Rehberg & M. Paluch. Effect of free volume and temperature on the structural relaxation in polymethylphenylsiloxane: A positron lifetime and pressure-volume-temperature study. *J. Chem. Phys.* **126**, 024906 (2007).
- 143 E. Riande, R. Diaz-Calleja, M.G. Prolongo, R.M. Masegosa & Salom., C. *Polymer Viscoelasticity: Stress and Strain in practice*, . 71-72 (Marcel Dekker Inc., 2000).
- 144 R. Srithawatpong *et al.* Positron annihilation lifetime studies of changes in free volume on cross-linking cis-polyisoprene, high-vinyl polybutadiene, and their miscible blends. *Journal of polymer science. Part B. Polymer physics* **37**, pp. 2754-2770 (1999).
- 145 C. Lianxi, T. Hua, L. Quanwen & W. Jun. Curing Reaction Kinetics of Epoxy Resin Using Dicyandiamide Modified by Aromatic Amines. *Wuhan University Journal of Natural Sciences* **12**, 1105-1108 (2007).
- 146 M.R. Kamal. *Polym. Eng. Sci.* **14**, 231 (1974).
- 147 Jürgen Schawe. Kinetic studies of complex reactions Part 1: model free kinetics *Usercom - Mettler Toledo* **2**, 13-16 (2003).
- 148 J. Schawe. Kinetic studies of complex reactions, Part 2:Description of diffusion control,. *Usercom- Mettler Toledo* **1**, 8-12 (2004).
- 149 H. F. Mark. in *Encyclopedia of polymer science and technology. Vol. 9, Epoxy resins.* (ed H. F. Mark) pp.757 (John Wiley & Sons, 2004).
- 150 K. Horie, H. Hiura, M. Sawada, L.Mita & H. Kambe. Calorimetric investigation of polymerization reactions. III. Curing reaction of epoxides with amines. *J. Polym. Sci. (Part A-1)* **8**, 1357-1372 (1970).
- 151 N. Gupta & I.K. Varma. Effect of structure of aromatic diamines on curing characteristics, thermal stability, and mechanical properties of epoxy resins. I. *Journal of Applied Polymer Science* **68**, 1759-1766 (1998).
- 152 D. Olmos, A.J Aznar, J. Baselga & J. González-Benito. Kinetic study of epoxy curing in the glass fiber/epoxy interface using dansyl fluorescence *Journal of Colloid and Interface Science* **267**, 117–126 (2003).
- 153 J.K. Gillham. in *Encyclopedia of Polymer Science and Engineering* Vol. 4 p. 519 (Wiley, New York, 1989).
- 154 Boltzmann Function. Microcal Origin 7.5. (2010).
- 155 M. Pollard & J.L. Kardos. Analysis of epoxy resin curing kinetics using the Avrami theory of phase change. *Polym. Eng. Sci.* **27**, 829-836 (1987).
- 156 M.G. Lu, M.J. Shim & S.W. Kim. The macrokinetic model of thermosetting polymers by phase-change theory. *Mater. Sci. Commun.* **56**, 193-197 (1998).
- 157 K. Schulte, F.H. Gojny & B. Fiedler. in *Polymer Composites: From Nano to Macro Scale* (ed S. Fakirov K. Friedrich, Z. Zhang) 3-22 (Springer, 2005).
- 158 R. Dagani. Nanostructured materials promise to advance range of technologies. *C&EN* **70**, 18 (1992).
- 159 M. Z. Rong, M. Q. Zhang, Y. X. Zheng, H. M. Zeng & K. Friedrich. Improvement of tensile properties of nano-SiO₂/PP composites in relation to percolation mechanism. *Polymer* **42**, 3301 (2001).
- 160 M. Q. Zhang, M. Z. Rong & K. Friedrich. in *Polymer Composites: From Nano to Macro Scale* (ed S. Fakirov K. Friedrich, Z. Zhang) 25-43 (2005).
- 161 J. Ch. Gaukler & W. Possart. Functional Nano fillers in hot curing epoxies for prolonged shelf life and reduced curing temperature. (2009).
- 162 M. Noeske, P. Schiffels & J. Trautmann. Jahresbericht 2007/2008. (Fraunhofer Institut für Fertigungstechnik und Angewandte Materialforschung (IFAM), Bremen, Germany, March 2008).
- 163 P.L.M. Noeske. (Private Communication, Fraunhofer Institute for Manufacturing Technology and Applied Materials Research in Bremen, 2010).
- 164 S. Gramm. (Private Communication, AWOK University of Kaiserslautern, 2010).
- 165 W. Xu, R. Huang, B. Cai & W. Fan. Nano-CaCO₃ filled HDPE composites. *China Plastics* **12**, 30-34 (1998).
- 166 L.S. Schadler, K.O. Laul, R.W. Smith & E. Petrovicova. Microstructure and mechanical properties of thermally sprayed silica/nylon nanocomposites. *Journal of Thermal Spray Technology* **6**, 475 (1997).

- 167 A. Bhattacharya, J. W. Rawlins & P. Ray. *Polymer Grafting and Crosslinking*. (John Wiley & Sons Inc., 2009).
- 168 C.N. Bowman & N.A. Peppas. Development of a novel kinetic gelation method for the simulation of free radical polymerizations. *Chemical Engineering Science* **47**, 1411-1419 (1992).
- 169 Degussa AG. in *Technical Bulletin Free Particles No. 56, Highly Dispersed Metallic Oxides Produced by the AEROSIL Process, 4th ed.* (D-40402 Düsseldorf, 1989).
- 170 Degussa AG. in *Technical Bulletin Fine Particles No. 27, AEROSIL® Fumed Silica for Solvent-Free Epoxy Resins* (D-40402 Düsseldorf, 2009).
- 171 T. Schlosser & R. Nowak. (Evonik Degussa GmbH, *personal communication*, 60287 Frankfurt am Main, Germany, 2010).
- 172 J.H. Koo. in *Polymer Nanocomposites: Processing, Characterization, and Applications* (ed J.H. Koo) pp. 38-40 (McGraw-Hill Professional, 2006).
- 173 H. Nakanishi & Y.C. Jean. in *Studies in Physical Theoretical Chemistry Vol. 57* eds D.M. Schrader & Y.C. Jean pp. 159-192 (Elsevier, 1988).
- 174 T. Goworek, B. Jasinska, J. Wawryszczuk, K. Ciesielski & J. Goworek. in *Studies in Surface Science and Catalysis Vol. 128* eds V.K.K. Unger, G. Kreysa, & J.P. Baselt) pp. 557-564 (Elsevier, 2000).
- 175 B. Nagasaka, T. Eguchi, H. Nakayama, N. Nakamura & Ito, Y. Positron annihilation and ^{129}Xe NMR studies of free volume in polymers. *Radiation Physics and Chemistry* **58**, 581-585 (2000).
- 176 W.R. Ashcroft. in *Chemistry and Technology of Epoxy Resins, 1st ed.* (ed B. Ellis) pp. 37, 71 (Blackie Academic & Professional, 1993).
- 177 M.D. Gilbert, N.S. Schneider & W.J. McKnight. Mechanism of the dicyandiamide/epoxide reaction. *Macromolecules* **24**, 360-369 (1991).
- 178 S.A. Zahir. in *Advances in Organic Coatings Science and Technology, Vol. IV: Sixth International Conference in Organic Coatings Science and Technology* eds G.D. Parfitt & A. V. Patsis) pp.83 (Technomic Publishing Co. Inc., 1982).

APPENDICES

A. Derivation of Tao-Eldrup equation

The *o*-Ps in a spherical bubble or pore can be regarded as a particle in a spherical potential well with finite rectangular boundaries, having quantized levels in that well. The pore radius corresponds to the radius r_h of the spherical well. In its lowest state, the wave-function, Ψ , of the Ps inside the well is thus $(\sin Ar)/r$ if $0 \leq r \leq r_h$ and $\exp(-Kr)/r$ if $r > r_h$ (= in the wall).¹⁷³ The rate of *o*-Ps annihilation then is equal to the annihilation rate in bulk multiplied with the probability to find the Ps outside the well. Integration of $|\Psi(r)|^2 * r^2$ starting from r_h , where the electron density starts to be non-zero (boundary of the potential well), up to infinity calculates this probability. In order to substitute these complex calculations by more simple ones, Tao proposed a model based on rectangular potential wells with infinitely high walls. In an infinite potential well the wave-function has no extension outside the well. In order to realize the penetration of the wave-function outside the well, Tao defined a broadening of the well by an electron layer of thickness δr ,³ as shown in Fig. 2.8 (in Chapter 2 of this thesis). To calculate the overlap of the wave function with the electron layer, integration has now to be performed from r_h to $r_h + \delta r$, whereby the pick-off rate was assumed empirically to be the same as in the finite potential well (λ_a = pick-off rate in the bulk material). Only the electrons in this layer are assumed to interact with the positrons in *o*-Ps.

The *o*-Ps pick-off rate λ_{po} then calculates as the product of pick-off rate λ_a in this layer and the probability p of finding the positron in that layer

$$\lambda_{po} = \lambda_a p \quad (\text{A.1})$$

The probability, p , of finding the Ps inside the electron layer between r_h and $r_h + \delta r$ is

$$p = 1 - \left(\frac{\int_0^{r_h} |\Psi(r)|^2 r^2 dr}{\int_0^{r_h + \delta r} |\Psi(r)|^2 r^2 dr} \right) \quad (\text{A.2})$$

with $\Psi(r)$ = radial part of wave function, r_h = radius of potential well (= pore radius), δr = thickness of electron layer on the wall of the well. For particles in a potential well with

spherical geometry, the wave-functions are spherical Bessel functions $j_i(r)$ and for the lowest state $j_0 = (\sin(Ar)/r)$. The value for A is obtained by considering that the wave function $\Psi(r) = (\sin(Ar)/r)$ of the *o*-Ps does not extend outside the radius $r_h + \delta r$, which means it has to be zero at $r = r_h + \delta r$. This is fulfilled if $Ar = \pi$, and with $r = r_h + \delta r$ follows that $A = \pi/(r_h + \delta r)$. The wave-function thus has the form

$$\psi(r) = \frac{\sin\left(\frac{\pi r}{r_h + \delta r}\right)}{r} \quad (\text{A.3})$$

and the pick-off rate calculates as,

$$\lambda_{po} = \lambda_a \left[1 - \frac{\int_0^{r_h} \sin^2\left(\frac{\pi r}{r_h + \delta r}\right) dr}{\int_0^{r_h + \delta r} \sin^2\left(\frac{\pi r}{r_h + \delta r}\right) dr} \right] \quad (\text{A.4})$$

The integrals calculate according to

$$\sin^2(x) dx = \frac{1}{2} x - \frac{1}{4} \sin(2x) \quad (\text{A.5})$$

As the result one obtains the well known Tao-Eldrup equation,³⁻⁴

$$\lambda_{po} = \lambda_{2\gamma} = \lambda_a \left(1 - \frac{r_h}{r_h + \delta r} + \frac{1}{2\pi} \sin \frac{2\pi r_h}{r_h + \delta r} \right) \quad (\text{A.6})$$

The annihilation rate in the bulk λ_a is usually set equal to the spin averaged annihilation rate ($\lambda_a = \lambda_p/4 + 3\lambda_0/4 = 2ns-1$, with $\lambda_p = 1/\tau_p$ and $\lambda_0 = 1/\tau_0$)¹⁷⁴ λ_a is basically the pick-off probability in the electron layer on the surface of the holes.

$$\tau_{po} = 0.5ns \left[\left(1 - \frac{r_h}{r_h + \delta r} + \frac{1}{2\pi} \sin \frac{2\pi r_h}{r_h + \delta r} \right) \right]^{-1} \quad (\text{A.7})$$

For small holes no further contributions are considered and the total annihilation rate $\lambda(r_h)$ is in good approximation equal to λ_{po} . Empirically, Eldrup et al. defined δr to 0.166nm,⁴ a value which is very frequently used.¹⁷⁴⁻¹⁷⁵ This function is suitable for the calculation of positron lifetimes in the free volume holes of the sub-nanometer range. It was successfully applied to positroniums in bubbles in liquids, vacancies in polymers, and cages in zeolites. However, it fails when the positroniums are confined in larger holes. The agreement between calculated and experimental data is acceptable for free volume holes of less than approximately 0.8nm but for larger pores the calculated lifetimes are drastically overestimated.

B. Epoxy and Dicyandiamide curing mechanism

The curing mechanism is rather complex, involving several simultaneous reactions. There are a number of conflicting proposed mechanisms in the literature. One study proposed the initial reaction of all four active hydrogens with epoxy resin catalyzed by tertiary amine catalysts followed by epoxy homo-polymerization. The last step involves reactions between the hydroxyl groups of the epoxy resin with the cyano group.¹⁷⁶ One of the more recent and plausible mechanism of DICY cure with epoxies is that of Gilbert and co-workers.¹⁷⁷ The Gilbert mechanism is summarized in Figure 4. Gilbert and co-workers investigated the reaction of DICY with methyl glycidyl ether of bisphenol A (MGEBA). Products were analyzed using HPLC, NMR, and FTIR. On the basis of products that were isolated and characterized, Gilbert and co-workers proposed the mechanism shown in Figure B.1.

The first step in the mechanism is the reaction of DICY with epoxy to form the alkylated DICY. This was confirmed by the imide IR peak at 1570 cm^{-1} .

Step 1

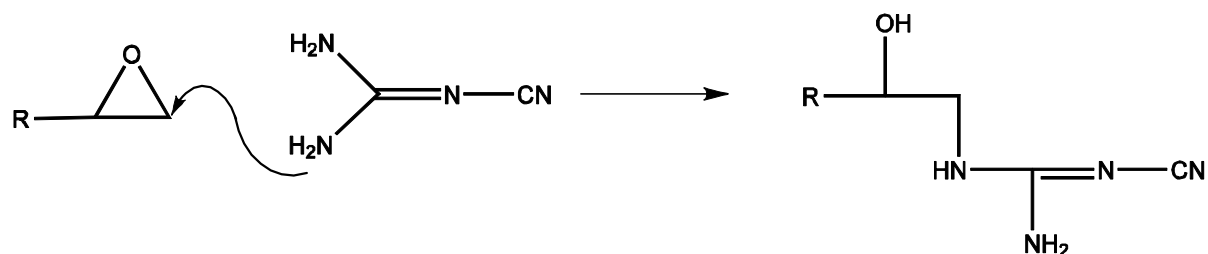


Fig B.1: Step 1 indicating reaction of DICY with epoxy

The second step involves further alkylation of the nitrogen that reacted in step 1, to form the N,N-dialkyldicyandiamide. No alkylation of the other amino group was suggested.

Step 2

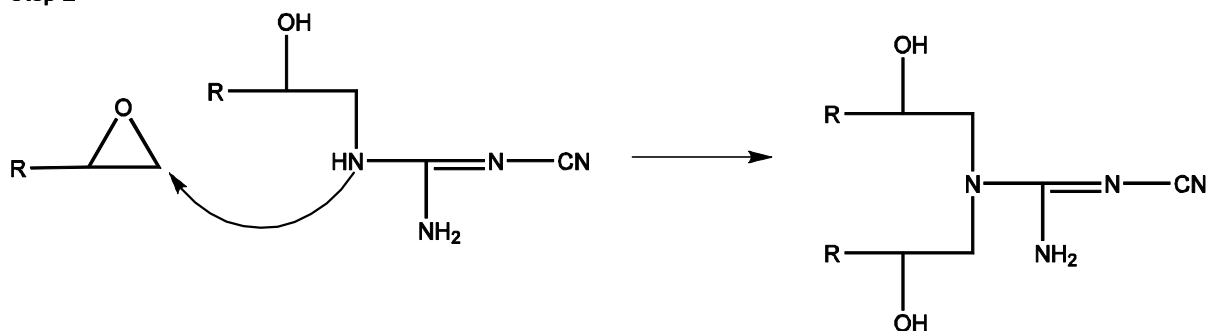


Fig B.2: Step 2 showing further alkylation of the nitrogen.

The third step is the intramolecular cyclization step to form a zwitterionic five-membered intermediate. This involves the intramolecular reaction of the secondary alcohol formed in

step 2 with the imide functionality (-C=N-). This is in contrast with the Zahir mechanism¹⁷⁸ where the intramolecular cyclization involves the hydroxy and the nitrile groups.

Step 3

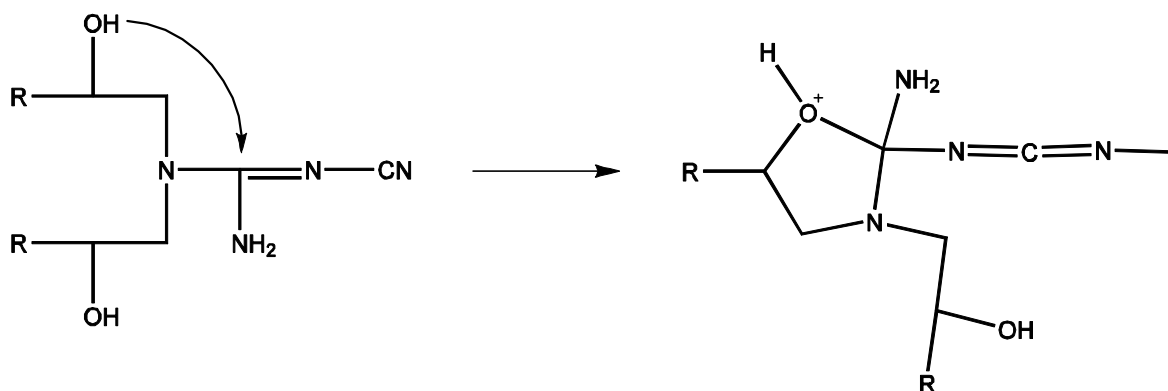


Fig B.3: Formation of a zwitterionic five-membered intermediate (Step 3).

The fourth step involves the elimination of ammonia and the formation of 2-cyanimidooxazolidine. The formation of this hetero-cycle is consistent with the observed bathochromic IR shift from 1570 cm^{-1} to 1650 cm^{-1} . The ammonia that is eliminated can then react with epoxy to form a tri-functional crosslink.

Step 4

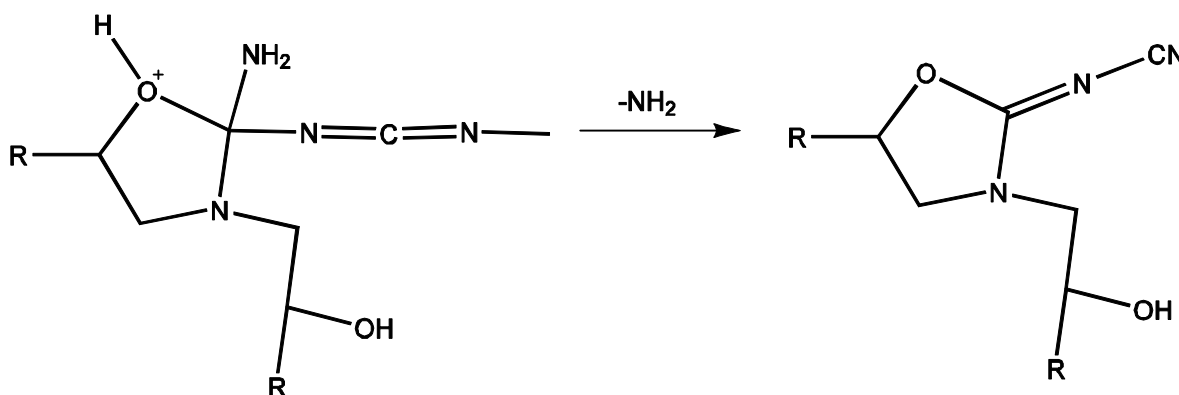


Fig B.4: Step 4, elimination of ammonia and the formation of 2-cyanimidooxazolidine.

The last step involves the hydrolysis of the oxazolidine to form the oxazolidone and cyanamide. The hydrolysis step accounts for the formation of the carbonyl group.

Step 5

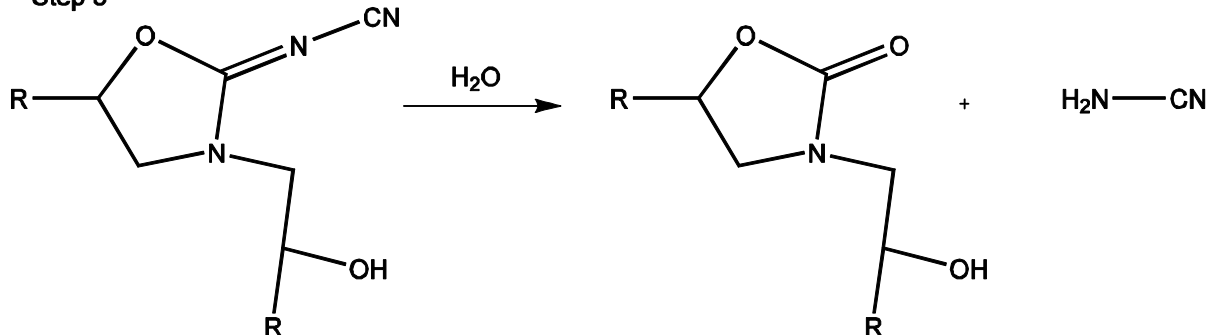
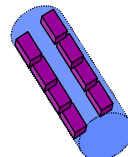
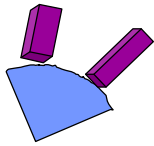


Fig. B.5: Finally the hydrolysis of oxazolidine to form the oxazolidone and cyanamide.¹⁷⁷

C. PALS and JMAK table for all 1K-formulations

Nanomodule	S. No.	Description	Accelerator in DICYLEP	T (°C)	τ_0	τ_{∞}	$\Delta\tau$	n	k	$t_{1/2}$ (PALS)	T_H °C(DSC)
Free Accelerator	1	Anhydride Benchmark (DGEBF + MHHPA)	-	50	2,70	2,20	0,50	3,77	1,68E-09	200, ~ 4 months	150,
	2	DICY Benchmark System + Uronone	0.43wt%	30	-	-	-	-	-	-	150,
	3	DICY Benchmark System + Uronone	0.43wt%	50	2,59	1,90	0,69	3,60	1,18E-08	140,3	150,
	4	DICY Benchmark System + Uronone	0.43wt%	60	2,53	1,91	0,62	3,63	1,12E-07	73,3	150,
	5	DICY Benchmark System + Uronone	0.43wt%	70	2,56	1,96	0,60	3,61	3,84E-07	51,7	150,
	6	DICY Benchmark System + Uronone	0.43wt%	80	2,41	1,98	0,43	3,67	1,89E-06	6,1	150,
	7	DICY Benchmark System + Acc.2	0.5 wt%	60	-	-	-	-	-	-	140,77
	8	DICY Benchmark System + Acc.3	0.5 wt%	60	-	-	-	-	-	-	-
	9	DICY Benchmark System + Acc.4	0.5 wt%	60	-	-	-	-	-	-	-
Activatory Energy	10	Benchmark System + Acc.1	0.5 wt%	30	2,21	1,68	0,53	1,26	3,30E-03	100,	124,93
	11	Benchmark System + Acc.1	0.5 wt%	40	2,36	1,88	0,48	1,30	8,96E-03	30,0	124,93
	12	Benchmark System + Acc.1	0.5 wt%	50	2,51	1,89	0,62	2,10	1,17E-03	18,3	124,93
	13	Benchmark System + Acc.1	0.5 wt%	60	2,45	1,86	0,59	2,02	1,31E-03	5,9	124,93
	14	Benchmark System + μ -Zeolite + Acc.1	0.5 wt%	50	2,47	2,08	0,39	3,03	4,19E-07	113,	-
	15	Benchmark System + μ -Zeolite + Acc.1	0.5 wt%	60	2,45	1,83	0,62	3,03	1,90E-06	67,8	-
Saarbrücken series	16	Benchmark System + μ -Zeolite + Acc.1	0.5 wt%	70	2,55	1,98	0,57	3,06	3,00E-05	28,6	-
	17	BK1 (Saarbrücken)	-	60	-	-	-	-	-	> 3 weeks	125,
	18	BK2 (Saarbrücken)	0.5 wt%	60	2,44	1,84	0,6	3,08	1,28E-03	6,	-
	19	BK3 (Saarbrücken)	-	60	-	-	-	-	-	> 3 weeks	-
	20	BK4 (Saarbrücken)	0.5 wt%	60	2,35	1,87	0,48	1,96	1,03E-03	26,	-
	21	BK5 (Saarbrücken)	-	60	-	-	-	-	-	-	-
	22	BK6 (Saarbrücken)	0.5 wt%	60	2,34	1,72	0,62	1,96	1,23E-03	23,	-
	23	μ -Zeolite + 11 wt% Acc.1	0.5 wt%	60	2,55	1,98	0,57	3,99	4,75E-09	114,	-
	24	μ -Zeolite + 13 wt% Acc.1	0.5 wt%	60	2,46	2,00	0,46	3,91	1,23E-08	91,	-
	25	μ -Zeolite + 15 wt% Acc.1	0.5 wt%	60	2,36	1,93	0,43	3,79	4,54E-07	43,	-
	26	μ -Zeolite + 16 wt% Acc.1	0.15 wt%	60	2,48	1,94	0,54	3,20	2,29E-08	-	-
	27	μ -Zeolite + 16 wt% Acc.1	0.5 wt%	60	2,48	1,95	0,53	3,30	1,35E-08	38,	-
	28	μ -Zeolite + 17 wt% Acc.1	0.5 wt%	60	2,46	2,00	0,46	3,96	2,10E-07	41,	-
	29	μ -Zeolite + 22 wt% Acc.1	0.5 wt%	60	2,35	1,94	0,41	3,93	1,30E-06	28,	-
	30	μ -Zeolite + 25 wt% Acc.1	0.15 wt%	60	2,59	2,01	0,58	3,21	1,44E-08	-	-
	31	μ -Zeolite + 25 wt% Acc.1	0.5 wt%	60	2,56	1,95	0,61	3,29	2,00E-05	24,	-
	32	μ -Zeolite2 + 11.4 wt% Acc.1	0.5 wt%	60	2,60	2,07	0,57	2,36	1,00E-04	40,	-
	33	μ -Zeolite2 + 12.3 wt% Acc.5	0.8 wt%	60	-	-	-	-	-	> 300,	-
	34	μ -Zeolite + 16 wt% Acc.1	0.5 wt%	60	2,59	2,02	0,57	4,80	3,40E-08	40,	-
	35	μ -Zeolite + 12 wt% Acc.1	1.0 wt%	60	2,55	1,95	0,60	2,20	1,72E-04	33,1 h	-
	36	μ -Zeolite + 12 wt% Acc.1	0.5 wt%	60	2,6	1,99	0,61	4,02	4,68E-07	13,5 h	-
	37	N31+10wt% Acc.1	1.0 wt%	60	2,6	1,99	0,61	4,02	4,68E-07	33,	-
	38	μ -Zeolite + 12 wt% Acc.1 (2. Charge)	0.5 wt%	60	2,58	1,95	0,63	2,06	3,06E-02	14,	-
	39	N30 + 10 wt% Acc.1 / Multi-stage encapsulation	1.0 wt%	60	2,44	1,90	0,54	3,69	4,10E-06	26,	-
	40	N37 + 12 wt% Acc.1	1.0 wt%	60	2,48	1,90	0,58	4,02	6,05E-07	33,	-
41	N38 + 12 wt% Acc.1	0.5 wt%	60	-	-	-	-	-	-	139,8	
42	μ -Zeolite + 16 wt% Acc.2 (2. Charge)	1.0 wt%	60	2,45	1,89	0,56	3,64	5,26E-06	25,	-	
43	μ -Zeolite + 16 wt% Acc.2 (2. Charge)	1.0 wt%	60	2,49	1,90	0,59	4,00	4,61E-07	34,	-	
44	N39 + 12 wt% Acc.1	1.0 wt%	60	2,47	1,94	0,53	3,91	9,66E-07	32,	-	
45	N40 + 12 wt% Acc.1	1.0 wt%	60	2,47	1,94	0,53	3,91	9,66E-07	32,	-	
46	N41 + 12 wt% Acc.3	0.67 wt%	60	2,46	1,89	0,57	3,01	4,00E-05	25,	-	
47	μ -Zeolite + 16 wt% Acc.1	1.0 wt%	60	-	-	-	-	-	-	-	
48	N42 + 12 wt% Acc.1	1.0 wt%	60	2,42	1,91	0,51	3,94	3,27E-06	21,	-	
49	N43 + 12 wt% Acc.1	1.0 wt%	60	2,47	1,91	0,56	3,30	3,82E-06	22,	-	
50	N45 + 12 wt% Acc.1	1.0 wt%	60	2,71	2,24	0,47	2,90	3,33E-06	50,	-	
51	N46 + 14 wt% Acc.1	1.0 wt%	60	2,71	2,24	0,47	2,90	3,33E-06	64	-	
		N47 + 12 wt% Acc.1	1.0 wt%	60	2,43	1,85	0,58	3,50	1,12E-06	45	-

Nanomodule	Description	Accelerator in DIC/EP	T (°C)	τ_0	τ_{∞}	$\Delta\tau$	n	k	$t_{1/2}$ (PALS)	T_H (DSC)	
	52	A200 + 5 wt% Acc.1	60	-	-	-	-	-	310,		
	53	A200 + 5 wt% Acc.1	60	2,44	1,98	0,46	3,48	6,78E-08	102,		
	54	A200 + 5 wt% Acc.1	60	2,58	1,98	0,60	3,49	2,36E-07	70,		
	55	A200 + 5 wt% Acc.1	60	2,56	2,02	0,54	2,49	2,00E-05	69,		
	56	A200 + 5 wt% Acc.1	60	2,37	1,86	0,51	2,17	1,50E-04	42,		
	57	A200 + 5 wt% Acc.1	60	2,55	2,00	0,55	3,51	2,69E-06	34,		
	58	A380 + 14.5 wt% Acc.1	0.5 wt%	60	2,52	2,02	0,50	3,4	1,51E-06	45,	
	59	A380 + 9.1 wt% Acc.1	0.5 wt%	60	2,59	2,03	0,56	3,39	5,97E-07	61,	
	60	OX50 + 1.4 wt% Acc.1	0.5 wt%	60	2,26	1,82	0,44	3,19	8,27E-07	71,	
	61	OX50 + 0.8 wt% Acc.1	0.5 wt%	60	-	-	-	-	-	> 250,	
	62	A380 + 6.5 wt% Acc.1	0.5 wt%	60	-	-	-	-	-	> 200,	
	63	N33-A380 + 6.5 wt% Acc.1	0.6 wt%	60	2,41	1,91	0,50	3,40	2,56E-08	159,	
	64	N33-A380 + 6.5 wt% Acc.1	0.75 wt%	60	2,39	1,87	0,52	3,20	1,63E-07	125,	
	65	N33-A380 + 6.5 wt% Acc.1	1.0 wt%	60	2,55	2,05	0,55	3,20	1,67E-06	60,7 h	
	66	N34-R816 + 5.3 wt% Acc.1	0.8 wt%	60	2,51	1,92	0,59	2,10	6,60E-04	26,3 h	
	67	N35-R9200 + 2.4 wt% Acc.1	0.8 wt%	60	-	-	-	-	-	111,	
	68	N36-A380 + 16 wt% Uron	0.43 wt%	60	2,60	2,07	0,53	3,50	6,20E-08	106,8	154,32
	69	N36-A380 + 16 wt% Uron	1.0 wt%	60	2,60	1,98	0,62	3,60	4,20E-07	51,3	147,35
	70	N43 + 7.8 wt% Acc.1 / Multi-stage encapsulation	0.75 wt%	60	2,47	1,89	0,58	2,50	2,00E-04	71,	
	71	N43 + 7.8 wt% Acc.1 / Multi-stage encapsulation	0.9 wt%	60	2,45	1,91	0,54	3,50	9,31E-07	40,	
	72	N48 + 12 wt% Acc.1 / Multi-stage encapsulation μ -Zeolite	1.0 wt%	60	2,50	1,93	0,57	4,09	2,04E-08	70,	
	73	N49 + 12 wt% Acc.1 / Multi-stage encapsulation n-Zeolite	1.0 wt%	60	2,59	2,05	0,54	3,51	3,28E-07	65,	
	74	N43 + 7.8 wt% Acc.1 / Multi-stage encapsulation	0.9 wt%	60	2,43	1,91	0,53	3,46	4,58E-07	61,	
	75	A380 + 7.8 wt% Acc.1 (2. Charge)	0.9 wt%	60	2,49	1,88	0,61	3,50	4,47E-09	217,	
	76	NM1-A380 + 7.8 wt% Acc.1	0.9 wt%	60	2,52	1,96	0,56	2,74	3,00E-05	39,	
	77	NM2-A380 + 12 wt% Acc.1	0.5 wt%	60	2,54	1,92	0,63	2,87	2,00E-05	41,	
	78	DGEBA + MHHPA (1:0.9)		30	-	-	-	-	-	-	
	79	DGEBA + MHHPA (1:0.9) + 25% SiO ₂ nanoparticles		30	-	-	-	-	-	-	

T_H = Hardening temperature measured by DSC at 10K/min (S. Gramm, personal communication, AWOK-Kaiserslautern)

N45 + 12 wt% Acc.1 (1.0 wt% Acc.1 in DIC/EP) only < 250 μ m μ -Zeolite used

N46 + 14 wt% Acc.1 (1.0 wt% Acc.1 in DIC/EP) Multi-stage encapsulation Acc.1/nano-Zeolite system

N47 + 12 wt% Acc.1 (1.0 wt% Acc.1 in DIC/EP) Multi-stage encapsulation Acc.1/ μ -Zeolite system (same like N45 but higher levels of encapsulation)

N48, Multi-stage encapsulation (12wt% Acc.1 / μ -Zeolite)

N49, Multi-stage encapsulation (12wt% Acc.1 / highSilica nano-Zeolite)

Acknowledgements

I am deeply grateful to Prof. Dr. Franz Faupel for accepting me as a PhD candidate in his group at the Institute for Material Science, Multi-component Materials, Christian-Albrechts University of Kiel and the German Ministry of Education and Research (BMBF) for the financial support under the Project No.:03X0026F “Nanomodule”. The last four years of my life have been no less than a roller coaster ride, both in terms of the academics and my personal life. But before going into details I would like to thank one of the most important person, who’s scientific knowledge and discussions helped me to finally complete my PhD thesis, my mentor, my guide and my “Doktorpapa”; Prof. Dr. Klaus Rätzke. It was an honor learning under his supervision, not just the academic part but also the social part i.e. punctuality, good sense of humor and team skills. I’m sure all these qualities will go a long way in building my personality as a qualified researcher and most important of all a more responsible individual.

Special thanks for Emeritus Prof. Dr. Günter Dlubek from the Institute for Innovative Technologies (ITA), in Halle (Saale). He is the “See of Knowledge” when it comes to positron annihilation science and I consider myself really lucky to grab a few buckets of knowledge for myself. Dr. Michael Noeske and colleagues from Fraunhofer Institute for Manufacturing Technology and Applied Materials Research (IFAM) in Bremen, Prof. Dr. Wulff Possart and Dipl.-Ing. Jan Gaukler from the University of Saarland in Saarbruecken were really cordial with their expert opinions and the scientific discussions during the half yearly meetings within the framework of the BMBF project, along with other industrial and academic partners.

It’s never easy to settle in a completely new environment, but thanks to Dr. Ing. Jan Kruse and Dr. Ing. Alexandar Bartsch for not only a smooth transition into the “Kieler Positronerei”, but also for the scientific knowledge and healthy discussions. Dipl.-Ing. Rainer Kloth made sure that my PC kept running and the huge data analysis in my work was not possible without his technical assistance. Dipl. Ing. Stefan Rehders is simply the best when it comes to the engineering skills and knowledge. It was always relaxing to know that he is on the standby, whenever it comes to troubleshooting. Another Stephan I would like to thank is my lab mate, Dipl. Phys. Stephan Harms, we always had a very good level of understanding when it comes to sharing not only the three PALS machines but also our lab duties. It was the same case

when I use to share the lab with Dipl. Ing. Dennis Ehlers. There was a time when the three of us worked together to assemble the new PALS baby “MCB4”, it was an interesting phase of my thesis, as I never thought that learning can be so fun, I think we were a great team.

The “Chair Symposiums” together with the groups of Prof. Dr. Rainer Adelung and Prof. Dr. Mady Elbahry helped a lot in increasing the general scientific knowledge and also improved my presentation skills. The famous “Two Questions” of Dr. Vladimir Zaporojtchenko are particularly appreciated for the gain in scientific knowledge, although most of the times one used to ask “and what was the other question please?” ☺

My “Mittags Gruppe”, including Dr. Ing. Seid Jebril, M.Sc Arfat Pradana, M.Sc Dawit Gedamu and M.Sc Ahmed Fazir, deserve a big thank for all the politically in-correct discussions. Dr. rer. nat. Ulrich Schürmann, Dr. Ing. Sebastian Wille, Dr. Ing. Christian Hanisch, Dr. Ing. Henry Greeve, M.Sc Sören Kaps, Dipl. Phys. Tomislav Hrkac and Dipl. Chem. Christina Pakula made sure that living in Kiel was fun. My “Kicker” mates and the “WM-2010” group, for giving me such wonderful memories to cheer, it would have been great if the “Nationalmannschaft” were the champions. M.Sc Chakravadhanula Venkata Sai Kiran was really helpful for all the tips regarding the loopholes in the German bureaucratic system. Big thanks to all the significant members of the AG Faupel, AG Adelung and AG Elbahry for the coffee and cake parties.

I would also like to thank my family back in Pakistan, for their continued support and prayers. Last but definitely not the least; I would like to thank my wife Ayesha for her continued support and love, which helped a lot even through some of the darkest and the lowest phases of my life. She always believed that I can do it and her love gave me strength to keep striving for the best, which eventually resulted in achieving this work.

Curriculum Vitae

Name: Muhammad Qasim Shaikh
Address: Preetzer Str. 64, 24143 Kiel
Born: 14.November 1977 in Karachi
Parents: Muhammad Shamim Shaikh
Feroza Nigar

School Education

1991 Secondary School Certificate
1993 Higher Secondary School Certificate (Graduation)

Academic Education

01/1994 - 08/1998 Bachelors of Mechanical Engineering (B.E.)
at the N.E.D University of Engineering and Technology, Karachi
10/2004 - 09/2006 Masters in Applied Polymer Science (M.Sc)
at the Martin-Luther University of Halle-Wittenberg
09/2006 Master Thesis: "Investigation of Free Volume in Polymers by Positron
Annihilation Lifetime Spectroscopy (PALS)"

Occupational History

09/1998 - 09/2004 Manager Production and Quality control
at Nasarun Exports, Karachi
09/2006 - Scientific Researcher
at the Institute of Material Science, Multicomponent Materials
Engineering Department, Christian-Albrechts University of Kiel

List of Publications

Publications related to this work:

1. "Shelf stability of reactive adhesive formulations: A case study for dicyandiamide-cured epoxy systems". K. Raetzke, **M.Q. Shaikh**, F. Faupel, P.-L.M. Noeske, International Journal of Adhesion and Adhesives, Vol. 30, Issue 2, 105-110, (2010).
2. "Effect of accelerator encapsulation on the curing kinetics and the activation energies of one-component epoxy-resin formulations". **M.Q. Shaikh**, K. Raetzke, F. Faupel, P.-L.M. Noeske, in preparation.
3. "IR-spectroscopy, DSC and PALS studies of several epoxy precursors and their cured composites". **M.Q. Shaikh**, K. Rätzke, J. Ch. Gaukler, W. Possart, F. Faupel, in preparation.

Other Publications:

4. "Positron Annihilation studies on Metal Organic Frameworks". **M.Q. Shaikh**, K. Raetzke, F. Faupel, I. Senkovska and S. Kaskel, in preparation.
5. "From small molecules to polymers: The free volume from PALS and PVT experiments in relation to the dynamics", G. Dlubek, **M.Q. Shaikh**, Y. Yu, J. Pionteck, M. Paluch, K. Rätzke, F. Faupel, R. Krause-Rehberg, 14th International Conference Polymeric Materials'2010 (P2010), Halle (Saale), Sept. 15-17, 2010. Submitted.
6. "Open volume in bioadhesive detected by positron annihilation lifetime spectroscopy ". K. Raetzke, M. Wiegemann, **M.Q. Shaikh**, S. Harms, R. Adelung, W. Egger and P. Sperr, Acta Biomaterialia Vol. 6, 2690-2694, (2010).
7. "Free volume from positron lifetime and pressure-volume-temperature experiments in relation to structural relaxation of van der Waals molecular glass-forming liquids". G. Dlubek, **M.Q. Shaikh**, K. Raetzke, M. Paluch and F. Faupel, Journal of Physics: Condensed Matter, Vol. 22, 235104, (2010).
8. "Subnanometre size free volumes in amorphous Verapamil hydrochloride: A positron lifetime and PVT study through T_g in comparison with dielectric relaxation spectroscopy". G. Dlubek, **M.Q. Shaikh**, K. Rätzke, J. Pionteck, M. Paluch, F. Faupel, European Journal of Pharmaceutical Sciences. Vol. 41, 388–398 (2010).
9. "Molecular Dynamics Approach to Structure-Property Correlation in Epoxy Resins for Thermo-Mechanical Lifetime Modeling" B. Wunderle, E. Dermizaki, O. Hoelck, J. Bauer, H. Walter, **M.Q. Shaikh**, K. Raetzke, F. Faupel, B. Michel, H. Reich; The 59th Electronic Components and Technology Conference (ECTC), San Diego, California USA, May (2009).
10. "The temperature dependence of free volume in phenyl salicylate and its relation to structural dynamics: A positron annihilation lifetime and pressure-volume-temperature study" G. Dlubek, **M.Q. Shaikh**, K. Raetzke, F. Faupel, J. Pionteck, and M. Paluch; Journal of Chemical Physics 130, 144906 (2009).
11. "Gas permeability and free volume in poly(amide-b-ethylene oxide)/polyethylene glycol blend membranes" W. Yave, A. Car, K.V. Peinemann, **M.Q. Shaikh**, K. Rätzke, F. Faupel; Journal of Membrane Science 339, 177 (2009).

12. *"Molecular Dynamics Simulation and Mechanical Characterization for the Establishment of Structure-Property Correlations for Epoxy Resins in Microelectronics Packaging Applications"* B. Wunderle, E. Dermitzaki, O. Hoelck, J. Bauer, H. Walter, **M.Q. Shaikh**, K. Raetzke, F. Faupel, B. Michel; Proceedings of the 10th EuroSimE, Delft, The Netherlands, April (2009).
13. *"Differences in Free Volume Elements of the Carrier Matrix Affect the Stability of Microencapsulated Lipophilic Food Ingredients"* S. Drusch, K. Raetzke, **M.Q. Shaikh**, Y. Serfert, H. Steckel, M. Scampicchio, I. Voigt, K. Schwarz, S. Mannino; Food Biophysics 4, 42 (2009).
14. *"Temperature dependence of the free volume from positron lifetime experiments and its relation to structural dynamics: Phenylphthalein-dimethylether"* G. Dlubek, **M.Q. Shaikh**, K. Raetzke, F. Faupel, M. Paluch; Physical Review E 78, 051505 (2008).
15. *"Free volume of an oligomeric epoxy resin and its relation to structural relaxation: Evidence from positron lifetime and pressure-volume-temperature experiments"* G. Dlubek, J. Pointeck, **M.Q. Shaikh**, E.M. Hassan, R. Krause-Rehberg; Physical Review E 75, 021802 (2007).
16. *"The free volume in two untreated, pressure-densified, and CO₂ gas exposed polymers from positron lifetime and pressure-volume-temperature experiments"* G. Dlubek, J. Pointeck, **M.Q. Shaikh**, L. Häußler, S. Thraenert, E. M. Hassan, R. Krause-Rehberg; e-Polymers no.108, 1 (2007).
17. *"Effect of free volume and temperature on the structural relaxation in polymethylphenylsiloxane: A positron lifetime and pressure-volume-temperature study"* G. Dlubek, **M.Q. Shaikh**, R. Krause-Rehberg, M. Paluch; Journal of Chemical Physics 126, 024906 (2007).

Declaration

I hereby declare that this thesis entitled "**Free Volume and Storage Stability of One-component Epoxy Nanocomposites**" is an authentic record of research work carried out by me and coworkers under the supervision of Prof. Dr. Klaus Rätzke, Multicomponent Materials, at Institute for Materials Science and Engineering, Christian Albrechts University of Kiel, Germany.

In keeping with the general practice of reporting scientific works, due acknowledgement has been made whenever work discussed has been based on the finding of other investigators. Any oversight due to error of judgment is regretted.

Muhammad Qasim Shaikh

Kiel, 2011